ELECTROLYTIC MAGNESIUM PRODUCTION
USING COAXIAL ELECTRODES

A THESIS SUBMITTED TO
THE GRADUATE SCHOOL OF NATURAL AND APPLIED SCIENCES
OF
MIDDLE EAST TECHNICAL UNIVERSITY

BY

GÖKHAN DEMİRCİ

IN PARTIAL FULFILLMENT OF THE REQUIREMENTS
FOR
THE DEGREE OF DOCTOR OF PHILOSOPHY
IN
METALLURGICAL AND MATERIALS ENGINEERING

AUGUST 2006

Approval of the Graduate School of Natural and Applied Sciences.

———————————————

Prof.Dr.Canan Özgen

Director

I certify that this thesis satisfies all the requirements as a thesis for the degree of Doctor of Philosophy.

———————————————

Prof.Dr.Tayfur Öztürk

Head of Department

This is to certify that we have read this thesis and that in our opinion it is fully adequate, in scope and quality, as a thesis for the degree of Doctor of Philosophy.

———————————————

Prof.Dr.İshak Karakaya

Supervisor

Examining Committee Members

Prof.Dr.Naci Sevinç   (METU, METE)   ———————————————

Prof.Dr.İshak Karakaya   (METU, METE)   ———————————————

Prof. Dr. Ali İhsan Arol   (METU, MINE)   ———————————————

Assoc.Prof.Dr. Kadri Aydınol   (METU, METE)   ———————————————

Assoc.Prof.Dr.Halil Arık   (Gazi Unv., Met. Edu.) ———————————————

I hereby declare that all information in this document has been obtained and presented in accordance with academic rules and ethical conduct. I also declare that, as required by these rules and conduct, I have fully cited and referenced all material and results that are not original to this work.

Last Name, Name : Demirci, Gökhan

Signature   :

ABSTRACT

ELECTROLYTIC MAGNESIUM PRODUCTION
USING COAXIAL ELECTRODES

Demirci, Gökhan

Ph.D., Department of Metallurgical and Materials Engineering

Supervisor : Prof.Dr. İshak Karakaya

August 2006, 152 pages

Main reason for the current losses in electrolytic magnesium production is the reaction between electrode products. Present study was devoted to effective separation of chlorine gas from the electrolysis environment by a new cell design and thus reducing the extent of back reaction between magnesium and chlorine to decrease energy consumption values. The new cell design was tested by changing temperature, cathode surface, current density, anode cathode distance and electrolyte composition.

Both the voltages and the current efficiencies were considered to be influenced by the amount and hydrodynamics of chlorine bubbles in inter-electrode region. Cell voltages were also found to be affected from the nucleation of magnesium droplets and changes in electrolyte composition that took place during the electrolysis. A hydrodynamic model was used to calculate net cell voltage by including the resistance of chlorine bubbles on anode surface to theoretical decomposition voltage during electrolysis. Good correlations were obtained between experimental and calculated voltages. The same model was used to calculate current efficiencies

by considering chlorine diffusion from bubble surfaces. A general agreement was obtained between calculated and experimental current efficiencies.

Desired magnesium deposition morphology and detachment characteristics from cathode were obtained when $MgCl_2$-$NaCl$-KCl-$CaCl_2$ electrolytes were employed. Current efficiencies higher than 90% could be achieved using the above electrolyte. The cell consumes around 8 kWh·kg^{-1} Mg at 0.43 A·cm^{-2} as a result of high chlorine removal efficiency and capability of working at low inter-electrode distances. Furthermore, the cell was capable of producing magnesium with less than the lowest energy consumption industrially obtained, at about double the commonly practiced industrial current density levels.

Keywords: Magnesium, Magnesium Chloride, Electrometallurgy, Molten Salt Electrolysis.

ÖZ

EŞ EKSENLİ ELEKTROTLAR İLE MAGNEZYUM ÜRETİMİ

Demirci, Gökhan

Doktora, Metalurji ve Malzeme Mühendisliği Bölümü

Tez Yöneticisi : Prof.Dr. İshak Karakaya

Ağustos 2006, 152 sayfa

Elektrolitik mağnezyum üretimindeki akım kayıplarının ana sebebi elektrot ürünlerinin kendi aralarında tepkimeye girmesidir. Bu çalışma enerji tüketim değerlerinin düşürülmesi için yeni bir hücre tasarımı ile klor gazının elektroliz ortamından etkin bir şeklide uzaklaştırılması ve dolayısı ile mağnezyum ve klor arasındaki geri reaksiyon miktarının azaltılmasını içermektedir. Yeni hücre tasarımı sıcaklık, katot yüzeyi, akım yoğunluğu, anot katot aralığı ve elektrolit kompozisyonu değiştirilerek test edilmiştir.

Hem voltaj hem de akım verimliliklerinin elektrotlar arası bölgedeki klor baloncuklarının miktar ve hidrodinamiğinden etkilendiği değerlendirilmektedir. Hücre voltajlarının aynı zamanda mağnezyum damlacıklarının çekirdeklenmesinden ve elektroliz sırasında meydana gelen elektrolit kompozisyonu değişimlerinden etkilendiği bulunmuştur. Net hücre voltajını hesaplamak amacı ile elektroliz sırasındaki teorik bozunma voltajına anot yüzeyindeki klor baloncuklarının etkisini dâhil eden bir hidrodinamik model kullanılmıştır. Deneysel ve hesaplanmış voltajlar arasında iyi bağıntılar elde edilmiştir. Aynı model baloncuk yüzeylerinden klor difüzyonu göz önüne alınarak

akım verimliliklerinin hesaplanmasında kullanılmıştır. Hesaplanmış ve deneysel akım verimlilikleri arasında genel bir uyum elde edilmiştir.

$MgCl_2$-NaCl-KCl-$CaCl_2$ elektrolitleri kullanıldığında istenilen magnezyum birikme yapısı ve katottan ayrılma özellikleri elde edilmiştir. Yukarıdaki elektroliti kullanarak %90 üzerinde akım verimlilikleri elde edilebilmiştir. Hücre, yüksek klor uzaklaştırma verimi ve düşük elektrotlar arası mesafede çalışabilme kabiliyeti nedeni ile 0.43 A·cm^{-2} akım yoğunluğunda 8 kWh·kg^{-1} Mg civarında enerji tüketmektedir. Buna ilaveten, hücre genelde uygulanan endüstriyel akım yoğunluğu seviyelerinin yaklaşık iki katında, elde edilen en düşük endüstriyel enerji tüketiminden daha aşağıda magnezyum üretme kapasitesine sahiptir.

Anahtar Kelimeler: Mağnezyum, Mağnezyum Klorür, Elektrometalurji, Erimiş Tuz Elektrolizi.

To my beloved Gamze

ACKNOWLEDGEMENTS

TABLE OF CONTENTS

LIST OF TABLES

LIST OF FIGURES

xv

xvi

LIST OF SYMBOLS AND ABBREVIATIONS

$E_{short\ circuit}$: Voltage drop at the electrical leads

$E_{applied}$: Cell voltage including the short circuit voltage

E_{net} : Cell voltage excluding the short circuit voltage

$E_{average\ net}$: Average of the net cell voltage after 10 minutes of electrolysis

$j_{cathode}$: Cathode current density ($A \cdot cm^{-2}$)

j_{anode} : Anode current density ($A \cdot cm^{-2}$)

I : Applied current (A)

$A_{cathode}$: Cathode area (cm^2)

A_{anode} : Anode area (cm^2)

$\%CE$: Current Efficiency (%)

$Mg_{collected}$: Deposited magnesium during electrolysis (g).

$Mg_{theoretical}$: Theoretical magnesium deposition from Faraday Equation (g).

EC : Energy consumption per kg of magnesium ($kWh \cdot kg^{-1}$)

$\%EE$: Energy efficiency (%)

E_{th} : Theoretical voltage calculated from Nernst Equation (V)

$E_{th\ (mean)}$: E_{th} value that corresponds to average composition of experiment

ACD : Anode-cathode distance

E^0 : Standard emf for the reaction when both reactants and products are in their standard states (V)

R : Gas constant (8.3145 J/mol.K)

T : Temperature

F : The Faradays number (96485.34 Coulombs/g-equivalent)

n : The number of Faradays of charge that passes through the cell when 1 g.atom of Mg is collected at the cathode at %100 efficiency

a_{MgCl_2} : $MgCl_2$ activity with respect to pure liquid standard state

P_{Cl_2} : Chlorine partial pressure of surrounding environment (atm)

a_{Mg} : Magnesium activity with respect to pure liquid standard state

κ : Electrolyte conductivity (ohm^{-1}·cm^{-1})

t : Electrolysis duration (min)

d_b : Mean bubble diameter

d_o : Orifice diameter, (cm)

$N_{Re\,o}$: Orifice Reynolds number, $d_o u_o \rho_l / \mu_l$

u_o : Gas velocity at the orifice (m·s^{-1})

ρ_l : Density of electrolyte (g.cm^{-3})

μ_l : Viscosity of electrolyte (Poise)

a : Bubble interfacial area per unit volume of dispersion (cm^2.cm^{-3})

u$_s$: Superficial velocity (cm.s^{-1})

v : Volumetric gas flow rate (cm^3.s^{-1})

A_{lc} : Cross sectional area of liquid column (cm^2)

g : Gravitational acceleration (cm.s^{-2})

σ : Surface tension (dyne.cm^{-1})

u_b : Bubble velocity (cm.s^{-1})

A_b : Single bubble area

RT : Residence time (second)

h : Half of the anode height (cm)

B : Number of bubbles

V_p : Plume volume (cm^3)

A_g : Surface area of anode covered by chlorine bubbles

IR_{bubble} : IR drop due to bubbles (V)

$IR_{electrolyte}$: IR drop across bulk electrolyte (V)

N_{Cl_2} : Chlorine flux from bubble surface in mol.m^{-2}.sec^{-1},

D_{Cl_2} : Diffusivity of Cl$_2$ (m^2.sec^{-1})

ΔC_{Cl_2} : Concentration gradient of Cl$_2$ (mol.m^{-3})

δ : Boundary layer thickness (mm)

CHAPTER 1

INTRODUCTION

Magnesium is the lightest structural metal. It is 4.5 times lighter than iron and 1.6 times lighter than aluminum. Although the magnesium consumption has increased over time, its use is still restricted due to its high productions costs despite its better properties.

Magnesium is the eighth most abundant element that constitutes about 2% of the earth's crust. It is the third most plentiful element dissolved in seawater with a concentration averaging 0.13% [1]. Seawater contains 3.7% of the total magnesium present in the earth's crust [2]. Despite its abundance, magnesium is never found in its free state in nature because of its high chemical reactivity. Dolomite ($MgCO_3 \cdot CaCO_3$), magnesite ($MgCO_3$), brucite ($Mg(OH)_2$), carnallite ($MgCl_2 \cdot KCl \cdot 6H_2O$), and serpentine ($3MgO.2SiO_2.2H_2O$) are the magnesium bearing minerals of commercial importance for the magnesium production. Magnesium can also be produced from seawater, brine and bitterns as well.

Magnesium metal was first produced in the form of an amalgam by Sir Humphrey Davy in 1808 and free metallic magnesium was first isolated by Bussy by reduction of magnesium chloride with potassium vapor in 1831. Then, Michael Faraday obtained magnesium metal by the electrolysis of fused anhydrous magnesium chloride in 1833 [3]. Metallothermic reaction and molten salt electrolysis are still the two principal magnesium metal production methods today.

Magnesium production by using aqueous electrolytes is not possible because of the high decomposition potential of magnesium chloride. For that reason magnesium production is carried out by molten salt electrolysis. Pure $MgCl_2$ has a high

melting point and high magnesium solubility in molten $MgCl_2$ increases current losses. Moreover electrical conductivity of the molten $MgCl_2$ is low and its vapor pressure is high. A chloride salt mixture is used to eliminate these disadvantages.

The main reason for the losses in electrolytic magnesium production was the back reaction between the electrode products. More effective separation of the electrode products decreases the production costs associated with the electrolytic magnesium production. Energy consumption values attained by various producers and the theoretical minimum for $20\%MgCl_2$-$40\%NaCl$-$40\%KCl$ electrolyte are given in Table1. The lowest energy consumption is around 10.0 kWh·kg^{-1} Mg and achieved by multipolar cells using a high purity $MgCl_2$ feed. The large difference between the theoretical and actual energy consumption values indicates the possibility of decreasing the industrially attained energy consumption further.

The effect of cathode material and the impurities in the magnesium electrodeposition process in molten chloride melts were investigated in considerable detail through the years. However, studies involving the effects of different electrolysis parameters on electrolysis performance are absent for both those representing the industrial production and new designs [4]. Therefore it is necessary to have more studies on magnesium production to decrease the gap between the theoretical and the actual energy consumptions.

Table 1 Energy consumptions for different electrolytic magnesium producers [5].

Producer	Cell Type	Voltage, V	Energy Consumption, kWh·kg^{-1}
Norsk Hydro	Monopolar	5.3	13.0
Alcan Int.	Multipolar	NA	10.5
MagCorp	Monopolar	5.0	12.6
AVISMA	Monopolar	4.7	13.5
UKTMP	Monopolar	4.8	13.2
Theoretical	Monopolar	2.7	6.0

Magnesium and chlorine are the electrolysis products and reacts with each other when they come into contact during the electrolysis. This reaction is called "back reaction" and it is the main reason for the low current efficiencies in electrolytic magnesium production. The separation of chlorine and magnesium increased by increasing the inter-electrode distance and employing a diaphragm in early cell designs. Recent cell designs make use of electrolyte circulation and lifting action of chlorine gas to separate the magnesium and chlorine in shortest time possible by means of the chlorine gas evolution at a smaller inter-electrode distance. However the drastic decrease in energy consumption that has to be achieved to have a considerable decrease in production costs has not been experienced with newer cell designs yet.

The present study was devoted to the effective separation of chlorine gas from the electrolysis environment by a new cell design and thus reducing the extent of back reaction. Effective separation of the electrolysis products in the new cell design was achieved by the graphite anode geometry that was machined to ease the chlorine gas removal from the anode surface. The design of the anode requires a high dimensional stability of the anode that is achievable by the dehydrated cell feed when using conventional graphite anodes. The utilization of the proposed non-consumable anodes would further help to implement the special anodes that are machined to help chlorine removal.

New cell design was tested under the conditions involving the variations of the following seven parameters; current density, temperature, NaF concentration, NaCl/KCl ratio, $CaCl_2$ concentration, cathode surface and anode to cathode distance. Anode geometry was kept as fixed during this study. Cell performance was attempted to be optimized by selecting the best combinations of those parameters. So that it would lead to a decrease in the energy consumption without compromising from capacity and the purity.

3

CHAPTER 2

THEORETICAL BACKGROUND

2.1. World Magnesium Production and Markets

Primary magnesium production increases with time as it can be seen in Table 2. Alloying with aluminum, using as a structural material, iron and steel processing are the main magnesium markets.

Aluminum alloying is one of the largest single applications for magnesium. Relatively small additions of magnesium to aluminum will improve its strength and corrosion resistance. Many aluminum alloys contain some magnesium.

Magnesium alloys are also used in a wide variety of structural applications. Generally, the alloys of lower aluminum content are used for the production of wrought products while those of higher aluminum content are used mainly for castings. One of the largest structural markets for magnesium is die castings, particularly since the introduction of the corrosion resistant high purity alloys in the early 1980's. Special alloys containing Zn, Zr, Ag, Y and rare earth's are used for components operating at temperatures up to 300°C for extended periods of time.

Magnesium reduces the sulfur content dramatically when injected into molten iron or steel. Mg is also an important element in nodular cast iron production. Graphite forms spherical particles instead of flakes inside the iron in the presence of magnesium. This imparts higher strength and much greater ductility to the casting.

Table 2 World primary magnesium production [6].

Country	1994	1995	1996	1997	1998	1999	2000	2001	2002	2003	2004
United States*	128	142	133	125	106	45	45	45	45	45	45
Brazil	10	10	9	9	9	9	9	6	6	6	6
Canada	29	48	54	58	77	71	80	83	80	60	54
China	11	40	50	92	67	83	140	200	230	340	426
France	9	12	14	12	14	14	14	4	-	-	-
Israel	-	-	-	8	15	25	34	32	34	34	28
Kazakhstan	15	-	-	9	9	10	10	16	18	14	18
Norway	28	35	30	28	28	28	35	36	10	-	-
Russia	25	38	35	40	42	35	45	48	50	52	50
Serbia and Montenegro	2	2	3	3	1	1	1	1	1	2	2
Ukraine	7	13	13	10	1	1	-	-	-	-	
Total	267	340	341	394	369	322	413	471	474	553	629

* Production in USA is not given by USGS after 1999 to avoid disclosing proprietary data of the only magnesium producer in USA. The production capacity of the Magcorp is used instead to complete the table.

- Data in thousand metric tons.

Mg is also used in the metallothermic production of beryllium, titanium, zirconium, hafnium and uranium. Organic chemistry applications of Mg include important industrial syntheses such as the Grignard reaction.

Mg anodes are used to prevent galvanic corrosion of other metals. The use of sacrificial Mg anodes suppresses corrosion and thus decrease leaks in pipelines and vessels.

2.2. Electrolytic production

2.2.1. Theoretical Background

Decomposition voltage of water is lower than that of the $MgCl_2$. Therefore, magnesium metal can not be produced in aqueous solutions despite the high over voltages associated with the hydrogen and oxygen evolution. Reactivity of magnesium in water is another factor that precludes the utilization of aqueous electrolytes. Instead, molten salt solutions are used to produce magnesium metal. The following is a brief information about the molten salts related with the electro-winning of the magnesium.

2.2.1.1. Structure of Molten Salts

Molten salts are called ionic liquids or molten electrolytes and its structure is intermediate between the gaseous and solid states. They have neither the structural regularity of solid crystals nor the typical disorder of gases.

Molten salts consist of ions, and the coulombic interactions are the principal forces inside the electrolyte. High melting and boiling points, surface tensions and electrical conductivities observed in molten salts when compared to other liquids are due to the existence of those coulombic interactions. Much of their other properties are of the same order of magnitude as for non-polar liquids.

An ordering at short distance is observed after melting. Inter-ionic distances decreases between the oppositely charged ions (nearest neighbors) and increases for ions of the same charge (next nearest neighbors). The number of nearest neighbors (coordination number) becomes lower around a central ion. Molten salt volume increases 10–25% at melting and this increase is not associated with the corresponding increase of the distance between the nearest neighboring atoms.

Molten salts consist of partially maintained elements of crystalline lattice and holes produced between these elements. The holes explain the volume increase by melting and also the short range ordering. The holes in molten salt have no definite shape and size and they can expand or shrink spontaneously.

Interaction forces are very strong in molten salts [7], therefore, there is no random distribution and that the nearest neighbors of the cations are anions and the nearest neighbors of the anions are always cations. As a result two sublattices formed; one for cations and one for anions. Temkin's model proposes an ideal mixture of molten salts which assumes the existence of two interlocking sublattices of cations and anions. An ideal mixture of molten salts has no heat of mixing and change of volume due to mixing. Deviations from the ideal behavior are mainly due to the formation of ion associations and complex ions as a result of the reactions of type (2) and (3) below.

$$MX = M^+ + X^- \qquad\qquad\qquad (1)$$
$$2MX = M_2X^+ + X^- \qquad\qquad\qquad (2)$$
$$3MX = M_2X^+ + MX_2^- \qquad\qquad\qquad (3)$$

$MgCl_2$ does not exist as simple Mg^{2+} cations and Cl^- anions when dissolved in alkali chloride melts. Reactions (2) and (3) are energetically favored and there is a tendency to form some ion associations by the dissociation of a simple molten salt. Raman spectroscopy results showed that $MgCl_4^{-2}$ is the predominant specie [8,9] and small amounts of other species like $MgCl_3^-$ are also present in $MgCl_2$ rich

melts [10]. The cryoscopy data show that for low contents of $MgCl_2$, all $MgCl_2$ present in the melt is completely complexes [11,12] according to the reaction below.

$$2M^+ + 2Cl^- + MgCl_2 = 2M^+ + MgCl_4^{-2} \tag{4}$$
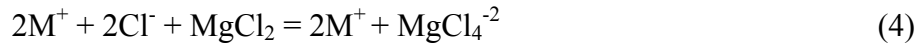
where M^+ is an alkali ion.

The low equilibrium constant for the dissociation reaction

$$MgCl_4^{-2} = Mg^{+2} + 4Cl^- \tag{5}$$

that was calculated as 1.8×10^{-3} [13] indicates the stability of the $MgCl_4^{-2}$ ion.

Complex ion formation affects electrical conductivity, viscosity, molecular refraction, diffusion and thermodynamic properties like molar volume, compressibility, heat of mixing, thermodynamic activity, surface tension.

2.2.1.2. Electrolysis of $MgCl_2$

The overall magnesium chloride decomposition reaction can be written as,

$$MgCl_2 \text{ (l)} = Mg \text{ (l)} + Cl_2 \text{ (g)} \tag{6}$$

The standard Gibbs energy change of the decomposition reaction is [14]

$$\Delta G^\circ = 607469.6 - 124.4T(K) \qquad \text{Joule·mol}^{-1} \tag{7}$$

and the standard reversible decomposition potential, E°, is

$$E^\circ(V) = 3.148 - 6.448 \times 10^{-4}T(K) \tag{8}$$

8

Standard reversible decomposition potential, $E°$, is calculated as 2.51 V from Equation (8) at 700ºC. Experimentally determined $MgCl_2$ formation voltages are 2.80 and 2.73 V at 10 and 20 % $MgCl_2$ respectively in $MgCl_2$-KCl-NaCl melts at 700ºC [15].

The half reaction at the cathode,

$$MgCl_4^{-2} + 2e^- = Mg + 4Cl^- \tag{9}$$

takes place in three steps. Firstly, the tetrahedral complex formed at high alkali chloride concentrations dissociates according to equation below

$$MgCl_4^{-2} = Mg^{+2} + 4Cl^- \tag{10}$$

Reduction of the Mg^{2+} ion to metallic Mg at a liquid magnesium electrode in pure molten $MgCl_2$ has two charge transfer steps [16].

$$Mg^{+2} + e^- = Mg^+(ads) \tag{11}$$
$$Mg^+(ads) + e^- = Mg \tag{12}$$
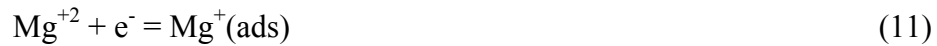
The first charge transfer step is the rate determining step and has an exchange current density of greater than 2 A·cm^{-2}. The second charge transfer step has an exchange current density about 20 A·cm^{-2} at 725° C. Deposition is diffusion controlled in dilute solutions of Mg^{2+} solutions. There is also an under potential deposition of a magnesium monolayer at potentials 100mV positive to the Mg deposition potential [17]. This is due to alloy formation observed at cathode surface [17]. The half reaction at the anode can be defined as follows,

$$2Cl^- = Cl_2 (g) + 2e^- \tag{13}$$

Possible reasons for the current efficiency losses are given below [3]:

1. Reaction between the dissolved magnesium and chlorine inside the melt.

2. Direct reaction of the chlorine gas with magnesium metal.

3. Co-deposition of other ions present inside the electrolyte.

4. Redox reactions of some multivalent ions.

5. Sinking of the magnesium droplets and forming sludge at the bottom of the cell.

6. Oxidation of magnesium metal

Most important reason for the current losses is the reaction between the electrode products that is called as recombination or back reaction:

$$Mg + Cl_2 = MgCl_2 \qquad\qquad (14)$$

Dissolution of magnesium or chlorine inside the melt is the rate determining step [18,19]. Solubility of magnesium in electrolyte increases with temperature. Magnesium dissolution is considered as associated with the formation of monomer or dimer monovalent magnesium ions as given by the reactions below [20].

$$Mg + Mg^{+2} = Mg_2^{+2} \qquad\qquad (15)$$
$$Mg + Mg^{+2} = 2Mg^{+} \qquad\qquad (16)$$
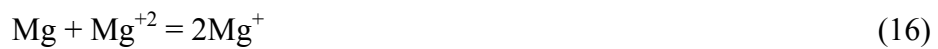
2.2.1.3. Physicochemical Properties of the Electrolyte

It is possible to electrolyze pure $MgCl_2$ but its physicochemical properties are not suitable for the industrial operation. Melting temperature of the $MgCl_2$ is high and electrical conductivity is low. Introducing other chlorides lower melting point, improve chemical stability and conductivity and modify the electrolyte density.

The salts that have higher decomposition potentials than the $MgCl_2$ can be used for modifying the physicochemical properties of the electrolyte. Relative stabilities of the various chlorides with the temperature are given in Figure 1 and standard decomposition potentials of the electrolyte components are also given in Table 3.
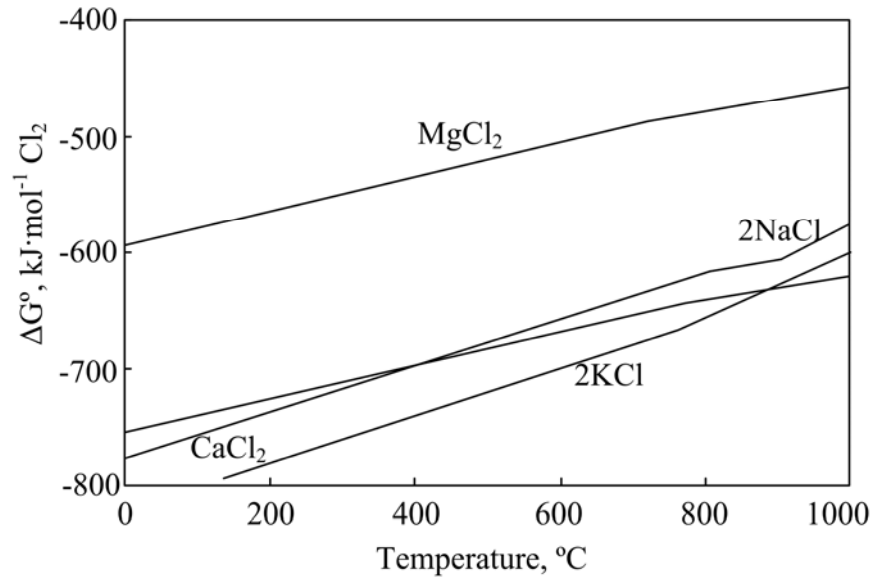
Figure 1 ΔG° of formation vs. temperature for typical electrolyte components [21].

Table 3 Standard decomposition potentials of typical electrolyte components at 700˚C [22].

MgCl$_2$	NaCl	KCl	CaCl$_2$
2.531 V	3.332 V	3.549 V	3.392 V

Reduction obtained in melting point of magnesium chloride by addition of NaCl, KCl and CaCl$_2$ is shown in Figure 2 and Figure 3. The melting temperature of the electrolyte should be lower than that of magnesium to eliminate the problems with solid magnesium deposition. Lower operating temperatures helps to minimize the metal losses associated with evaporation, oxidation and dissolution in the melt as well as the lower heating energy required. However electrolytes that have a very low melting point penetrate and attack the refractory cell liner. Therefore, electrolyte should be chosen with a liquidus temperature close to melting point of magnesium.

11
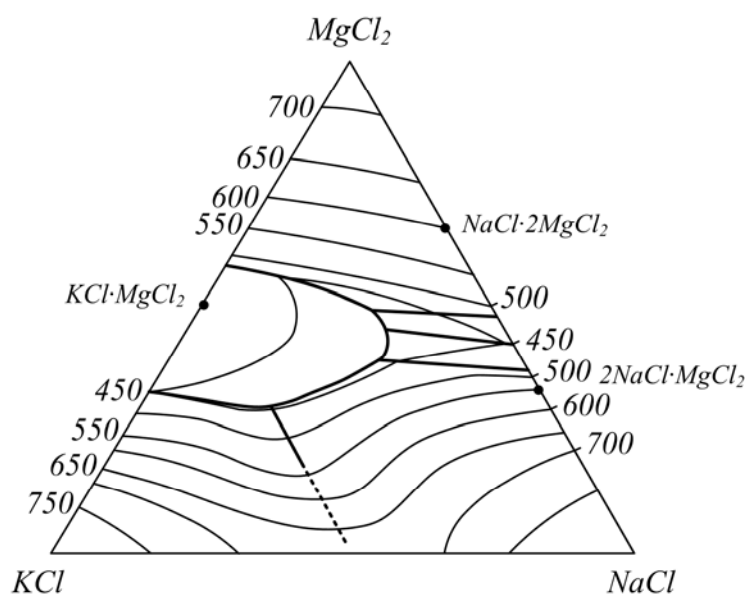
Figure 2 Liquidus surface of the system $MgCl_2$-KCl-$NaCl$ [23].
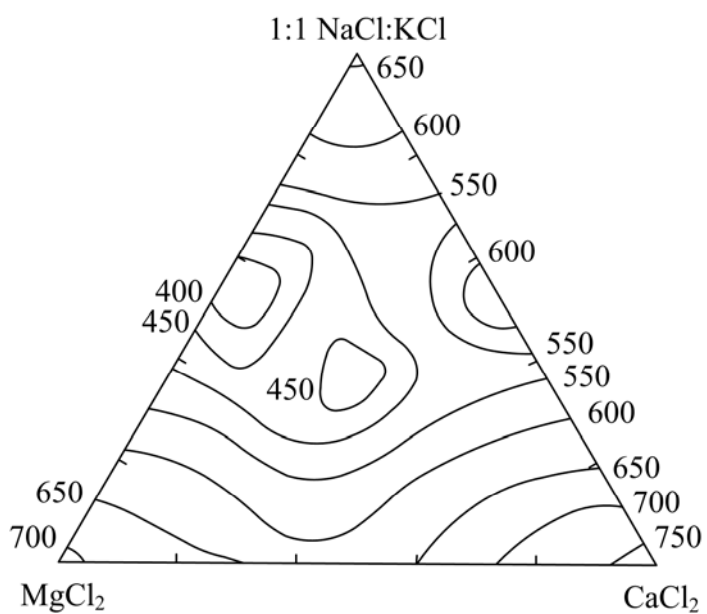
Figure 3 Liquidus surface of the system $MgCl_2$-$CaCl_2$ -1:1 (KCl:$NaCl$) showing some of the isotherms [24].

Conductivity of the $MgCl_2$ is lower than the other electrolyte constituents as it can be seen in Figure 4. Addition of the other salts increases the electrolyte conductivity and lower energy consumption. Conductivity of the 10% $MgCl_2$-NaCl-KCl-$CaCl_2$ electrolyte at 700ºC is given in Figure 5.
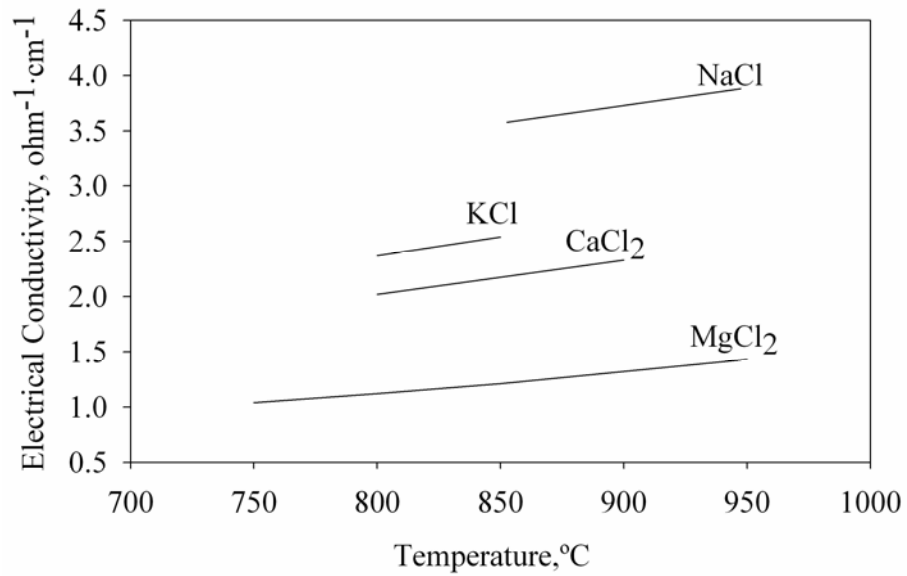
Figure 4 Electrical conductivities of typical electrolyte components [25].
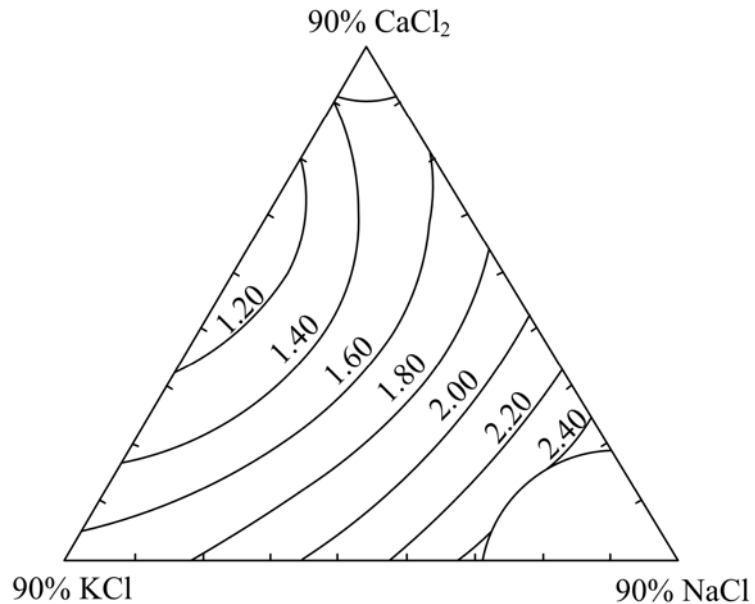
Figure 5 Equal conductivity, $ohm^{-1} \cdot cm^{-1}$, lines at 10% $MgCl_2$ and 700˚C [2].

Density of the electrolyte is one of the most important factors in cell operation. The electrolysis produces liquid metallic magnesium. It is possible to force the magnesium metal to collect at the bottom of the cell by employing LiCl containing lighter electrolytes. However their commercial application seems not possible due to the cost of dehydrated LiCl. Moreover the sludge that also sinks to the bottom of the cell also introduces problems in collecting the magnesium [26]. The density of the electrolyte and hence the separation of the magnesium from the cathode can be adjusted by the amount of $MgCl_2$ and $CaCl_2$ inside the electrolyte as it can be seen form Figure 6 and Figure 7. $BaCl_2$ can also be used for adjusting the density of the electrolyte.
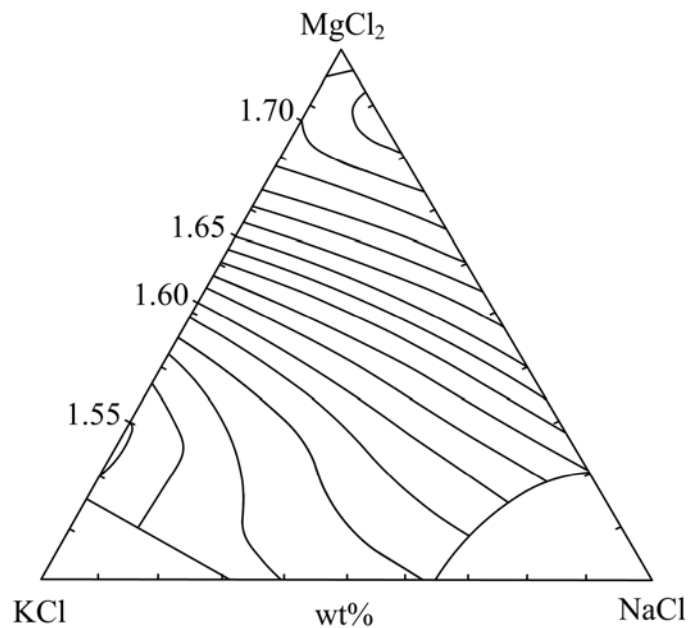
Figure 6 Densities, $g \cdot cm^{-3}$, for $MgCl_2$-KCl-NaCl system at 700˚C [27].
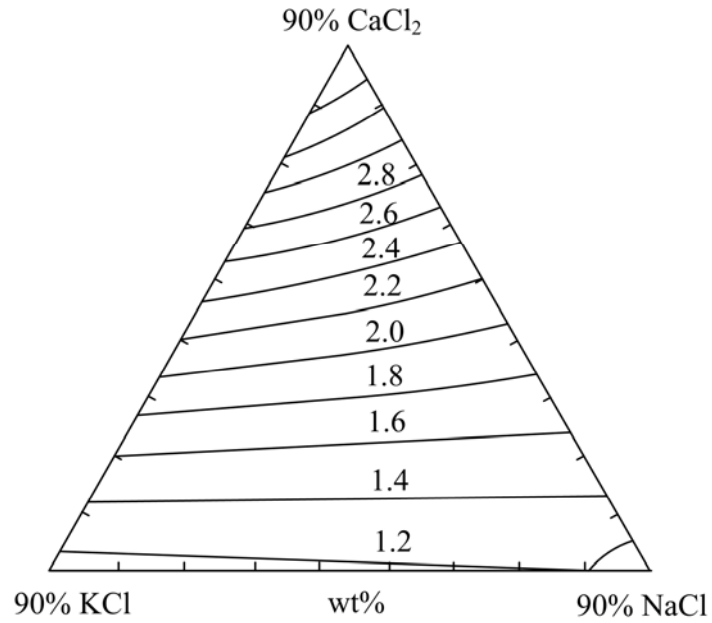
Figure 7 Densities, g·cm^{-3}, for 10%MgCl$_2$-KCl-NaCl-CaCl$_2$ system at 750˚C [28].

As it can be seen in Figure 8, the surface tensions of the other pure electrolyte components are higher than that of pure MgCl$_2$. The magnesium wetting over the cathode surface increases when other electrolyte components are added due to higher surface tensions as it can be seen from Figure 9 and Figure 10.
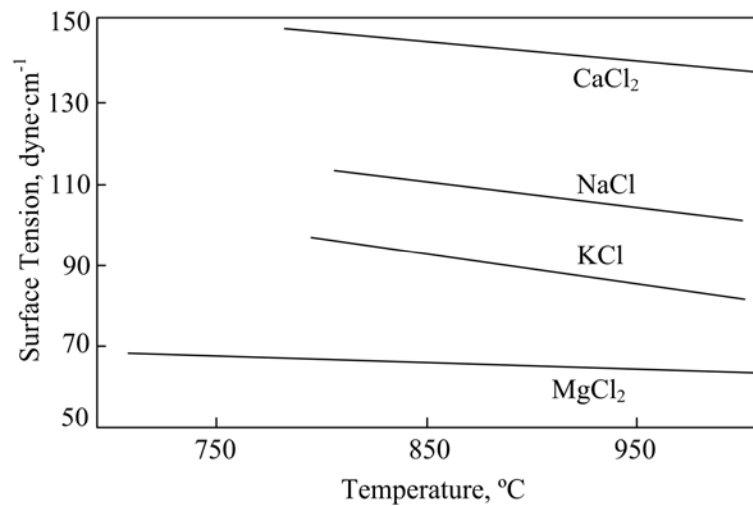
Figure 8 Surface tension of pure electrolyte components [2].
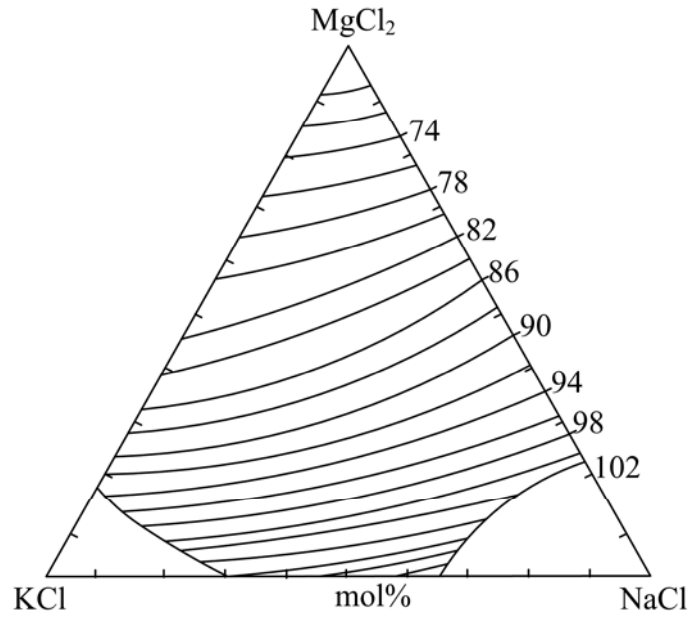
Figure 9 Surface tensions, dyne·cm^{-1}, of MgCl$_2$-NaCl-KCl system at 800°C and gas interface [2].
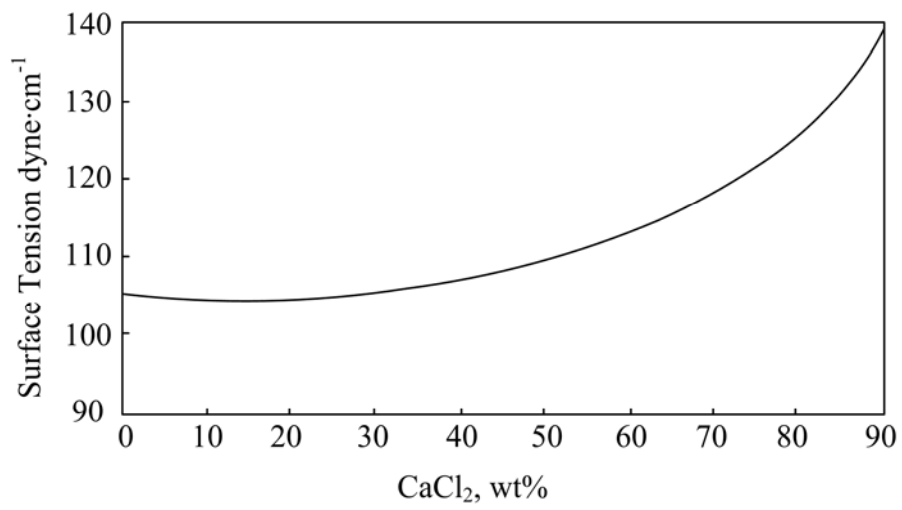
Figure 10 Surface tensions of the electrolytes at different CaCl$_2$ concentrations at 10% MgCl$_2$-NaCl:KCl=1 and 750°C [28].

16

2.2.1.4. Production of Anhydrous MgCl₂

All electrolytic magnesium production plants operate on anhydrous $MgCl_2$ today. Electrolytic magnesium production depends on the quality of the feed $MgCl_2$. $MgCl_2$ is very hygroscopic and a series of magnesium chloride hydrates can be found ($MgCl_2 \cdot nH_2O$, n=1,2,4,6,8,12). The schematic phase diagram of the hydrated magnesium chloride is given in Figure 11. Schematic drawing of stability regions of hydrated magnesium chloride compounds in moist atmosphere when HCl pressure is 0.001 atm. is given in Figure 12. At room temperature magnesium chloride hexahydrate is stable. Hydrated magnesium chloride dehydration is a stepwise process. Dehydration is straightforward until dihydrate and proceeds as follows:

$$MgCl_2 \cdot 6H_2O_{(s)} \rightarrow MgCl_2 \cdot 4H_2O_{(s)} + 2H_2O_{(v)} \qquad (17)$$

$$MgCl_2 \cdot 4H_2O_{(s)} \rightarrow MgCl_2 \cdot 2H_2O_{(s)} + 2H_2O_{(v)} \qquad (18)$$
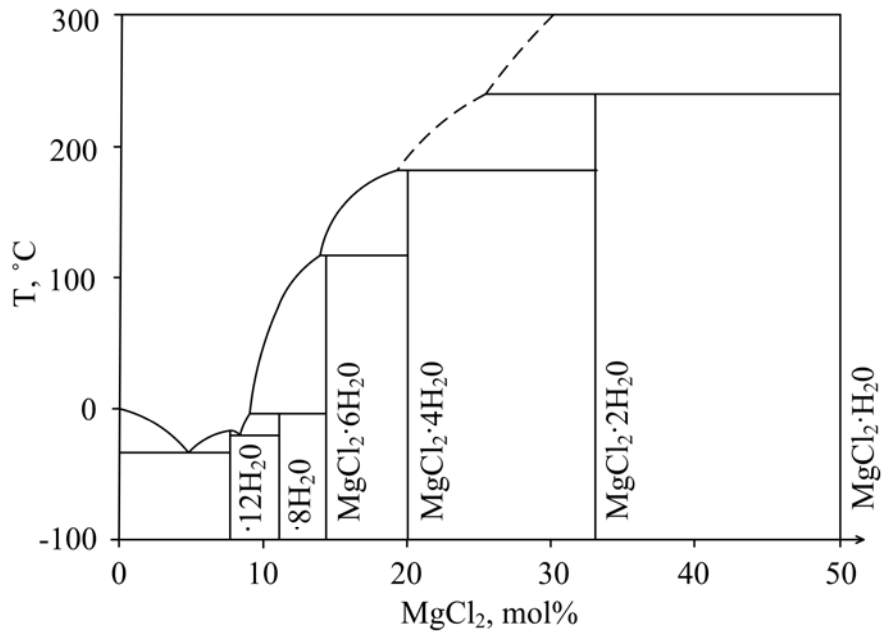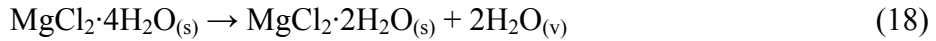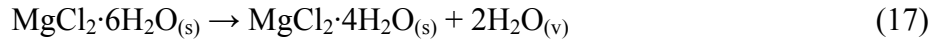
Figure 11 Schematic Phase Diagram of $MgCl_2$-H_2O [3].

17
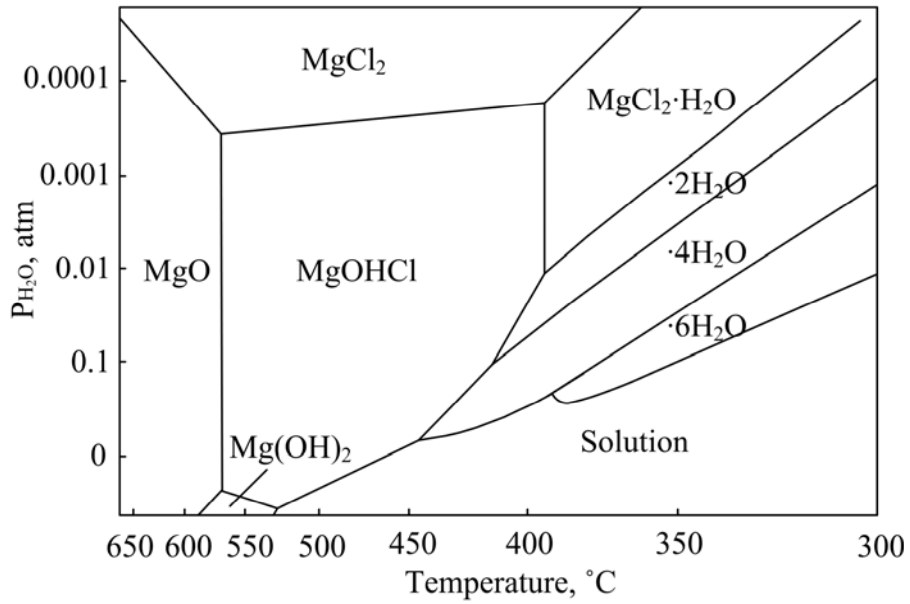
Figure 12 Stability regions of magnesium chloride hydrates under H_2O pressure, $P_{HCl} = 0.001$ atm [29].

Dehydration continues after dihydrate as follows:

$$MgCl_2 \cdot 2H_2O_{(s)} \rightarrow MgCl_2 \cdot H_2O_{(s)} + H_2O_{(v)} \qquad (19)$$

$$MgCl_2 \cdot H_2O_{(s)} \rightarrow MgCl_{2(s)} + H_2O_{(v)} \qquad (20)$$
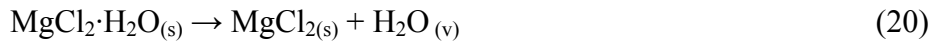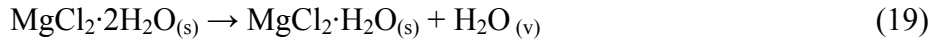
However hydrolysis and HCl formation also take place upon further dehydration after dihydrate [30,3].

$$MgCl_2 \cdot 2H_2O_{(s)} \rightarrow MgOHCl_{(s)} + H_2O_{(v)} + HCl_{(v)} \qquad (21)$$

$$MgCl_2 \cdot H_2O_{(s)} \rightarrow MgOHCl_{(s)} + HCl_{(v)} \qquad (22)$$
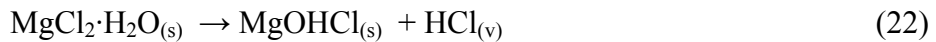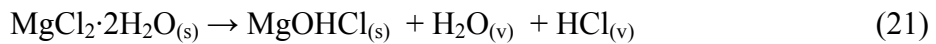
Reaction 20 is inhibited by the high water vapor pressure due to Reaction 19. However an HCl rich environment is required to suppress the formation of MgOHCl as result of Reactions 21 and 22, as it can be seen in Figure 12. The

amount of MgOHCl increases with the $MgCl_2$ content of the melt [31]. The MgOHCl decomposes directly to MgO and HCl as a result of the first order reaction with respect to amount of MgOHCl remaining as given below.

$$MgOHCl \rightarrow MgO + HCl \qquad (23)$$

Mass transfer of the HCl removal from the MgOHCl particles is the rate determining step. The time required for complete decomposition of MgOHCl is around 20 minutes for the industrial feeds [32].

Carnallite is also used as the starting material for the magnesium metal production. Dehydration of carnallite takes place according to the equations given below.

$$KCl \cdot MgCl_2 \cdot 6H_2O_{(s)} \rightarrow KCl \cdot 2MgCl_2 \cdot H_2O_{(s)} + 4H_2O_{(v)} \qquad (24)$$

$$KCl \cdot MgCl_2 \cdot 2H_2O_{(s)} \rightarrow KCl \cdot MgCl_{2(s)} + 2H_2O_{(v)} \qquad (25)$$
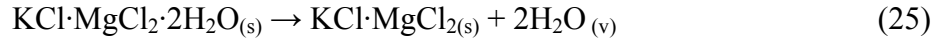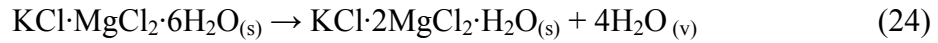
Hydroxychloride formation also takes place in carnallite feed but forms solid solutions with the dehydrated carnallite. Hydroxchloride dissociates and generates cationic impurities that interfere with the magnesium deposition according to Reaction 26. A dry HCl gas environment is required to prevent hydrolysis and the process offer no advantages over the dehydration of hydrated magnesium chloride.

$$MgOHCl \rightarrow MgOH^+ + Cl^- \qquad (26)$$

Chlorination of magnesium oxide from the calcination of magnesite or magnesium hydroxide precipitated by mixing seawater with dolime is another alternative to produce anhydrous magnesium chloride. The reaction rate depends on the particle size. The reaction is controlled by the diffusion of Cl_2 in $MgCl_2$ that covers the particle surface [33].

$$MgO_{(s)} + Cl_{2(g)} \rightarrow MgCl_{2(s/l)} + 1/2O_{2(g)} \qquad (27)$$
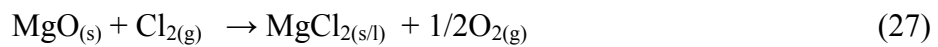
Direct chlorination of MgO requires low oxygen levels. However oxygen level must be high to achieve high production rates. For that reason carbon is used to decrease the oxygen present inside the chlorinator.

$$MgO_{(s)} + Cl_{2(g)} + C_{(s)} = MgCl_{2(l)} + CO_{(s)} \tag{28}$$

$$MgO_{(s)} + Cl_{2(g)} + 2CO_{(g)} = MgCl_{2(l)} + CO_{2(g)} \tag{29}$$
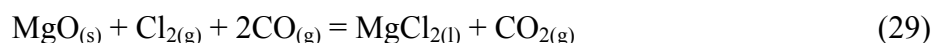
It is also possible to chlorinate magnesite ore directly in the presence of carbonmonoxide and chlorine gas as given in equations below.

$$MgCO_{3(s)} + CO_{(g)} + Cl_{2(g)} = MgCl_{2(l)} + 2CO_{2(g)} \tag{30}$$

$$CO_{2(g)} + O_{2(g)} + 3C_{(s)} = 4CO_{(g)} \tag{31}$$
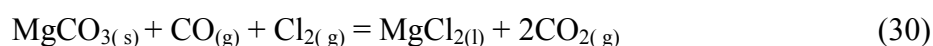
The magnesium chloride is purified as a result of the formation of volatile chloride compounds of the impurities. Magnesium chloride production by chlorination eliminates the problems related with the use of hydrated magnesium chloride. However, it possesses process dependent problems like chlorinated hydrocarbons. And for improved process efficiency process parameters must be closely controlled.

2.2.1.5 Cell Feed Impurities

One of the impurities that are present in $MgCl_2$-containing cell feed is MgO. MgO is not soluble inside the molten salt electrolyte. MgO present inside the electrolyte is chlorinated at the anode surface and $MgCl_2$ is formed. Graphite is consumed during the chlorination process. Therefore the dimensional stability of the anode is impaired and the inter-electrode distance increases.

The worst effect of MgO is observed when it is deposited at the cathode surface. MgO deposited at the cathode as a black film containing some iron [34] and

decreases the magnesium wettability. MgO prevents magnesium particle coalescence and stimulates the formation of tiny particles [2]. The cell voltage increases due to the deposition at the cathode surface. The MgO coated tiny particles sinks to the bottom of the cell and they are lost with the sludge. Therefore it is important to control the formation of MgO inside the electrolyte.

Alkali and alkaline earth fluorides, CaF_2 or NaF, are added to the electrolyte to overcome problems associated with the MgO remaining inside the melt. The fluorides enhance the surface tension of the electrolyte at the boundary between the fused magnesium and the solid cathode, thereby favoring the persistence and growth of magnesium metal drops at the cathode. Furthermore, fluxing action on the surface oxide deposited at the produced magnesium leading to increased rate of coalescence of small magnesium droplets dispersed in the melt. Moreover, fluorides decrease the Cl_2 diffusion coefficient. This retard the chlorine diffusion through the electrolyte resulting in a decrease in back reaction between magnesium and chlorine [35]. Since the solubility of CaF_2 in the electrolyte is limited NaF is preferred as the magnesium electrolyte additive [2]. On the other hand, not to cause undesirable sodium discharge at the cathode, its level should be kept low.

Most detrimental impurities can be given as Fe, Cr, Ni, Al, Si, Mn, B, sulfates, MgO and MgOHCl. Maximum permissible levels of impurities in anhydrous electrolytic cell feed are given in Table 4.

Table 4 Maximum permissible impurity levels for the cell feed [3].

B	0.001%
MgO	0.2%
SO_4^{-2}	0.05%
Fe	0.005%
C (for anhydrous feed)	0.2%

21

Sulfates are precipitated with the addition of $CaCl_2$ while using hydrated $MgCl_2$. In sea water process, sulfuric acid is used to precipitate excess calcium after dissolving $Mg(OH)_2$ in HCl. $CaCl_2$ also precipitates other solids like clays and silica. $BaCl_2$ or Barium carbonate is used for the complete removal of residual sulfates.

Oxide and sulfate impurities are removed as volatile chlorides in carbo-chlorination of MgO that consumes both the chlorine and carbon. Remaining oxides forms a slag that has to be removed from the cells [3].

$$CaO_{(s)} + C_{(s)} + Cl_{2(g)} = CaCl_{2(l)} + CO_{(g)} \tag{32}$$

$$2Fe_2O_{3(s)} + 3C_{(s)} + 6Cl_{2(g)} = 4FeCl_{3(v)} + 3CO_{2(g)} \tag{33}$$

$$SiO_{2(s)} + 2C_{(s)} + 2Cl_{2(g)} = SiCl_{4(v)} + 2CO_{(g)} \tag{34}$$

$$2Al_2O_{3(s)} + 3C_{(s)} + 6Cl_{2(g)} = 4AlCl_{3(v)} + 3CO_{2(g)} \tag{35}$$

$$MgSO_{4(s)} + C_{(s)} + Cl_{2(g)} = MgCl_{2(l)} + SO_{2(g)} + CO_{2(g)} \tag{36}$$

$$CaSO_{4(s)} + C_{(s)} + Cl_{2(g)} = CaCl_{2(l)} + SO_{2(g)} + CO_{2(g)} \tag{37}$$

$$2H_2O_{(v)} + 2Cl_{2(g)} + C_{(s)} = 4HCl_{(g)} + CO_{2(g)} \tag{38}$$

$$H_2O_{(v)} + Cl_{2(g)} + C_{(s)} = 2HCl_{(g)} + CO_{(g)} \tag{39}$$
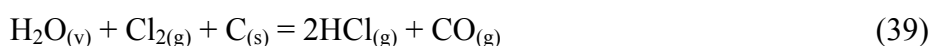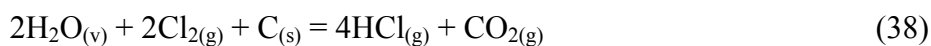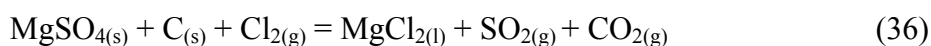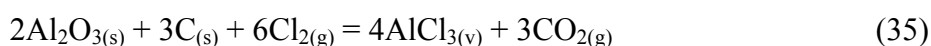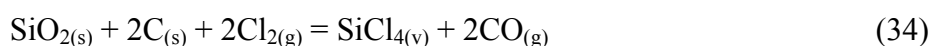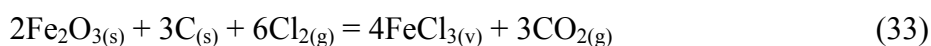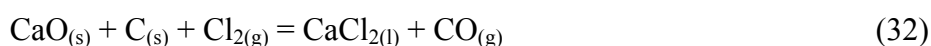
2.2.2. Industrial Applications

Various starting materials are possible for electrolytic magnesium production. The design of the cells used for the magnesium production and magnesium chloride feed preparation procedures varies for each producer.

2.2.2.1. Partially Dehydrated MgCl$_2$ Feed

Dow Chemical Company was the only manufacturer that used partially dehydrated magnesium chloride so far. Process includes the electrolysis of $MgCl_2$ feed dried to approximately dihydrate as it can be seen from the process diagram of the Dow

process given in Figure 13. Magnesium present in seawater is precipitated as magnesium hydroxide using either caustic soda or the calcined dolomite, dolime $MgO \cdot CaO$. Settled magnesium hydroxide is dewatered, washed and mixed with water. This slurry reacts with HCl to form $MgCl_2$ liquor in neutralizers. Excess calcium is removed by precipitation with sulfuric acid. Calcium sulfate is filtered along with other solids such as clays and silica. This brine is purified to remove sulfate and boron. The purified brine is dried in a fluid-bed dryer to produce granules of approximately 70% $MgCl_2$.

The Dow cells are fed semi continuously and constructed with steel as it can be seen in Figure 14. Graphite anodes can be lowered into the cell to compensate for graphite loss. Independently suspended cylindrical anodes pass through the refractory cover. Because the feed is aqueous, the graphite consumption is high and frequent adjustments of the anodes must be made while maintaining a tight seal on the cell system. The bottom of the cell pot is surrounded by a gas-fired refractory chamber.

Using partially dehydrated cell feed promotes magnesium detachment from the cathode. Therefore it is possible to work at relatively smaller inter-electrode distances. However, the energy consumption remained high as compared to its competitors and the only plant that operates with the partially dehydrated magnesium chloride was closed by the Dow Chemical Inc. in 1998.
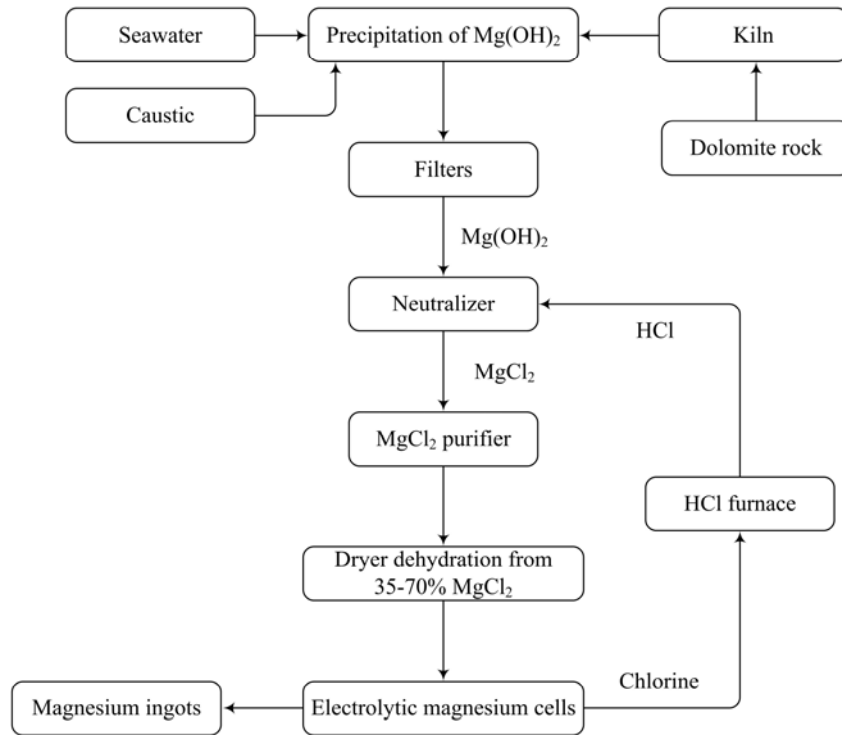
Figure 13 Dow process diagram [1].
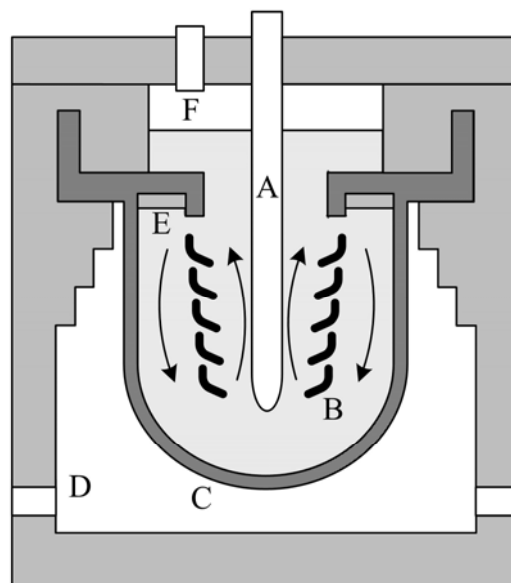
Figure 14 Schematic drawing of the Dow cell.

A. Graphite anode, B. Cathode, C. Cast iron pot, D. Gas burner openings, E. Collected magnesium, F. Chlorine gas outlet.

2.2.2.2. Anhydrous MgCl$_2$ Feed

The I.G. Farben process, Figure 15, is the basic flow sheet of numerous cell designs that operates on the dehydrated MgCl$_2$ feed. Mg(OH)$_2$ obtained from the seawater and dolomite mixed with carbon and aqueous MgCl$_2$ is pelletized. Pellets containing approximately 50% MgO, 15–20% MgCl$_2$, 15–20% H$_2$O, 10% C, and other alkali metal chlorides are conveyed to the chlorinators after drying. Chlorine from electrolyzers is used to obtain MgCl$_2$. The anhydrous magnesium chloride produced contains less than 0.1% MgO, 0.1% SiO$_2$, and 20 ppm boron.

Molten magnesium chloride is collected at the bottom of the furnace. The molten material is transported to the electrolytic cells in closed containers and fed into cells to replenish MgCl$_2$.

A schematic drawing of I.G. Farben cell is given in Figure 16. The I.G. Farben Cell employs a semi wall that surrounds the graphite anode and forms a chlorine collection compartment. The partitioning wall is also called as diaphragm. Anode compartment is surrounded by two cast steel cathodes. The rising chlorine bubbles cause an electrolyte motion during the electrolysis. The moving electrolyte carries the magnesium droplets to the cathode compartment and brings fresh electrolyte containing magnesium chloride to the inter-electrode space. Operating temperature is about 750° C, and the cell life is about one year. The current efficiency is around 90%.

The inter-electrode distance must be high since the magnesium removal from the cathode is poor when using completely dehydrated feed. Physical barriers were used at these cells to ensure good separation and reduce the back reaction. However the use of a diaphragm increases the inter-electrode distance and cell resistance.
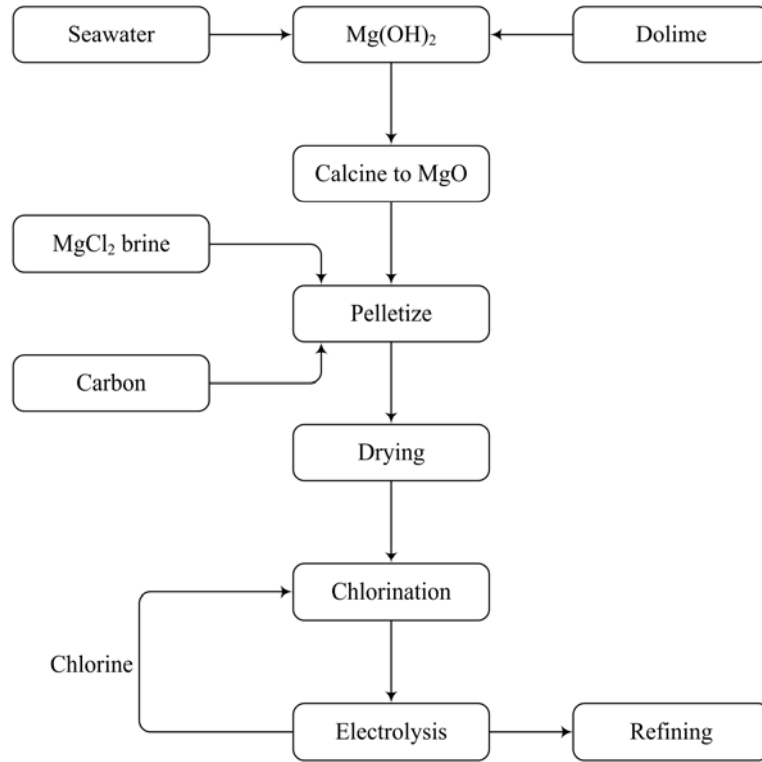
Figure 15 I.G. Farben process diagram [1].
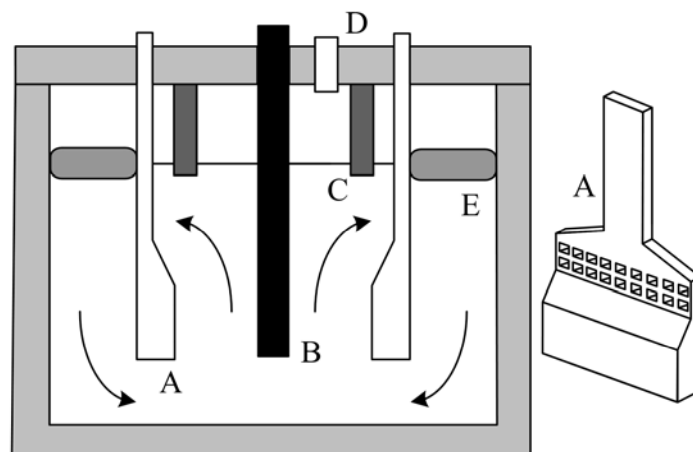
Figure 16 Schematic drawing of the I.G. Farben cell.

A. Cathode, B. Anode, C. Refractory partition wall, D. Chlorine gas outlet and
E. Collected magnesium metal.

Norsk Hydro started to operate with I.G. Farben electrolytic cells with current loads of 32–62 kA at Porsgrunn, Norway in 1951 [1]. Then they established a second plant at Becancour, Canada. Norsk Hydro has been using its own process, for the preparation of $MgCl_2$ cell feed [36] and electrolysis [37] since 1978. The diaphragms are not used in the new cell design. Separation is controlled by the electrolyte circulation in current cell design that necessitates working with a completely dehydrated electrolyte to ensure dimensional stability.

The process in Norway is based on raw material from the potash industry and the brine in Canada is obtained by dissolving magnesite in hydrochloric acid. Purified brine concentrated to 45–50% $MgCl_2$ in steam heated evaporators before prilling, Figure 17. In the first stage of dehydration, the prills are dried to $MgCl_2\cdot2H_2O$ with hot air. Dihydrate prills are contacted with a hot, anhydrous HCl gas stream and anhydrous $MgCl_2$ is formed at the second stage. $MgCl_2$ prills are transported pneumatically to the electrolytic cells [1].
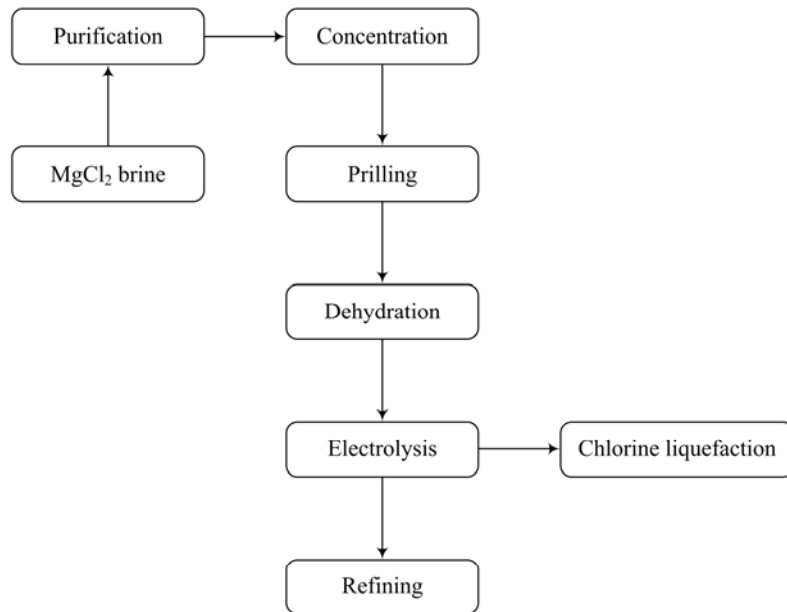
Figure 17 Norsk Hydro process diagram [1].

Norsk Hydro electrolytic cell includes one chamber for electrolysis and one for metal collection. The cell is a sealed brick-lined unit. Graphite anode plates enter through the top and they are cooled since they are densely packed. Cathode plates enter through the wall of the cell since they are cooled and double sides of the hollow cathode is used during electrolysis.

The hollow cathodes and the metal collecting chamber can be seen in Figure 18. Chlorine is collected from one central pipe in the anode compartment. Metal passes to the collection chamber by the circulation of the electrolyte. Molten magnesium extracted by vacuum from the collection chamber. The cell is operated at 700–720°C and the energy consumption is of the order of 12–13 kWh·kg^{-1} Mg.
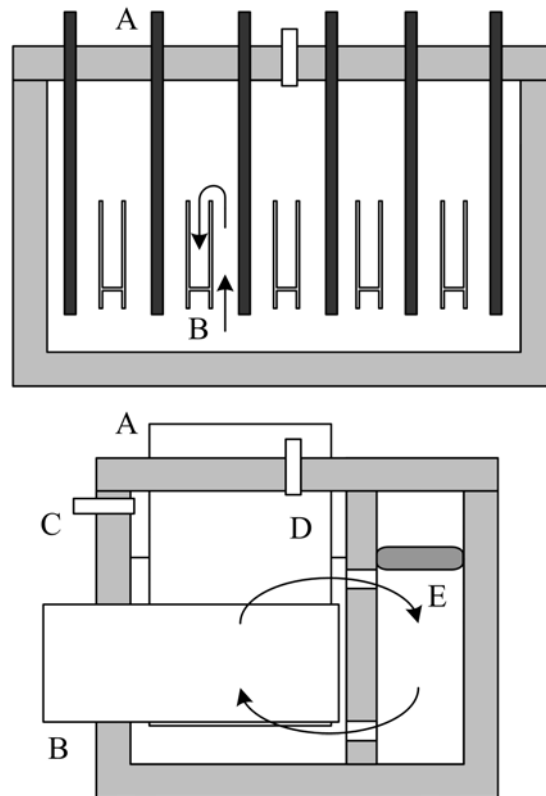
Figure 18 Schematic drawing of the Norsk Hydro cell.
A. Graphite anode, B. Hollow steel cathode, C. Chlorine gas outlet, D. Feeding port and E. Collected magnesium [37].

The cells of the Magcorp magnesium facility in Rowley, Utah, are also essentially a modification of the I.G. Farben cell. Brine from the Great Salt Lake solar evaporation ponds is further concentrated and treated with $CaCl_2$ to remove sulfate. Brine is dried into powder by spray dryers. Dried $MgCl_2$ powder is melted and further purified with chlorine and other reactants, Figure 19. The molten $MgCl_2$ is then fed to the electrolytic cells. Excess chlorine is sold as a by-product. Liquid magnesium is removed from the electrolytic cells under vacuum and transferred to the cast house.
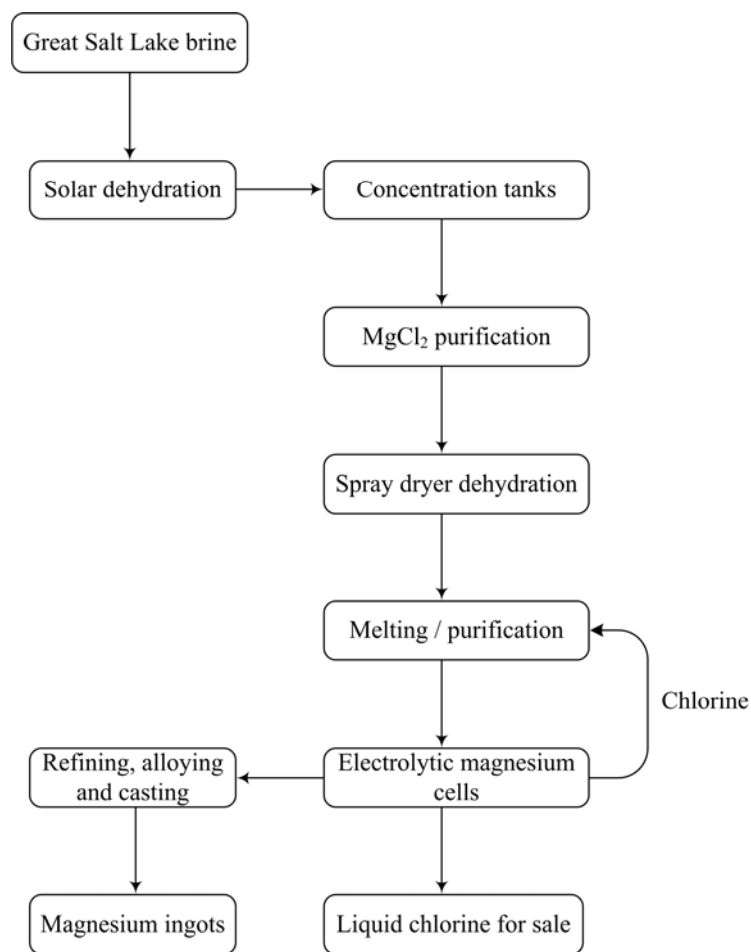
Figure 19 Magcorp process diagram [1].

2.2.2.3. Dehydrated Carnallite Feed

Magnesium production in the former Soviet Union is done by the electrolysis of carnallite, $MgCl_2 \cdot KCl \cdot 6H_2O$ that is obtained either from natural deposits or as a by-product of processing natural salt deposits. Drying is done in fluid-bed/moving-bed furnace with temperature increasing from 130 to 200°C in three distinct zones. Partially dried carnallite that contains 1–2% MgO and 3–6% H_2O is chlorinated at 700–750°C. The molten $MgCl_2/KCl$ is either fed to the cells while still molten or after solidification [1].

The cells used in Russia were basically I.G. Farben diaphragm cells until the late 1960s. Diaphragmless cells [38] have been used since 1970s operated in the temperature range of 680–720°C and at currents of 150–200 kA. Current efficiencies are somewhat lower in carnallite fed cells [1].

The Dead Sea Works magnesium plant at Beer-Sheva is based on Russian carnallite technology and designed to use an existing potash plant for the source of carnallite. The chlorine is the by-product waste streams from the process and spent electrolyte can be returned to the potash plant.

2.2.2.4. Pure MgCl$_2$ Feed from Kroll Process

Pure anhydrous magnesium chloride is produced in industrial titanium production as a byproduct. Alcan has developed cells for the production of magnesium from anhydrous magnesium chloride obtained as by product from the Kroll process, Figure 20.
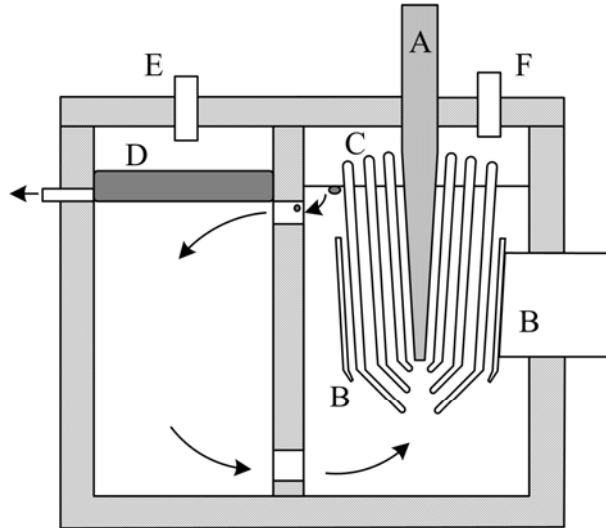
Figure 20 Schematic drawing of the Alcan multi-polar cell.

A. Graphite Anode, B. Cathode, C. Bipolar Electrodes, D. Collected magnesium,
E. Feeding port and F. Chlorine outlet.

In Alcan multi-polar cell, chlorine is collected at the electrolysis compartment where the bipolar electrodes are placed while magnesium metal accumulates in a separate chamber [39]. The electrolysis temperature, 660-680°C, is just above the melting point of the metal. The energy consumption when operating on high-purity $MgCl_2$ is 9.5–10.0 kWh·kg^{-1} Mg [1]. The cell operates at 100 kA with a life of up to two years.

Multipolar cells use bipolar electrodes that are electrically conductive plates inserted between the anode and the cathode of a conventional electrolytic cell. Anode side of the bipolar electrode becomes cathodic and the cathode side becomes anodic. The metal produced is swept by the evolved chlorine. All the Alcan cells show excellent operation characteristics with $MgCl_2$ from titanium plants, but none is in use with brine or ore-based feed processes [1].

Another multipolar cell is the Ishizuka cell [40]. The cell operates at 670°C. Steel plates are attached to the cathode side of the graphite bipolar electrodes in the cell

31

developed by the Ishizuka Research Institute in Japan. The cell operates at 50 kA current. The current density is 0.56 A·cm^{-2}, and the inter-polar gap is 4 cm. The power consumption is 11 kWh·kg^{-1} Mg when operated on molten magnesium chloride from titanium production by the Kroll process at a current efficiency of 76%. The cell life is about three years.

Oremet Titanium (Albany, Oregon) and Timet (Henderson, Nevada) are the other plants that use monopolar Alcan cells. Osaka Titanium Co. (now Sumitomo Sitex) in Osaka, Japan also utilizes multipolar cells.

2.2.2.5. MgCO$_3$ Based Feed

The Magcan process uses anhydrous MgCl$_2$ directly produced from magnesite ore [3]. Crushed and screened magnesite ore is fed from the top of a vertical reactor. It reacts with chlorine produced during MgCl$_2$ electrolysis and CO obtained from a gas generator at 1000° C [41]. The magnesite is chlorinated by the Reactions 30 and 31.

Anhydrous molten magnesium chloride is collected at the bottom of the reactor. Iron, aluminum, and silicon-based impurities evaporate out of the reactor since they are also chlorinated and they have low boiling points. The Magcan plant (Aldersyde, Alberta, Canada) that used Russian diaphragmless cells was shut down in 1991 after an operation of one year.

2.2.2.6. MgCl$_2$ Feed from Serpentine Tailings

Magnola plant is designed to operate with serpentine (3MgO.2SiO$_2$.2H$_2$O) tailings from the asbestos mine operations [5,42]. Magnetic separation is required to remove Fe compounds that are about 5% in the serpentine tailings. Firstly the ore is made slurry to apply magnetic separation. The slurry medium is leached with HCl and hydrochloric acid vapor is recycled from the fluidized bed dryer and

chlorinator. Chlorinated solution is neutralized with MgO and the residue is filtered. In the purification step chlorine gas is injected to oxidize impurities such as Fe, Ni, Mn. Then MgO and %50 NaOH are added to precipitate the impurities and neutralize the solution, and the solution is filtered again. Filtrate is sent to ion exchange columns. Remaining detrimental ions to the electrolysis operation such as Fe, Ni, Mn and B are removed by the ion exchange. Brine is dehydrated by evaporation using fluidized bed dryer and prills are formed. Prills contained around 2 moles of water per $MgCl_2$. Prills are sent to chlorinator. Prills are added to externally heated chlorinator that holds liquid electrolyte. HCl gas is injected and prills give the water off and they are dissolved into the electrolyte. Any MgO that is formed is chlorinated and the oxide-free electrolyte is taken from the chlorinator via overflow launder.

Magnola plant utilizes the Alcan's Multi-Polar Cells to electrowin the magnesium. Electrolyte is fed from the metal collection chamber and the electrolysis takes place at another compartment. Electrolyte contains $MgCl_2$, $CaCl_2$, NaCl, KCl and NaF. Anode and bipolar electrodes are made from graphite and the cathode is steel. Magnola plant was closed down in 2003 after operating for 2 years.

2.2.3. New Approaches in electrolytic production

Anhydrous magnesium chloride production accounts for about the half of total expenses in electrolytic magnesium extraction. Therefore direct utilization of magnesium ores has a large potential to reduce the production costs. There are two different approaches that are greatly different than the conventional chloride electrolysis. The first one utilizes rare earth chloride constituents that have the capacity of dissolving more MgO than the conventional cell components. The second one is the direct electrolysis of oxide components that have promising results in many systems. It is also possible to produce magnesium alloy directly instead of pure metal.

2.2.3.1. Dissolved Magnesium Oxide Electrolyte

Magnesium oxide is practically insoluble in any melt consisting alkali and alkali-earth metal chlorides at cell operating temperatures. Rare earth chlorides are known to dissolve magnesium oxide by converting oxide in to a complex as given by the reaction below:

$$MgO(l) + NdCl_3(l) \rightarrow MgCl_2(l) + NdOCl(l) \qquad (40)$$
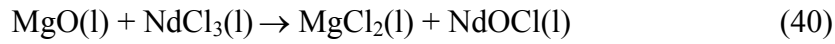
Rare earth chlorides introduced to the electrolyte are claimed to dissolve sufficient magnesium oxide to produce magnesium metal and oxygen gas[18]. Proposed process is similar to the dissolution of alumina in cryolite used in the production of aluminum in the Hall-Heroult process. Magnesium is produced by the reaction at the cathode:

$$Mg^{2+} + 2e^- \rightarrow Mg(l) \qquad (41)$$

At the graphite anode, the probable pathway is as follows:

$$NdOCl_2^- \text{ (bath)} \rightarrow NdOCl_2^- (\text{ electrode}) \qquad (42)$$

$$NdOCl_2^- + C(s) \rightarrow Nd^{3+} + 2Cl^- + CO_{ads} + 2e^- \qquad (43)$$

$$NdOCl_2^- + CO_{ads} \rightarrow Nd^{3+} + 2Cl^- + CO_2(g) + 2e^- \qquad (44)$$
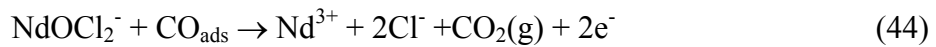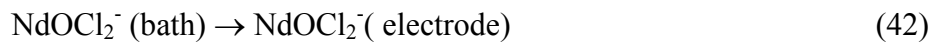
Process is expected to consume 12200 kJ/kg energy to produce magnesium. In Pechiney process 14080 kJ/kg energy required for aluminum production. That is, theoretically, the proposed process can produce magnesium at costs lower than aluminum.

2.2.3.2. Direct Oxide Electrolysis

It was reported that numerous metals can be produced by electrochemical reduction of metal oxides to metal in a molten salt as the electrolyte [43,44]. The proposed process that is based on the direct electrolysis of MgO to produce magnesium and oxygen totally eliminates the chloride metallurgy if it could be successfully commercialised.

2.2.3.3. Magnesium Alloy Production

Almost half of the magnesium produced is used for alloying with aluminum. So it may be beneficial to produce magnesium-aluminum alloys instead of pure metal. Such attempts are encountered in literature by electrolysis of magnesium oxide dissolved in fluoride salt baths [19] or magnesium-aluminum alloy production [20], by electrolyzing $MgCl_2$, resembling the study of collection of magnesium at the bottom of the cell by alloying with lead [45].

The cathode is molten aluminum at the bottom of the cell where magnesium is deposited in proposed process. This is a low cost method for the production of Al-Mg alloys [46]. Partially dehydrated $MgCl_2$ is dissolved and the electrolysis temperature is 750° C.

2.3. Post Production Processes

A refining operation is required after the production of magnesium especially by thermal process to remove nonmetallic inclusions, metallic impurities, and hydrogen. Magnesium oxide, magnesium nitride, and magnesium chloride may present and impair the appearance and corrosion resistance of magnesium alloys. Because of the higher density of the alkali metal chlorides and intermetallic compounds relative to magnesium, they sink to the bottom of melts as a slag. Fluxes added to magnesium melts to coat the surface of the melt to prevent oxidation [47].

Iron, nickel and copper form very small galvanic islands which act as cathodes and reduce the corrosion resistance of magnesium and magnesium alloys significantly. These are controlled by the choice of raw materials used for the electrolyte. Iron can be removed by addition of manganese or zirconium that forms an intermetallic complex and settles to the bottom of the cell [48]. Metallothermic reduction gives more control on their composition. Other impurities found in magnesium can be stated as aluminum, manganese, zinc, silicon and sodium. Intermetallic compounds of these impurities have also been found. Sodium, calcium, and strontium can be removed by the addition of magnesium chloride.

Hydrogen is formed as a result of the reaction between magnesium and moist air. The hydrogen content larger than 7 ppm may cause micro and macroporosity in metal castings. Hydrogen can be completely removed by blowing an inert gas into the melt.

CHAPTER 3

EXPERIMENTAL

3.1. Experimental Set-up

3.1.1. Cell Assembly

The cell assembly is shown schematically in Figure 21. An enlarged drawing of electrolysis cell is illustrated in Figure 22. A close ended 600 mm long quartz tube of 65 mm inner diameter was used to accommodate the cell assembly. The cell vessel was aligned vertically and its open end at the top was used for the entrance of the cell components. A Teflon lid was used to close the cell vessel. Connections to cell were made through the Teflon lid by employing o-rings to each hole. Hence the quartz anode protection tube, stainless steel cathode connection rod and alumina thermocouple shield were vertically movable while preventing gas leak. A 10 mm diameter central hole was used to introduce the quartz tube of the graphite anode. Other holes were located around the central hole. The 4 mm diameter holes were used to place argon inlet and gas outlet. The hole with 2.5 mm diameter was used to introduce the cathode extension rod into the cell.

Upper portion of the cell vessel remained outside the vertical tube furnace during the electrolysis. Thus the necessary electrode movements were made possible by electrode leads extended from the top of the cell vessel while the bottom of the cell was still inside the furnace. Furthermore electrical and gas connections at a temperature close to room temperature enabled an easier operation.

37

A. Quartz cell vessel
B. Alumina crucible
C. Electrolyte
D. Graphite leveller
E. Graphite anode
F. Stainless steel cathode
G. Magnesium droplets
H. Quartz tube
I. Thermocouple
J. Graphite lid
K. Cathode extension rod
L. Anode extension rod
M. Teflon lid
N. Chlorine outlet
O. Argon inlet
P. Argon outlet
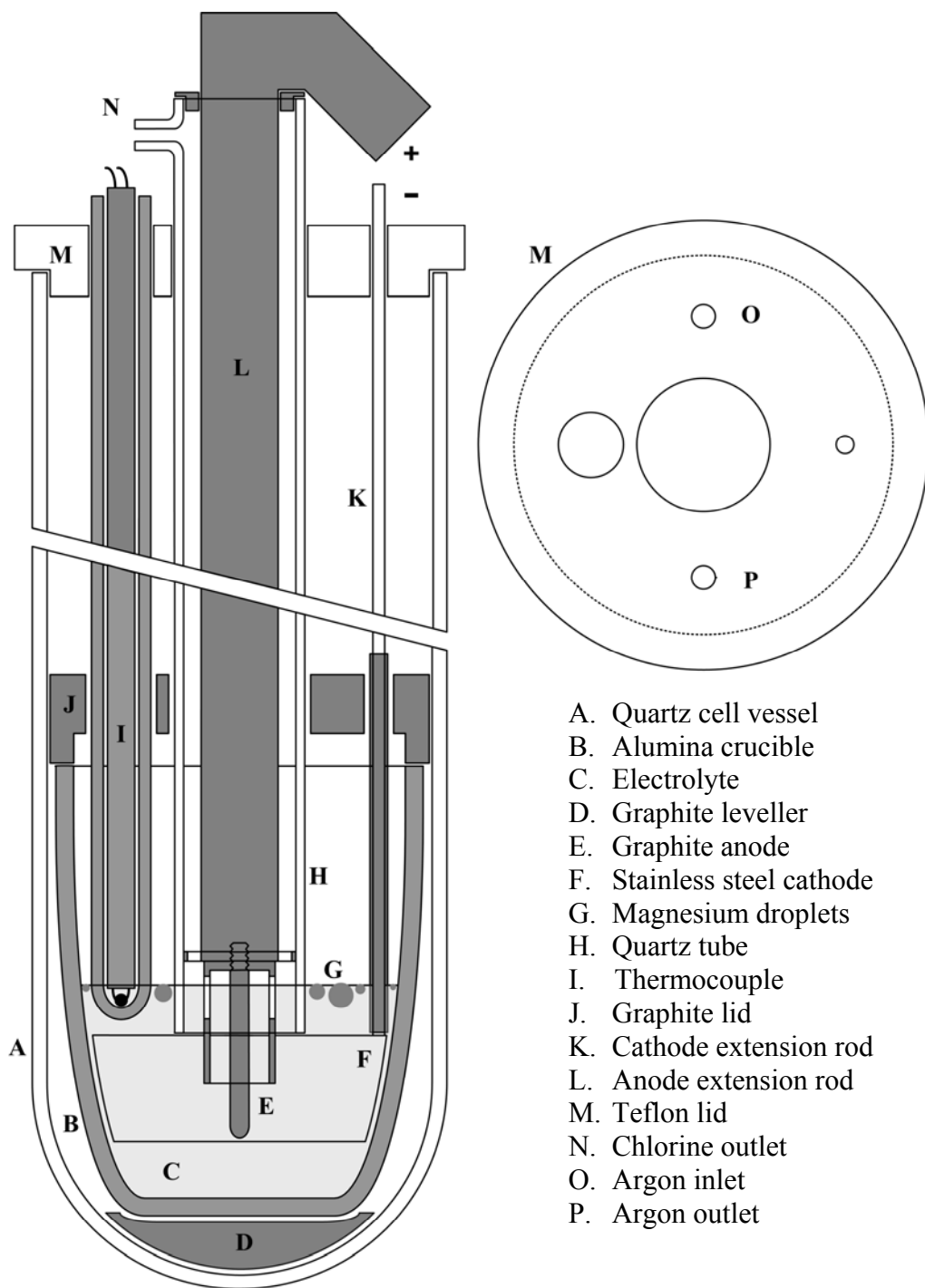
Figure 21 Schematic drawing of the cell assembly and the Teflon lid.
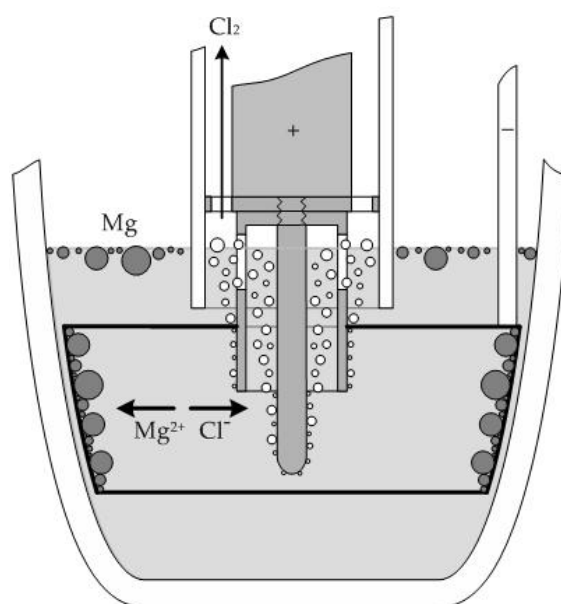
Figure 22 Schematic drawing of the electrolysis process.

Quartz was used to withstand the high operating temperatures as well as the high temperature differences along the height of the cell vessel. The temperature difference between the top and the bottom of the quartz vessel was close to 700°C during the experiments. In addition quartz was very suitable as the vessel material because of its being chemically inert.

Pictures of anode and cathode can be seen in Figure 23 and Figure 24 respectively. Anode, anode connection rods and screws used to fasten different parts of the anode assembly were all made of graphite to prevent reaction with chlorine gas. Anode was designed to minimize the resistance to gas flow. Hollow graphite cylinder with a co-axial graphite rod design was chosen to remove chlorine from inter-electrode region as fast as possible. Anode and its connection rods were placed into a quartz tube that was extending out of the cell vessel from the top.

This tube was also immersed into the melt to collect chlorine bubbles. Chlorine produced at the working surface of the anode raised between anode rod and quartz tube and it was removed directly from the cell assembly without entering into the quartz cell vessel. By this way the extent of back reaction could be reduced.

Anode connection rod was centered inside the quartz tube by employing small graphite spacers. Quartz tube was also centered inside the quartz vessel. The position of the upper portion of the quartz tube was fixed at the center of the Teflon lid. Similarly, the lower portion was fixed by a graphite ring that was placed over the crucible as a lid. So the positions of the anode and cathode were fixed and a constant inter-electrode distance was obtained. The graphite ring had also other holes to accommodate cathode extension wire and thermocouple.

To protect electrical contacts from the chlorine gas attack, the direction of anode extension was turned down 150° from vertical at the exit of the quartz tube. Good electrical connections were obtained by means of above design when connections were made below the chlorine gas exit level.

Figure 23 Graphite anode with its extension rod.

Figure 24 Stainless steel cathode without extension rod.

Height of the cathode and the height of the active anode were made equal. Cathode was designed as circular around the anode. Cathode material was 18mm wide and 0.2mm thick stainless steel ribbons. Windows were opened through the ribbons to make cathode area compatible with the capacity of the DC source to achieve desired current densities. Windows were opened by electro erosion in an acidic electrolyte. The sizes and positions of the openings were kept constant through the study. A stainless steel rod was welded to the cathode to make electrical connection outside the cell vessel. The rod was extended out of the cell and connected to the negative terminal of the DC power supply. An alumina rod was used to prevent electrolysis at the immersed portions of the steel rod.

Circular cathode made up of these ribbons would have been very large regarding the total current that can be applied. Current density values had to be constant, so increasing the cathode area increases the current that had to be applied. On the other hand, increasing the current increases the depletion rate of magnesium chloride inside the electrolyte. If it falls below %7-8, current efficiency falls due to co-deposition of sodium and potassium. Unfortunately any addition of magnesium chloride was not possible and its amount was limited by the initial addition.

An alumina sheathed alumel-chromel thermocouple was placed into the molten salt electrolyte to measure the electrolyte temperature. The crucible material to hold the cell was also alumina to minimize any chemical reaction between cell components. The maximum outer diameter of the alumina crucible (slightly conical) was 62mm and its height was 76mm.

3.1.2. Auxiliary Apparatus

Since the cell assembly had to be maintained vertically, the furnace that accommodated the vessel was also a vertical furnace, Figure 25. A Lindberg split furnace was used during the experiments. A Maximel direct current power supply that had a capacity of providing 10 A current at 30 volts maximum was used for the experiments. The current was tuned at the beginning of each experiment, according to the required current density. Experiments were carried out galvonastatically. Cell voltage readings were taken by a portable multimeter, Goldstar DM 340, continuously every one to five minutes during the experiments.

Due to the high temperature difference between upper and the lower portions of the cell vessel there was convection inside the cell assembly. A positive pressure was beneficial to prevent air from entering into the vessel. An argon gas flow of 60ml/minute was used to supply a slightly positive pressure to the cell vessel.
Argon gas was passed through a drying column before it was introduced to the cell vessel. At the exit, a gas mixture of argon and chlorine was passed through a set of bubblers. By this way, NaOH solution in each bubbler could absorb chlorine gas before the exit gas was admitted to the atmosphere. An aspiration hood was placed above the cell assembly as a precaution against incidental gas leakage from the cell.

Figure 25 Auxiliary apparatus.

A. Furnace, B. Temperature Controller, C. DC Power Supply, D. Drying Column,

E. Argon Supply and F. Aspiration Hood.

3.2. Cell Operation

$MgCl_2$ used in these experiments were obtained from Aldrich Chemical Company. It contained 98% $MgCl_2$ and 1.5% H_2O. Dehydrated 97% $CaCl_2$ was also form Aldrich Chemical Company. 99.8% NaCl and KCl and reagent grade NaF were from Merck.

At the beginning of each run cathode was placed into its proper position in the alumina crucible. Required amounts of $MgCl_2$ and $CaCl_2$ were packaged under argon atmosphere. Electrolyte components were mixed together to yield about

43

20% by weight $MgCl_2$ initially for all the experiments. This was determined to be optimum concentration in a previous study [45] that employed $MgCl_2$-NaCl-KCl electrolyte. NaCl, KCl and NaF were dried in a Pyrex crucible at 25O°C for 3 hours and required amounts of above salts were mixed together. $MgCl_2$ and $CaCl_2$ were poured into the alumina crucible that was placed at the bottom of the quartz vessel by means of a quartz tube. Then NaCl, KCl and NaF mixture was added in to the alumina crucible. The cell vessel was closed and placed into the furnace. The heating process was started after the gas connections were made.

The cell vessel was heated to 500°C within 2-4 hours under continuous flow of argon gas. The furnace was then heated rapidly to 820°C to ensure complete melting of the electrolyte considering the highest melting point salt, NaCl (T_m= 801°C). Next, the furnace was cooled down to the test temperature. Anode was lowered and immersed into the electrolyte and the electrode connections were made to the DC power supply leads and the current was switched on when the temperature was stabilized.

Any crystal water that was left in the salt mixture evaporated at the bottom of the cell could condense at the higher regions of the quartz vessel outside the furnace. To overcome the condensation of water vapor, a heating tape was wound around the cell vessel outside the furnace. By this way entrance of atmospheric contaminants such as O_2, H_2O, N_2, and CO_2 could be minimized.

The current was switched off after a typical electrolysis period of 45-90 minutes. The electrodes were then withdrawn from the crucible while the electrolyte was still molten. The furnace was turned off while the argon flow being maintained. Cell vessel was taken out of the furnace as soon as possible after the electrolysis ended. Cell vessel was opened after complete cooling to room temperature.

Metallic magnesium was collected from, electrolyte surface and other parts of the cell after each experiment. Cathode and the magnesium that fused to the cathode

surface were washed together to dissolve the adhered salts. The cathode was then dried with compressed air. The washing and drying process were completed in the shortest time possible to reduce the magnesium losses. The cathode weight was recorded and then magnesium was dissolved in 300 ml water containing 1ml HCl to increase the dissolution rate [49]. Cathode was washed with water and brushed to remove MgOH remained at the cathode surface after dissolution of magnesium. The amount of magnesium at the cathode surface was determined form the weight difference of the cathode before and after dissolving the magnesium.

Some of the magnesium particles were easily collected from electrolyte surface after it was frozen. To collect the remaining metallic magnesium frozen salt mixture was crushed and grinded in a mortar to reduce particle size. Frozen salt was further milled for 24 hours in a rotating glass jar with 3 mm diameter stainless steel rods inside. Salt powder was screened with a 50 mesh sieve and the remaining magnesium particles were collected. Smaller particles were not washed with water during the cleaning process to prevent excessive dissolution due to their high surface area.

Larger magnesium particles were put inside a glass cup which was covered with a fine synthetic fabric. Then flushing water was applied inside the glass cup through the fabric. Excess water flowed back removing dissolved salt out. As soon as washing was completed, magnesium globules dried by compressed cold air again inside the glass cup through the fabric. All the salt that was ground was subjected to dissolution process using above procedure to not to loose any metallic magnesium. Since the salt was fine due to the milling, the washing step was finished in seconds. The method of utilizing glass cup covered with fine fabric was found very satisfying for both washing and drying of the fine magnesium particles that were difficult to collect.

The amounts of magnesium collected from cathode surface, cleaned magnesium droplets and small magnesium particles that were not washed were added together to determine the current efficiency.

3.3. Calculations

Observed cell voltage largely depends on the dimensions and electrical characteristics of the connection materials. Hence, to compare the cell voltage obtained at different runs, voltage due to the electrical resistance of the connections must be eliminated. Voltage drop across the electrical connections, $E_{short\ circuit}$, was measured by short-circuiting the electrodes in a molten Pb pool and applying the same current used in the experiment. The net cell voltage was found by subtracting short circuit voltage from the applied cell voltage, $E_{applied}$.

$$E_{net} = E_{applied} - E_{short\ circuit} \qquad (45)$$

Average Net Cell Voltage, $E_{average\ net}$, was obtained by calculating the average of the net cell voltage readings during experiments. The voltage readings of the first 10 minutes of each experiment were excluded because of the unstable cell voltages at the beginning of the experiments.

The following calculations were used for each experiment using the given operating parameters:

Current Density, j;

$$j_{cathode} = \frac{I}{A_{cathode}} \qquad \text{and} \qquad j_{anode} \frac{I}{A_{anode}} \qquad (46)$$

where,

$j_{cathode}$: Cathode current density ($A \cdot cm^{-2}$),

j_{anode} : Anode current density ($A \cdot cm^{-2}$),

I : Applied current (A),

46

$A_{cathode}$: Cathode area (cm^2),

A_{anode} : Anode area (cm^2).

The term current density is used for cathode current density unless otherwise stated. Current Efficiency, %CE, is the ratio of actual and theoretical magnesium deposition.

$$\%CE = \frac{Mg_{collected}}{Mg_{theoretical}} \times 100 \tag{47}$$

where,

$Mg_{collected}$: Deposited magnesium during electrolysis (g).

$Mg_{theoretical}$: Theoretical magnesium deposition from Faraday Equation (g).

Energy consumption per kg of magnesium, EC;

$$EC = \frac{E_{average\ net} \times 100}{0.4534\,g \cdot A^{-1} \cdot h^{-1} \times \%CE} \tag{48}$$

where,

$$0.4534\,g \cdot A^{-1} \cdot h^{-1} = \frac{3600\dfrac{\sec ond}{hour} \cdot \dfrac{24.305}{2} \cdot \dfrac{g}{g \cdot equivalent}}{96485\dfrac{coulombs}{g \cdot equivalent}} \tag{49}$$

Energy efficiency, %EE;

$$\%EE = \frac{E_{th}}{E_{net}} \times \%CE \tag{50}$$

where E_{th} is theoretical voltage calculated from Nernst Equation. The theoretical decomposition voltage, that is the minimum voltage that must be applied to electrodes at reversible conditions to decompose $MgCl_2$ is given by Nernst Equation for the reaction,

47

$$MgCl_2 \text{ (in electrolyte)} = Mg\ (l) + Cl_2\ (g,\ 1\ atm) \tag{51}$$
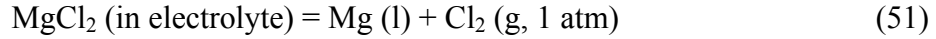
is:

$$E_{th} = E^0 - \frac{RT}{nF} \ln\left(\frac{a_{Mg} \cdot P_{Cl_2}}{a_{MgCl_2}}\right) \tag{52}$$

where,

E^0 : Standard emf for the reaction when both reactants and products are in their standard states. For decomposition of pure $MgCl_2$ to $Mg(l)$ and $Cl_2(g)$ it is given by Equation (8),

R : Gas constant (8.3145 J/mol.K),

T : Absolute temperature (K),

F : The Faradays number (96485.34 Coulombs/g-equivalent),

n : The number of Faradays of charge that passes through the cell when 1 g.atom of Mg is collected at the cathode at %100 efficiency,

a_{MgCl_2} : Magnesium chloride activity with respect to pure liquid standard state, Given as 0.0041 for 20% $MgCl_2$, 40 %NaCl, 40% KCl [50],

P_{Cl_2} : Chlorine partial pressure of surrounding environment (1 atm),

a_{Mg} : Magnesium activity with respect to pure liquid standard state (taken as 1).

When above data is used E_{th} can be obtained as 2.74 V at 700˚C for 20% $MgCl_2$, 40% NaCl, 40% KCl electrolyte.

CHAPTER 4

RESULTS AND DISCUSSION

4.1. The Effect of Current Density

Current density was the first parameter to evaluate the new cell design. Two sets of experiments were carried out to determine optimum current density at 13 mm and 20 mm ACD (anode-cathode distance). Although many different compositions of chloride electrolytes have been proposed, a $MgCl_2$-NaCl-KCl electrolyte is the most efficient due to the low slurry formation, less metal combustion, lower viscosity and higher electrical conductivity[51]. Composition of the electrolyte was 20% $MgCl_2$, 39.5% KCl, 39.5% NaCl and %1 NaF that was found as optimum electrolyte composition in a previous study that employed vertically aligned electrodes [45]. Additionally, this choice also makes possible the comparison of the results with the cells that use similar electrolyte compositions. The composition of the electrolyte was investigated in detail in subsequent sets of experiments.

A rapid initial rise in cell voltage was followed by a decrease at 13 mm ACD, forming a peak as shown in Figure 26. Then the cell voltage remained constant or decreased slightly until the end of the experiments. Both the magnitude of the peak and voltage relaxation rate at the latter portion was more pronounced at higher current densities. Similar variations were obtained for the 20 mm ACD, as it is shown in Figure 27.

Results obtained from the current density experiments and the calculations are summarized in Table 5. As it can be seen in this table an average $MgCl_2$ activity of 0.0025 was used to calculate theoretical decomposition voltage. This value

49
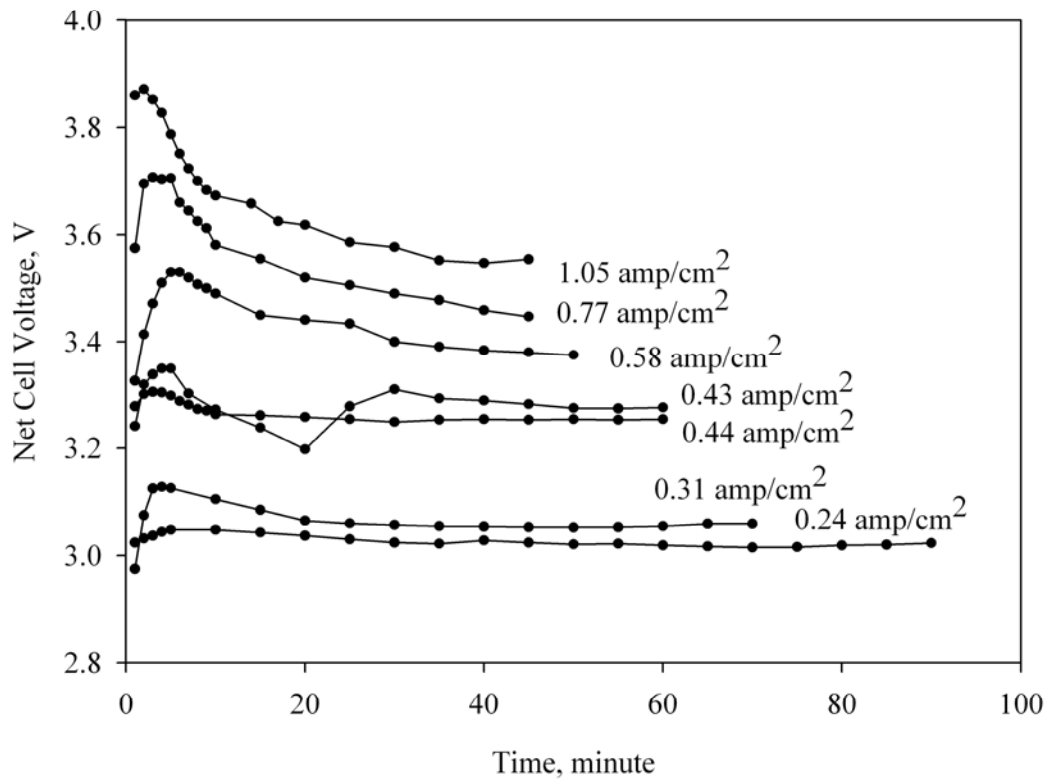
Figure 26 Net cell voltage vs. time at 13 mm ACD for the experiments involving
the effect of current density.
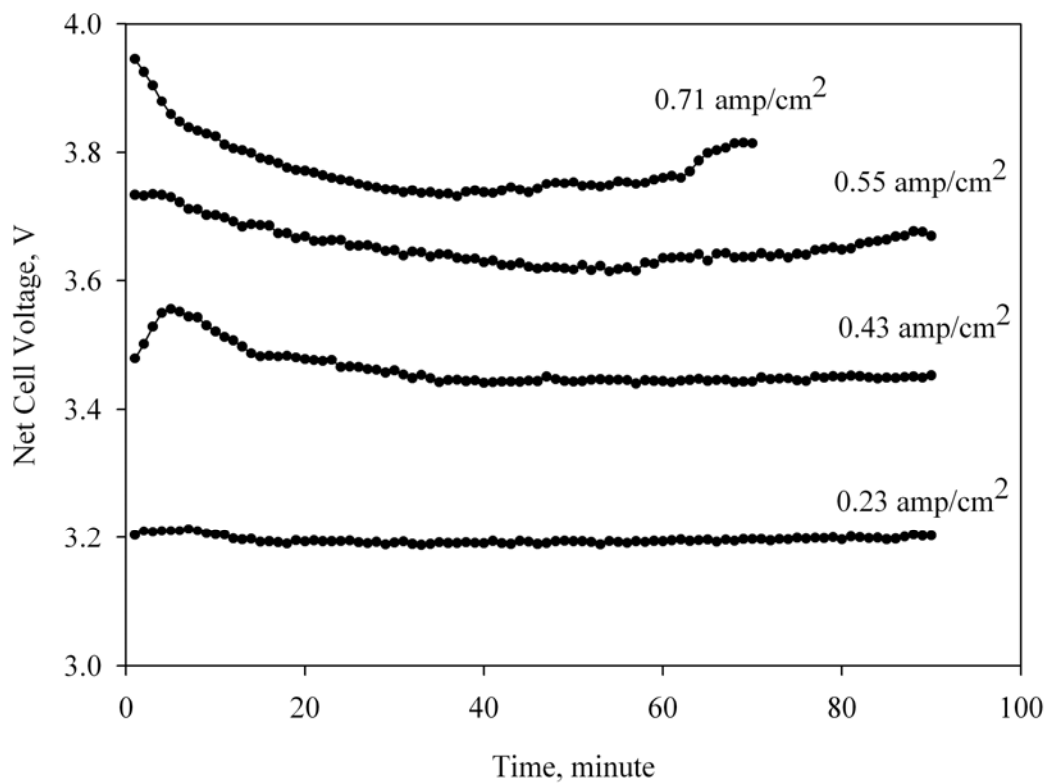
Figure 27 Net cell voltage vs. time at 20 mm ACD for the experiments involving the effect of current density.

Table 5 The details of the experiments involving the effect of current density.

Experiment	1	2	3	4	5	6	7
MgCl$_2$, wt%	20.2	20.4	22.2	20.2	20.2	20.2	20.2
NaCl, wt%	39.4	39.8	38.3	39.4	39.4	39.4	39.4
KCl, wt%	39.4	39.8	38.3	39.4	39.4	39.4	39.4
CaCl$_2$, wt%	0.0	0.0	0.0	0.0	0.0	0.0	0.0
NaF, wt%	1.0	1.0	1.1	1.0	1.0	1.0	1.0
Total Salt, g	100.2	99.2	90.0	100.2	100.2	100.2	100.2
T, °C	700	700	700	700	700	700	700
E^0, V	2.51	2.51	2.51	2.51	2.51	2.51	2.51
a_{MgCl_2} (mean)	0.0025	0.0025	0.0025	0.0025	0.0025	0.0025	0.0025
E_{th} (mean), V	2.77	2.77	2.77	2.77	2.77	2.77	2.77
κ (mean), ohm^{-1}·cm^{-1}	2.05	2.05	2.02	2.08	2.10	2.12	2.13
t, min	90	70	60	60	50	45	45
$Mg_{collected}$, g	2.01	2.03	2.57	2.55	2.72	3.02	3.11
$Mg_{theoretical}$, g	2.09	2.14	2.70	2.70	2.98	3.34	3.50
I, A	3.08	4.04	5.96	5.96	7.89	9.82	10.30
A_{anode}, cm^2	4.5	4.5	4.5	4.5	4.5	4.5	4.5
j_{anode}, A·cm^{-2}	0.68	0.90	1.32	1.32	1.75	2.18	2.29
$A_{cathode}$, cm^2	13.0	13.0	13.7	13.5	13.5	12.8	9.8
$j_{cathode}$, A·cm^{-2}	0.24	0.31	0.43	0.44	0.58	0.77	1.05
$E_{average\ net}$, V	3.03	3.06	3.27	3.26	3.42	3.50	3.60
CE, %	96.0	95.1	95.1	94.4	91.1	90.3	88.9
EC, kWh·kg^{-1}	7.0	7.1	7.6	7.6	8.3	8.6	8.9
EE, %	87.7	85.9	80.4	80.2	73.8	71.3	68.3
ACD, cm	1.3	1.3	1.3	1.3	1.3	1.3	1.3

Table 5 (continued).

Experiment	8	9	10	11
MgCl$_2$, wt%	20.4	20.4	20.4	20.4
NaCl, wt%	39.3	39.3	39.3	39.3
KCl, wt%	39.3	39.3	39.3	39.3
CaCl$_2$, wt%	0.0	0.0	0.0	0.0
NaF, wt%	1.0	1.0	1.0	1.0
Total Salt, g	159.7	159.7	159.7	159.7
T, °C	700	700	700	700
E^0, V	2.51	2.51	2.51	2.51
a_{MgCl_2} (mean)	0.0025	0.0025	0.0025	0.0025
E_{th} (mean), V	2.77	2.77	2.77	2.77
κ (mean), ohm^{-1}·cm^{-1}	2.06	2.10	2.16	2.10
t, min	90	90	90	70
$Mg_{collected}$, g	2.38	4.36	5.73	5.64
$Mg_{theoretical}$, g	2.40	4.46	5.82	5.82
I, A	3.53	6.56	8.55	11.00
A_{anode}, cm^2	5.0	5.0	5.0	5.0
j_{anode}, A·cm^{-2}	0.71	1.31	1.71	2.20
$A_{cathode}$, cm^2	15.4	15.4	15.4	15.4
$j_{cathode}$, A·cm^{-2}	0.23	0.43	0.55	0.71
$E_{average\ net}$, V	3.19	3.46	3.65	3.76
CE, %	99.1	97.7	98.5	97.0
EC, kWh·kg^{-1}	7.1	7.8	8.2	8.6
EE, %	85.8	78.2	74.7	71.3
ACD, cm	2.0	2.0	2.0	2.0

corresponds to the activity of 15% $MgCl_2$ electrolyte. That is the concentration of $MgCl_2$ obtained as the average between the initial and the final percentages of the $MgCl_2$-NaCl-KCl-NaF electrolyte

The average net cell voltage increases with increasing current density as it can be seen from the Figure 28. However the rate of increase decreases at the larger current densities. Extrapolated average net cell voltage curve intersects the voltage axis at 2.77 V that is the theoretical decomposition potential of $MgCl_2$ at the specified temperature and electrolyte composition. Current efficiency decreases with the current density as it can be seen in Figure 29. The decrease is more pronounced at the smaller anode cathode distance and both curves can be extrapolated to 100% current efficiency at 0 current density. Energy consumption increases from 7 $kWh \cdot kg^{-1}$ to 9 $kWh \cdot kg^{-1}$ in the current density range studied and both curves can be extrapolated again to the theoretical value that is 6.2 $kWh \cdot kg^{-1}$ as it can be seen from the Figure 30. Energy efficiency curves are given in Figure 31.

The peak formation observed in Figure 27 and Figure 28 is related with nucleation during the magnesium deposition. An extra energy other than the electrolysis potential had to be supplied to initiate the magnesium deposition on steel cathode. When the current density was high, higher deposition rate necessitated more nucleation. More nucleation required more energy, and the cell voltage increased accordingly. After nucleation, the process continued as magnesium deposition on molten magnesium. As a result, observed cell voltage decreased. The initial cell voltage rise was relatively small for 0.23 $A \cdot cm^{-2}$ in both sets of experiments due to the lower nucleation rates associated with the lower current density as explained above.
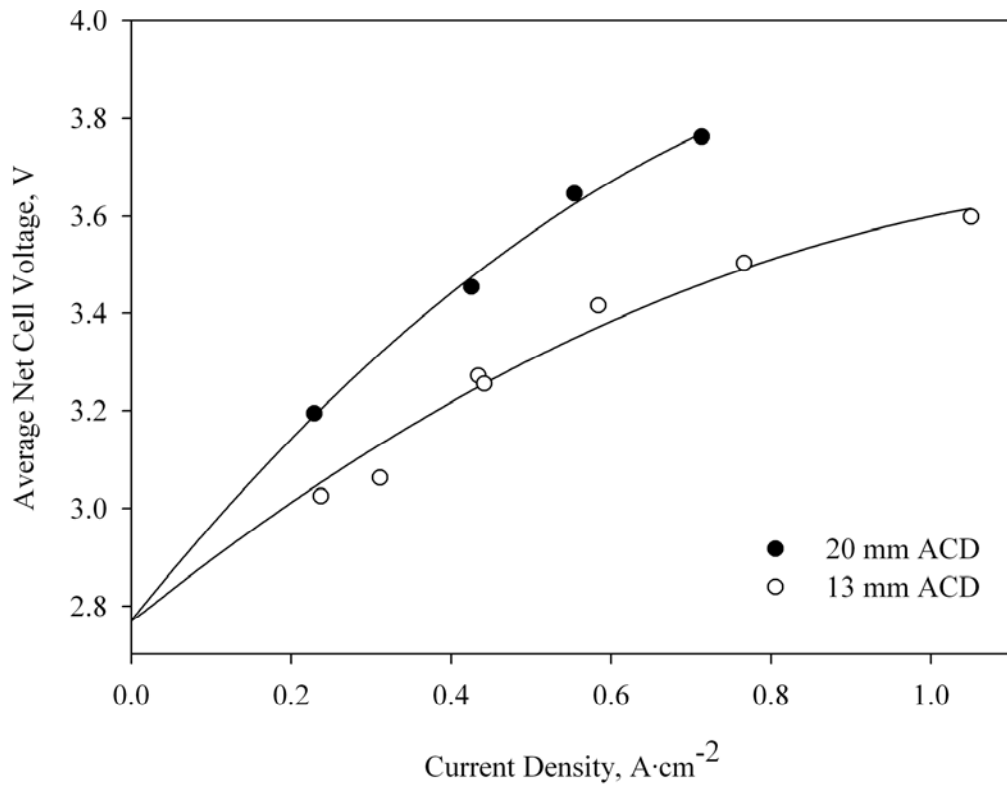
Figure 28 Average net cell voltages for the experiments involving the effect of current density.
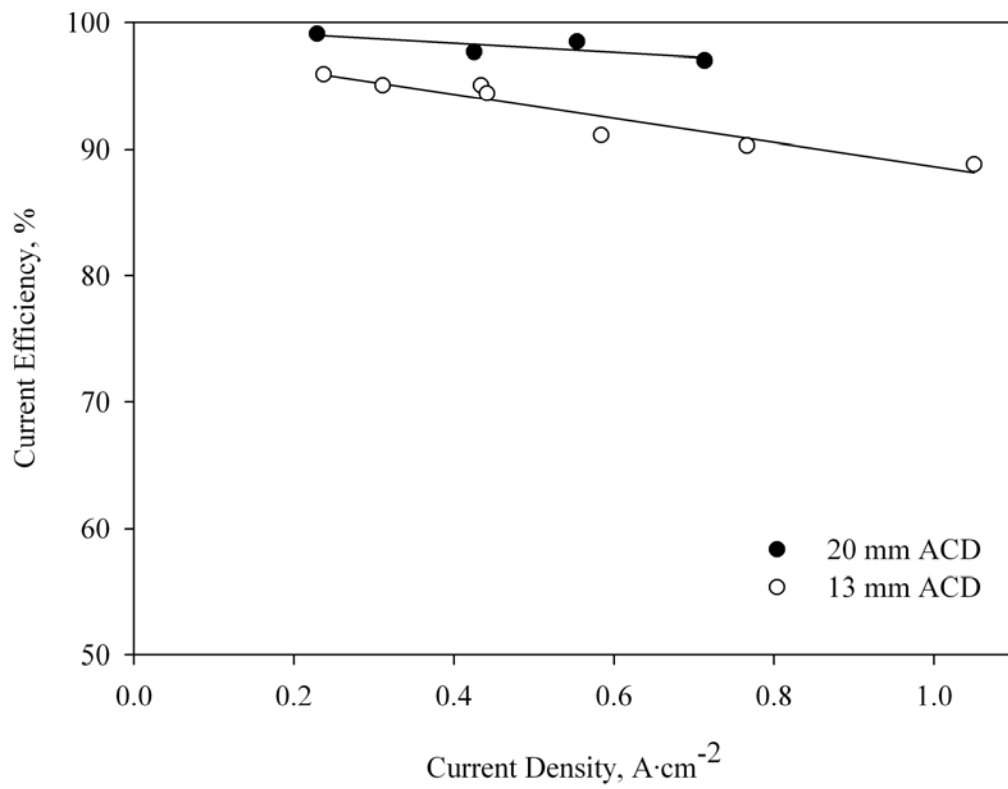
Figure 29 Current efficiencies for the experiments involving the effect of current density.
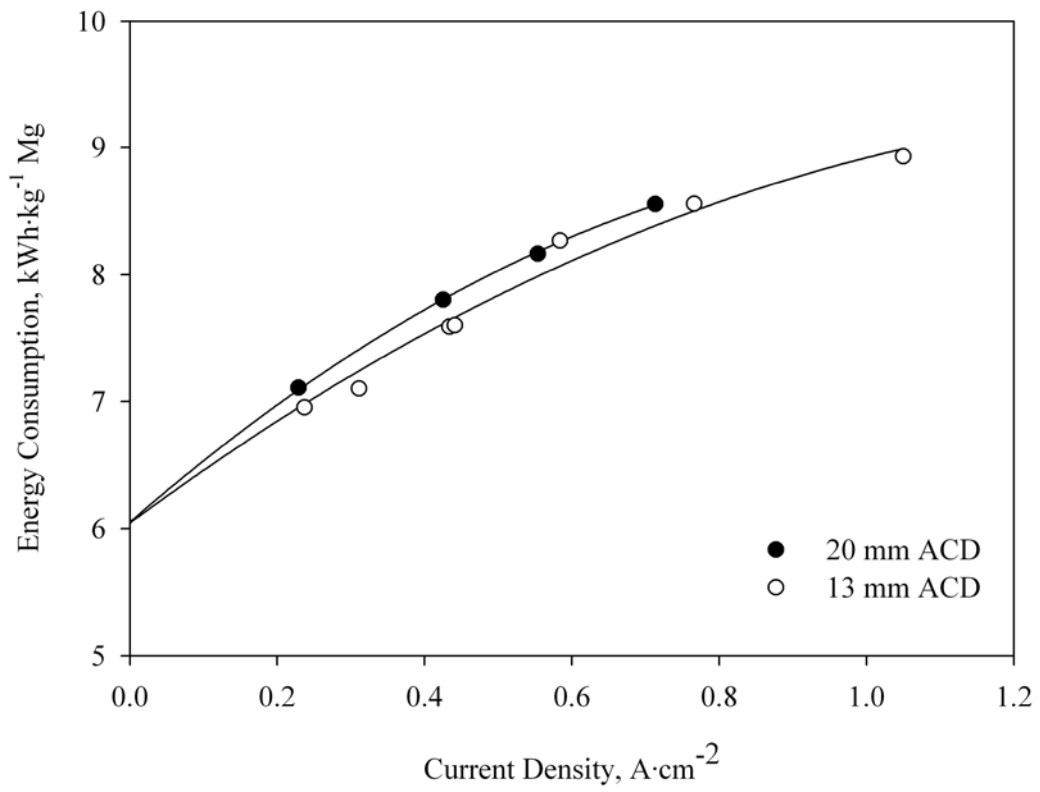
Figure 30 Energy consumptions for the experiments involving the effect of current density.
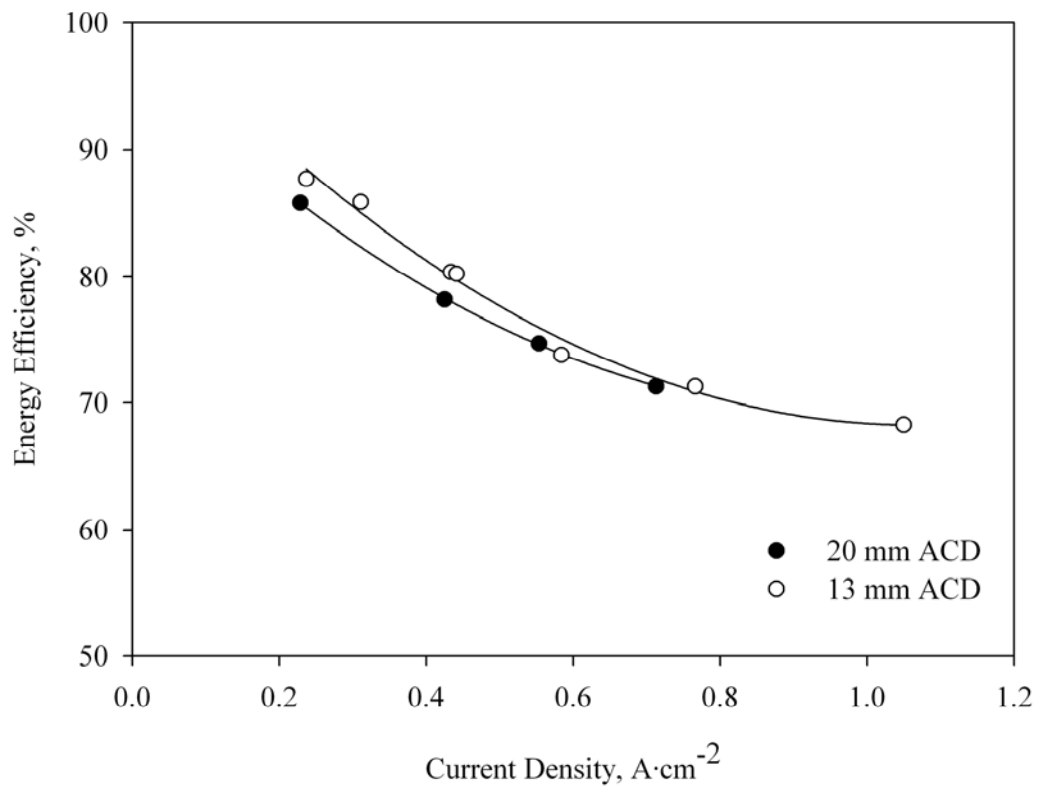
Figure 31 Energy efficiencies for the experiments involving the effect of current density.

Melt composition continuously changed during experiments since $MgCl_2$ was depleted as the electrolysis continued. As Mg is deposited at the cathode, chlorine gas escaped from the cell and $MgCl_2$ activity in the electrolyte decreased. Any decrease in $MgCl_2$ activity resulted in an increased cell voltage according to Nernst Equation. On the other hand, composition change also affected the IR drop across the electrolyte. As the $MgCl_2$ decreased, the electrolyte conductivity increased and IR drop became smaller. A decrease in IR drop had an effect of decreasing the cell voltage. Furthermore, effective ACD decreased with the deposition at the cathode surface that was proportional to the total time and the current.

The decrease in the $MgCl_2$ activity and the IR drop had an influence on the shape of the cell voltage variation during entire electrolysis. However, the shapes of the initial portions of the voltage transition curves were dominated by the effect of the magnesium nucleation at the cathode surface. Chemical composition change at the beginning of the experiments had no recognizable effect on the shape of voltage-time curve and a characteristic initial peak was observed for all the runs.

Although the decrease in $MgCl_2$ activity and the IR drop had more influence on the latter portions of the curves, the amount of voltage change remained small for most of the curves due to the low compositional change. The counteracting consequences of composition change seemed as balanced for much of the runs.

But relatively large changes were observed in Experiment 10 and Experiment 11 where the current densities were 0.55 and 0.71 A/cm^2 respectively and ACD was 20 mm. $MgCl_2$ concentration decreased more in experiments involving a high current density and long electrolysis duration. An increase in cell voltage indicated greater effect of the decreased $MgCl_2$ activity than the decreased IR drop at the final portions of the curves. In fact, similar cell voltage increase could have been observed for all runs if the duration of which was kept sufficiently long to cause such a composition change.

The main reason of the increase in average net cell voltage given in Figure 28 is the increased IR drop that is the voltage as a result of the electrolyte resistance with increased current density. More electrical energy is dissipated as heat through the electrolyte with an increase in applied current, where the electrical resistance is constant at a given chemical composition.

However the rate of increase, decreased at higher applied current densities. In fact, a region of an increased slope must follow the observed region where the cell voltage slope decreased. A critical current density could have been reached at the higher current densities where a small increase in current density could cause a large increase in cell voltage. The current density range involved in this study did not include the limiting current density region.

One of the reasons for the decrease in the slope of the curve was the electrode over-potentials. Electrode over potentials did not increase at the same rate as the IR drop with the increased current density. Since over-voltages are proportional with logarithm of applied current densities, their contributions to net cell voltage are small unless applied current densities are very close to limiting values.

The other reason is the change in the amount and hydrodynamics of chlorine bubbles in inter-electrode region. Increase in current density increases the production rate of chlorine gas. This affects the diameter, residence time and the coalescence of the evolving bubbles. Their effects can be calculated and compared with the experimental results.

The first attempt to correlate the average net cell voltage, $E_{average\ net}$, with the theoretical decomposition potential, $E_{th\ (mean)}$, involved the computation of IR drop from;

$$IR = \frac{jl}{\kappa} \tag{53}$$

Where j is current density in A·cm⁻². An inter-electrode distance, l, which is average separation distance between the electrodes, is taken as ACD directly disregarding the magnesium accumulation at the cathode surface. The current density is calculated by using the average of the electrode surfaces. Specific conductivity of the electrolyte, κ, was taken as 1.92 Ω^{-1}·cm⁻¹ [2]. Computation of IR drop using Equation (53) with 1.92 Ω^{-1}·cm⁻¹ specific conductivity involved the consideration of a homogenous unpolarized molten salt electrolyte between the electrodes.

The electrolyte is actually a heterogeneous mixture of molten salt electrolyte and chlorine gas bubbles especially near graphite anode during electrolysis. Therefore, IR drop computations during electrolysis should include the presence of resistance due to chlorine bubbles in the inter-electrode region since the chlorine gas formation at the anode surface increased the electrolyte resistance locally.

In order to introduce the effect of gas bubbles on cell voltage calculations, a simple hydrodynamic model was assumed. The change in the electrolyte resistance is related with the size and residence time of the bubbles in inter-electrode region. For this purpose variation in bubble size and bubble velocity with the applied current densities had to be determined to assess the effect of gas bubbles on the cell voltage.

The bubbles are assumed to be formed thorough multiple orifices distributed across the anode surface. The variation of bubble size in a single orifice with orifice diameter and Reynolds number is given by the equation below for $N_{\text{Re}o}$ <2100 [52]:

$$d_b = 0.286 d_o^{0.5} N_{\text{Re}o}^{0.33} \tag{54}$$

where,

      d_b : Mean bubble diameter, cm,

      d_o : Orifice diameter, cm,

$N_{\mathrm{Re}o}$: Orifice Reynolds number, $d_o u_o \rho_l / \mu_l$,

u_o : Gas velocity at the orifice, $\mathrm{m \cdot s^{-1}}$,

ρ_l : Density of electrolyte (1.59 $\mathrm{g \cdot cm^{-3}}$ at 10% $MgCl_2$ [2]),

μ_l : Viscosity of electrolyte (0.018 Poise at 10% $MgCl_2$ [2]).

To determine the diameter of the hypothetical orifices, bubble diameter and bubble residence time values in inter-electrode region are required. These values are taken as 0.1 cm and 0.05 second respectively from a previous study that was based on measurements involved the formation of gas bubbles on graphite electrodes of the same geometry in a room temperature water solution with kinematical properties similar to the magnesium cell electrolyte. Details of measurements are given elsewhere [53].

The data for Experiments 3 and 4 that have 2.26 $\mathrm{cm^3 \cdot s^{-1}}$ chlorine production rate, similar to gas flow rate used in previous study [53], was used to calculate bubble density in the electrolyte. This yielded 4320 bubbles per second when 0.1 cm bubble diameter was used. Bubble formation frequency at the orifices was taken as 20 bubbles per second, inverse of the residence time of the bubbles. Therefore the number of orifices was calculated as 216. Placing the values into above equation yields:

$$d_b = 0.286 d_o^{0.5} \frac{d_o^{0.33} \dfrac{\dfrac{2.26^{0.33}}{216}}{\left(\dfrac{\pi d_o^2}{4}\right)^{0.33}} \rho_l^{0.33}}{\mu_l^{0.33}} \tag{55}$$

$$\mathrm{d_b} = 0.069 \mathrm{d_o^{0.17}} \frac{\rho_l^{0.33}}{\mu_l^{0.33}} \tag{56}$$

And the orifice diameter, d_o, was found as 0.0148 cm. After determining the orifice diameter, bubble diameter, d_b, at different current densities were calculated as it can be seen from Figure 32.
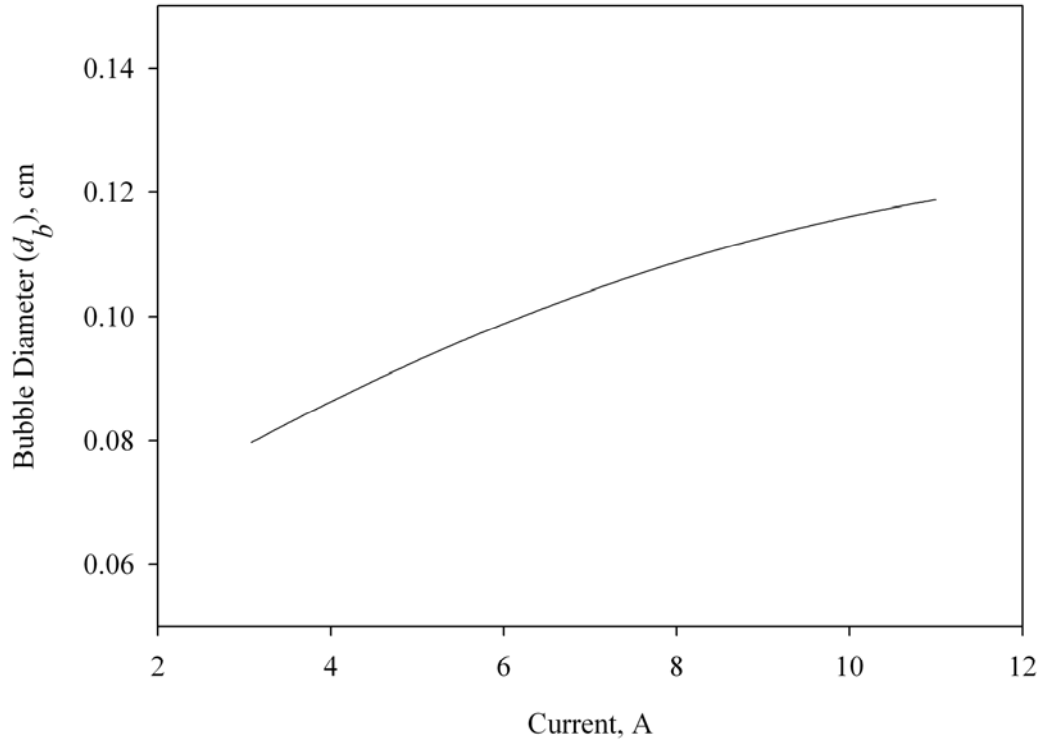
Figure 32 Calculated bubble diameter variation for the experiments involving the effect of current density.

Next, the relation between the bubble area formed and the size and the velocity of the rising bubbles is expressed as [54]:

$$a = 9.38(\frac{u_s}{u_b})^{0.775} N_{\mathrm{Re}o}{}^{0.125} (\frac{\rho_l g}{d_o \sigma})^{1/3} \tag{57}$$

where,

    a : Specific bubble interfacial area per unit volume of dispersion, $cm^2 \cdot cm^{-3}$,

    u_s : Superficial velocity, v/A_{lc}, $cm \cdot s^{-1}$,

v : Volumetric gas flow rate, $cm^3 \cdot s^{-1}$,

A_{lc} : Cross sectional area of liquid column, cm^2,

g : Gravitational acceleration, $cm \cdot s^{-2}$,

σ : Surface tension, $dyn \cdot cm^{-1}$,

u_b : Bubble velocity, $cm \cdot s^{-1}$.

Specific bubble interfacial area per unit volume of dispersion can be expressed as:

$$a = \frac{A_b \, x \, B \, x \, RT}{V_p} \qquad (58)$$

where,

A_b : Single bubble area,

RT : Residence time, h / u_b, second,

h : Half of the anode height, 0.9 cm,

B : Number of bubbles,

V_p : Plume volume, 1 cm^3.

$$\frac{A_b \, x \, B \, x \, \dfrac{h}{u_b}}{PV} = 9.38(\frac{v}{1300 d_b^2})^{0.775} N_{\mathrm{Re}o}^{\,0.125} (\frac{\rho_l g}{d_0 \sigma})^{1/3} \qquad (59)$$

$$u_b = \left(\frac{9.38(\dfrac{v}{1300 d_b^2})^{0.775} N_{\mathrm{Re}o}^{\,0.125} (\dfrac{\rho_l g}{d_0 \sigma})^{1/3}}{A_b \, x \, B \, x \, h} V_p \right)^{4.44} \qquad (60)$$

The $\rho_l g / d_0 \sigma$ ratio is calculated as 11691 by using 981 $cm \cdot s^{-2}$ and 90 $dyn.cm^{-1}$ for gravitational acceleration and surface tension of the electrolyte respectively using values for 10% $MgCl_2$ and 1:1 NaCl:KCl [2]. Plume volume is taken as 1 cm^3. Calculation results are given in Table 6. The variation of the bubble velocity with the applied current is given in Figure 33.

Table 6 Calculated bubble parameters for the experiments involving the effect of current density.

Experiment	1	2	3	4	5	6	7	8	9	10	11
I, A	3.08	4.04	5.96	5.96	7.89	9.82	10.30	3.53	6.56	8.55	11
d_b, cm	0.08	0.088	0.01	0.01	0.109	0.118	0.119	0.081	0.01	0.109	0.118
v, cm^3.s^{-1}	1.17	1.53	2.26	2.26	2.99	3.72	3.9	1.34	2.49	3.24	4.17
u_o, cm.s^{-1}	3139	4118	6075	6075	8042	10009	10498	3263	6063	7902	10167
N_{ReO}	411	539	794	794	1052	1309	1373	427	793	1034	1330
u_b, cm.s^{-1}	8.1	11.4	19.4	19.4	27.6	36.2	38.5	9.8	21.3	29.7	40.7
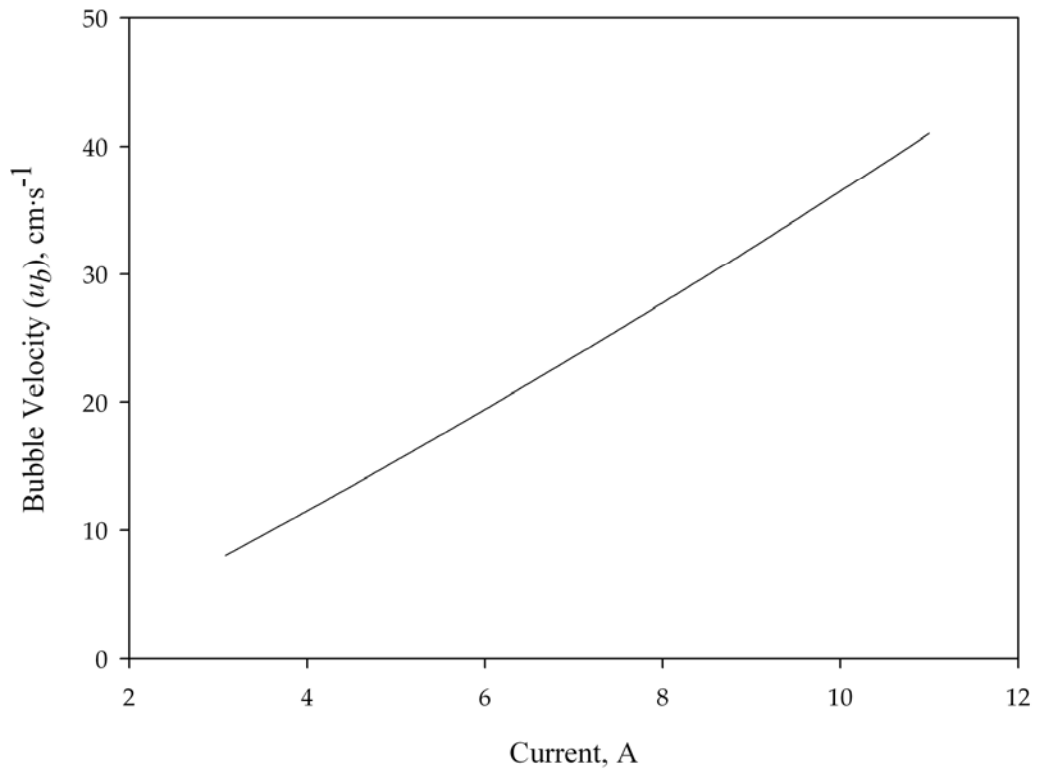
Figure 33 Calculated bubble velocities for the experiments involving the effect of current density.

After obtaining the diameter and the rising velocity for the bubbles it is possible to calculate the bubble surface area that shadows the graphite anode per unit time. The magnitude of shadowing is related with the cell resistance and the cell resistance was considered as composed of two series resistances between the electrodes. Most of the electrolyte was considered to be homogenous electrolyte with 1.92 ohm^{-1}·cm^{-1} specific conductivity. Remaining part of the electrolyte that is equal to one bubble diameter on the anode surface was considered as partly covered by chlorine bubbles. Since these bubbles sweep a volume as they move out of the electrolyte, cylinders with bubble diameter were assumed to restrict the current flow for a period of residence time for each bubble. Therefore IR drop was calculated from;

$$IR = \frac{j\,(l-d_b)}{\kappa} + \frac{j \times d_b}{\kappa}\,\frac{A_{anode}}{A_{anode} - A_g} \tag{61}$$

where, A_{anode} and A_g are the anode area and the surface area of anode covered by chlorine bubbles respectively. Using 0.413 $cm^3 \cdot A^{-1} \cdot s^{-1}$ chlorine production rates, A_g is calculated as;

$$A_g = \frac{0.413\,I}{\tfrac{4}{3}\,\pi r_b^3}\,\pi r_b^2\, t \tag{62}$$

Where I is applied current, r_b bubble radius and t residence time for each bubble. The results of the calculations are given in Table 7. Calculated net cell voltages obtained by adding IR drop to E_{th} are given in Figure 34. Full lines represent the values when electrolyte was considered to contain chlorine bubbles. The results of Equation (53) are added to $E_{th\ (mean)}$ and shown by dotted line in the same figure. As it can be seen in this figure, calculated net cell voltages represent experimental data better when chlorine bubbles were included near the surface of anode. The lower actual voltages than the calculated voltage at the higher current densities imply bubble combination. Reduction of total surface area of bubbles due to bubble combination was not included in the present calculation.

Table 7 Cell voltage calculation using IR drop for the experiments involving the effect of current density.

Experiment	1	2	3	4	5	6	7
ACD, cm	1.3	1.3	1.3	1.3	1.3	1.3	1.3
Mean Electrode Area, cm^2	8.75	8.75	9.12	9.01	9.01	8.66	7.16
r_b, cm	0.040	0.044	0.050	0.050	0.055	0.059	0.060
$A_{bubble\ cross\ section}$ x10^{-3}, cm^2	5.1	6.1	7.9	7.9	9.5	1.1	1.1
RT, second	0.103	0.073	0.045	0.045	0.032	0.024	0.023
Cl_2 rate x10^{-5}, mol·sec^{-1}	1.6	2.1	3.1	3.1	4.1	5.1	5.3
Cl_2 production rate, cm^3·sec^{-1}	1.275	1.672	2.467	2.467	3.266	4.065	4.264
Bubble Volume x10^{-4}, cm^3	2.7	3.6	5.3	5.3	7.0	8.7	9.1
Bubble rate, bubbles·sec^{-1}	4644	4656	4675	4675	4688	4698	4700
Blocked anode area, cm^2	2.43	2.08	1.66	1.66	1.41	1.24	1.21
Non blocked anode area, cm^2	2.07	2.42	2.84	2.84	3.09	3.26	3.29
Resistivity, ohm·cm	0.49	0.49	0.49	0.48	0.48	0.47	0.47
Bubbled Area Resistance, ohm	0.02	0.02	0.02	0.02	0.02	0.02	0.02
IR_{bubble}	0.06	0.07	0.10	0.10	0.13	0.17	0.18
ACD other than bubbles, cm	1.22	1.21	1.20	1.20	1.19	1.18	1.18
Electrolyte Resistance, ohm	0.07	0.07	0.07	0.06	0.06	0.06	0.08
$IR_{electrolyte}$	0.21	0.27	0.39	0.38	0.50	0.63	0.80
E_{th}+IR_{bubble} +$IR_{electrolyte}$	3.03	3.11	3.26	3.25	3.40	3.57	3.74
E_{th}+$IR_{electrolyte}$	2.99	3.06	3.19	3.18	3.31	3.46	3.65

Table 7 (continued).

Experiment	8	9	10	11
ACD, cm	2.0	2.0	2.0	2.0
Mean Electrode Area, cm^2	10.22	10.22	10.22	10.22
r_b, cm	0.041	0.050	0.055	0.059
$A_{bubble\ cross\ section}$ x10^{-3}, cm^2	5.2	7.9	9.4	11
RT, second	0.089	0.041	0.029	0.021
Cl_2 rate x10^{-5}, $mol \cdot sec^{-1}$	1.8	3.4	4.4	5.7
Cl_2 production rate, $cm^3 \cdot sec^{-1}$	1.461	2.716	3.540	4.554
Bubble Volume x10^{-4}, cm^3	2.9	5.3	6.8	8.8
Bubble rate, $bubbles \cdot sec^{-1}$	5123	5155	5169	5182
Blocked anode area, cm^2	2.38	1.66	1.42	1.23
Non blocked anode area, cm^2	2.62	3.34	3.58	3.77
Resistivity, ohm·cm	0.49	0.48	0.46	0.48
Bubbled Area Resistance, ohm	0.02	0.01	0.01	0.02
IR_{bubble}	0.05	0.09	0.12	0.17
ACD other than bubbles, cm	1.92	1.90	1.89	1.88
Electrolyte Resistance, ohm	0.09	0.09	0.09	0.09
$IR_{electrolyte}$	0.32	0.58	0.73	0.96
$E_{th}+IR_{bubble}+IR_{electrolyte}$	3.14	3.44	3.62	3.89
$E_{th}+IR_{electrolyte}$	3.10	3.38	3.54	3.79
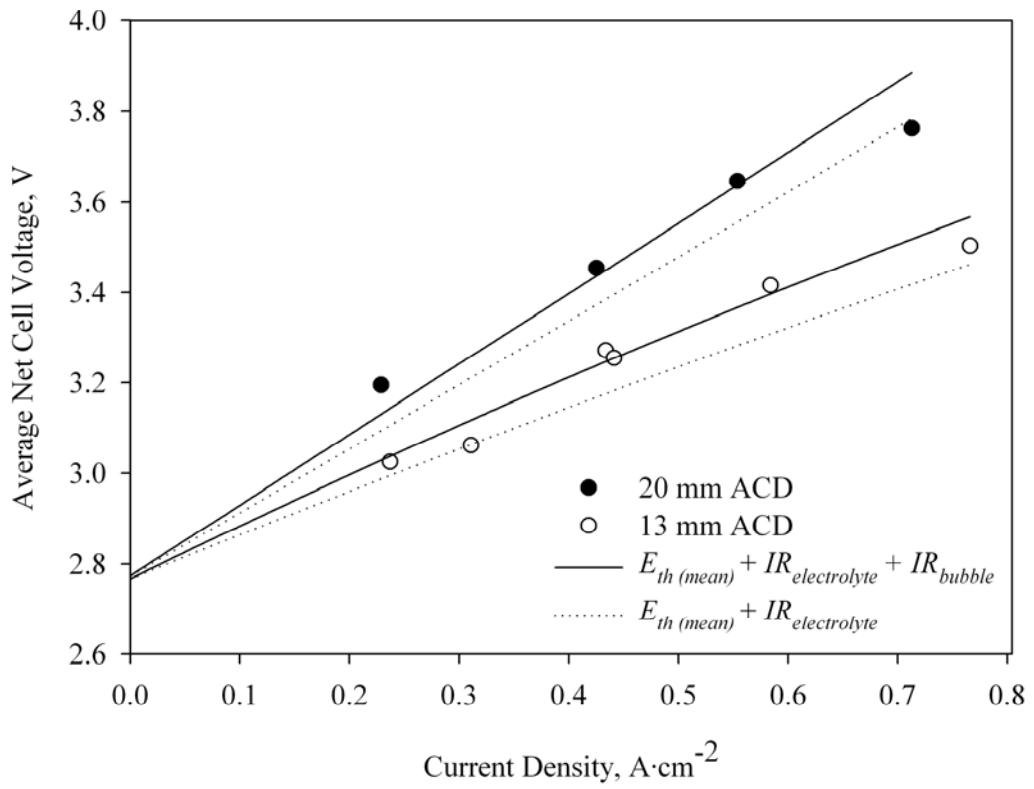
Figure 34 Calculated cell voltages for the experiments involving the effect of current density.

Current efficiencies more than 90% was easily achieved by the current cell design as shown in Figure 29. It was regarded as excellent when the short inter-electrode distances employed was considered. The results indicated that, the extent of contact between Cl_2 gas and Mg in the inter-electrode region was low, despite the low ACD employed in present cell design. This result could be due to low chlorine diffusion in to the melt as a result of high Cl_2 removal rate from the inter-electrode region.

The cell was capable of producing one kilogram of magnesium with less than 9 kWh of electrical energy at a current density of 1.05 A·cm^{-2}, as seen in Figure 30. This current density value corresponds to the largest current density level that is industrially practiced. Despite the high current density employed, energy consumption was well below the lowest energy consumption values industrially obtained; 10-12 kWh·kg^{-1} Mg. Energy efficiency decreases with increasing current density as seen in Figure 31. This is obvious because, increase in net cell voltage which in turn increases energy requirement with increasing current density. Major part of higher energy consumption which in turn decreasing the energy efficiency is coming from higher IR drop with increasing current density.

Chlorine diffusion across thin boundary layer between bubble and molten salt bath was assumed to be the rate determining step in recombination reaction of magnesium and chlorine. Therefore after obtaining the size and the residence time of chlorine bubbles in electrolyte, the extent of back reaction could be calculated from the chlorine dissolution into the melt.

Total chlorine bubble area produced per unit time was determined from the bubble size and the number of chlorine bubbles produced per unit time. Residence time of the bubbles in inter-electrode region was inversely proportional to the bubble rising velocities. The total chlorine surface area exposed to back reaction was calculated by multiplying total chlorine bubble area produced per unit time with

the residence time of the bubbles. Then the chlorine flux into the melt was calculated from the Fick's Law :

$$N_{Cl_2} = -D_{Cl_2} \frac{\Delta C_{Cl_2}}{\delta}$$

where,

N_{Cl_2} : Chlorine flux from bubble surface in $mol.m^{-2}.sec^{-1}$,

D_{Cl_2} : Diffusivity of Cl_2, 0.96 x 10^{-7} $m^2.sec^{-1}$ [2],

ΔC_{Cl_2} : Concentration gradient of Cl_2, 0.8 $mol.m^{-3}$ [55]. Electrolyte was assumed to be saturated with Cl_2 at the bubble surface,

δ : Boundary layer thickness, 0.022 mm [53].

The magnesium losses that correspond to the calculated chlorine flux multiplied by the total chlorine surface area exposed to back reaction and the theoretical current efficiencies were calculated as it was given in Table 8. The calculated current efficiencies were also plotted in Figure 35. As it can be seen from the figure current losses are calculated as decreasing with the increasing gas evolution rate based on the above model. This is contrary to the experimental current losses that are increasing at the higher current densities. Therefore it can be concluded that the reaction of dissolved magnesium and chlorine is not the only back reaction mechanism.

Higher current loss observations especially in experiments involving the use of 13 mm ACD may be attributed to the entrance of tiny magnesium droplets to the anode vicinity due to the convection inside the electrolyte. Thus some sounds heard during the experiments were considered as the result of chemical reactions between magnesium and chlorine in the anode compartment. Higher current loss observed at smaller ACD also supports that statement due to the more convection at the same gas evolution.

Table 8 Calculated current efficiency from chlorine surface area for the experiments involving the effect of current density.

Experiment	1	2	3	4	5	6	7
Current Density,	0.24	0.31	0.43	0.44	0.58	0.77	1.05
B. dia., d_bx10^4, m	8.02	8.77	9.97	9.97	1.09	1.18	1.19
SingleBubble Area, A_b x10^6, m^2	2.02	2.42	3.12	3.12	3.76	4.34	4.48
No. of Bubbles, *B*	4325	4337	4354	4354	4366	4376	4378
Residence Time, RT, s	0.1112	0.0792	0.0464	0.0464	0.0327	0.0248	0.0234
Cl$_2$ Area x10^4, m$^2 \cdot$s^{-1}	9.72	8.30	6.31	6.31	5.36	4.72	4.59
Cl$_2$ Flux x10^6, mol$\cdot$s^{-1}	3.39	2.90	2.20	2.20	1.87	1.65	1.60
Reacted Mg, g	0.440	0.292	0.190	0.190	0.135	0.107	0.106
Calculated CE, %	79.0	86.3	93.0	93.0	95.5	96.8	97.6
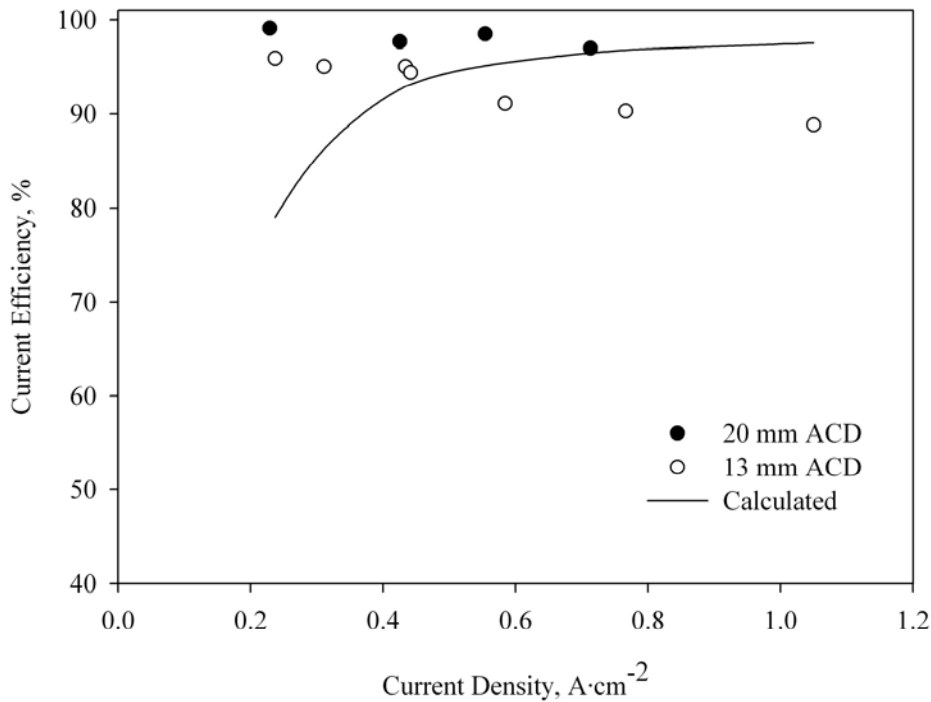
Figure 35 Calculated current efficiencies for the experiments involving the effect of current density.

Particle formation is known to be stimulated by the presence of water in cell feed and the formation of magnesium fog is reported in a see-through cell [56]. It seems that particle formation is also stimulated by the current density as it can be seen from the cathode and magnesium droplet photographs in Figure 36 that were obtained from the 20 mm ACD experiments. The giant particles easily distinguishable from other particles by their size should not be considered as particles that were detached from the cathode during electrolysis process. They dropped from the cathode surface in molten state because of the gravity during withdrawal of the cathode from the electrolyte after the electrolysis was completed. A giant particle remained just attached to the cathode surface can be seen in picture showing the cathode for Experiment 10.

Since the total charge were not the same in all experiments they could not be compared with each other directly. However photographs from Experiments 10 and 11 utilizing 0.55 and 0.71 A cm^{-2} current densities could be compared with each other. The amount of fine particles was more in Experiment 11 than in Experiment 10. Finer and more magnesium particles were obtained in Experiment 11 (j=0.71 A cm^{-2}). The reason might be related to the quantity of gas evolution from the anode. Increased gas evolution might stimulate particle detachment due to the increased turbulence inside the electrolyte. The total charge used in Experiment 9 were around 77% of the charges utilized in Experiments 10 and 11, the amount of fine magnesium particles also followed the same tendency by generating less small particles than the other two experiments. Slightly more particle formation at Experiment 8 when compared to Experiment 9 despite the lower current density employed could be explained by the open cathode areas that was not wetted by the magnesium. The total charge used in Experiment 8 was just the 41% of the charges employed in Experiment 10 and 11. Hence the total deposition was also lower leaving cathode regions uncovered by the liquid magnesium. Presence of open cathode regions seemed to stimulate particle formation. In addition to this low turbulence due to low gas evolution might have

protected the small particles from entering into the anode vicinity and the amount of the particles remained high.

Particle generation increase at higher production rates might be explained by two mechanisms or a combination of both. Increased turbulence inside the cell due to the increased chlorine gas formation might cause more particle separation from the cathode at the higher current densities. Increased current density might cause the formation of larger magnesium particles at a unit time that could be separated from some parts of cathode surface easier. These surfaces are either regions where cathode area is very small or parts where passivation may become effective. Formation and hydrodynamics of small particles could add to the current loss that was considered to be due to Cl_2 diffusion. Therefore decrease in current efficiency with increasing current density is not a surprise.

As explained above, a current efficiency decrease was expected with the increased current density, since both the total amount of particles and electrolyte circulation was increasing. Since more turbulence occurred at the lower ACD for a constant current density, the probability of chlorine and magnesium contact both in the elemental and dissolved form increased at the shorter inter-electrode distances. That is why current efficiency curve of 13 mm ACD was considerably deviated from the 20 mm ACD curve as seen in Figure 29. The magnitude of the decrease remained small and only 2.1% decrease was observed while increasing the current density from 0.23 A cm^{-2} to 0.71 A cm^{-2} at 20 mm ACD. Slightly higher decrease was observed at 13 mm ACD and current efficiency decreased 7.08% while increasing the current density from 0.24 A cm^{-2} to 1.05 A cm^{-2}.

The main reason of the high current efficiencies observed was the amount of the magnesium particles retained at the cathode surface. Less particle formation increases the current efficiency. Furthermore the magnesium was cathodic when remaining attached to cathode.

Another reason of the high current efficiencies might be the sinking of magnesium particles to the bottom of the melt after detaching from the cathode surface. Magnesium metal had a slightly lower density than the electrolyte used and magnesium metal would float to the surface of the electrolyte probably remaining in suspension for a long time. Therefore the probability of suspending magnesium particles to enter into the anode region increases. On the other hand MgO deposition at the droplet surfaces made them heavier and caused them to sink instead of floating or remaining in suspension. Therefore, most of the particles were found at the bottom of the crucible after the electrolysis might be protected from entering the anode vicinity during the electrolysis.

Although excellent current and energy efficiencies were obtained from the experiments involving the effect of current density, continuous growth of magnesium on the cathode surface was not suitable for working at small ACD. The amount of magnesium remained at the cathode surface during the electrolysis was too much due to the good wetting. This caused short circuiting at 13 mm ACD experiments. Experiment 3 (j= 0.43 A·cm^{-2}) is an example of the short circuiting as can be seen in Figure 26. The voltage decreased after the initial peak and electrolysis stopped at 20th minute. Voltage was recovered after moving electrodes slightly.

Experiment 8 (i=0.23 A cm^{-2})

Experiment 9 (i=0.43 A cm^{-2})

Experiment 10 (i=0.55 A cm^{-2})

Experiment 11 (i=0.71 A cm^{-2})

Figure 36 Cathodes and magnesium particles for the experiments involving the effect of current density (length of the line is 10 mm).

4.2. The Effect of Temperature

Experiments involving the effect of current density on cell performance yielded very high current and energy efficiencies. Observations of the cathode showed that, metallic magnesium was collected on cathode almost through the entire experiment duration. Continuous growth of magnesium in inter-electrode region could create problems related to short circuiting of electrodes for prolonged experiment duration. Therefore kinematic properties of the system have to be changed to obtain an industrially suitable condition. In this connection effect of temperature on cell performance was tested.

The temperature should be kept above 651°C to keep magnesium molten during the electrolysis. Since the vapor pressure of both liquid magnesium and the electrolyte was high, the operating temperatures close to the melting point of magnesium were preferred to prevent losses due to evaporation. In addition to the experiment performed at 700°C, experiments at 675°C and 725°C were conducted to see the effect of temperature. That temperature range covered the probable industrial operating temperatures that could be applied to the electrolyte composition used in the present study. The electrolyte composition was kept as 20% $MgCl_2$, 39.5% NaCl, 39.5% KCl and 1% NaF. The ACD and the current density were 20 mm and 0.42-0.43 A cm^{-2} respectively.

The net cell voltage vs. time graph is given in Figure 37. Similar to the previous results there were peaks at the beginning of the experiments and the cell voltage was stable after about 20 minutes. The area under the initial peaks decreased with the increasing temperature. It can be seen that voltage relaxation continues slightly after the initial peaks for 675°C and 700°C. However, continuous electrolysis results in a slight increase of net cell voltage at 725°C.
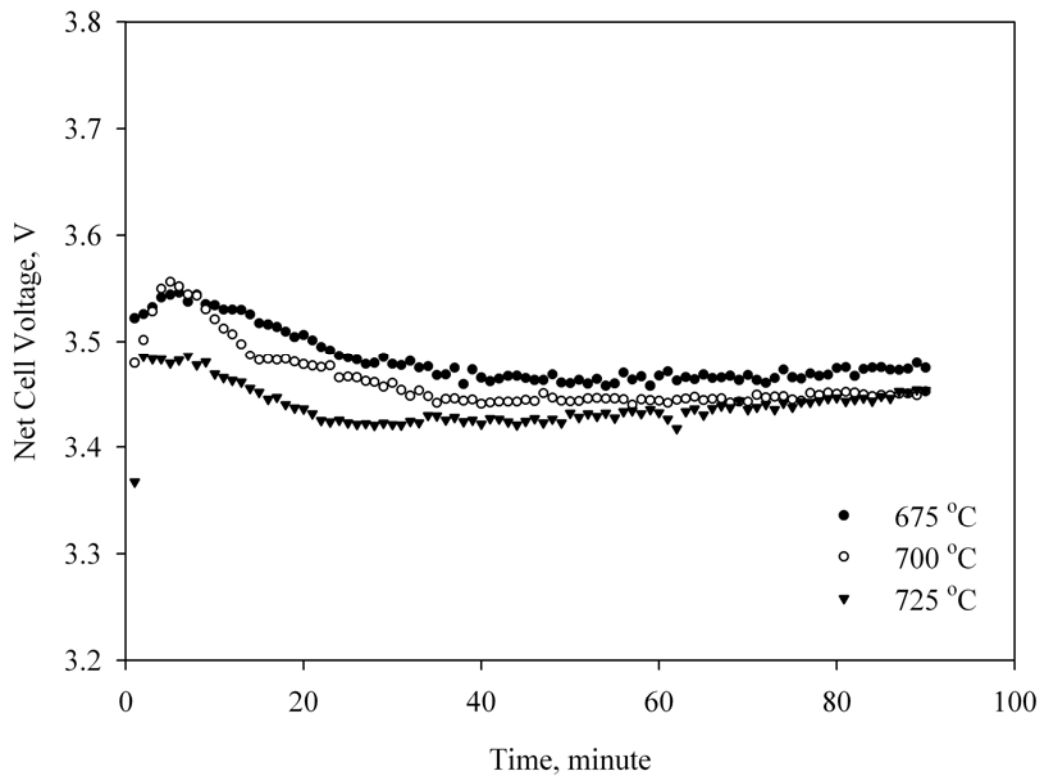
Figure 37 Net cell voltage vs. time at 20 mm ACD for the experiments involving the effect of temperature.

The effect of temperature on activity coefficient of $MgCl_2$ given in Figure 38 was used to calculate the change in $MgCl_2$ activity with temperature. The slopes of the four curves are close to each other although some of the lines correspond to NaCl rich compositions and the others KCl rich compositions. The same slope is used for the temperature dependency of $MgCl_2$ activity coefficients in electrolytes with 1:1 NaCl:KCl composition that falls in between NaCl rich and KCl rich electrolyte compositions. The $\ln \gamma_{MgCl_2}$ values were calculated as -3.83, -3.90 and -3.83 for the Experiments 12, 9 and 13 respectively from their corresponding average compositions and $MgCl_2$ activities at 700˚C. Then the $\ln \gamma_{MgCl_2}$ values were calculated by using the same slope obtained from the Figure 38 keeping the value for Experiment 9 as constant. Calculated activities are given in Table 9. The results of the experiments and the calculations were summarized in Table 10.
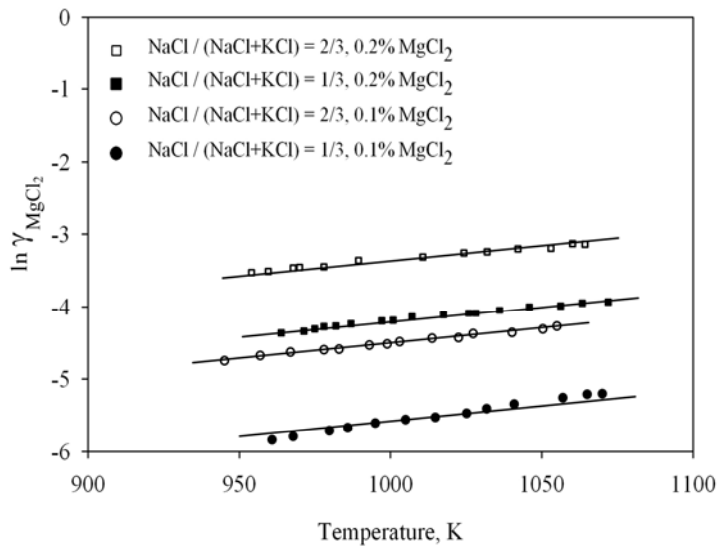
Figure 38 The change in $MgCl_2$ activity coefficient with temperature [57].

Table 9 The change in $MgCl_2$ activity with temperature.

Experiment (T°C)	12 (675°C)	9 (700°C)	13 (725°C)
$\ln \gamma_{MgCl2}$	-3.93	-3.90	-3.73
a_{MgCl2}	0.0023	0.0025	0.0028

Table 10 The details of the experiments involving the effect of temperature.

Experiment	12	9	13
$MgCl_2$, wt%	19.47	20.10	19.47
NaCl, wt%	39.76	39.45	39.76
KCl, wt%	39.76	39.45	39.76
$CaCl_2$, wt%	0.00	0.00	0.00
NaF, wt%	1.01	1.00	1.01
Total Salt, g	156.9	159.7	156.9
T, °C	675	700	725
E^0, V	2.531	2.514	2.498
$a_{MgCl_2 \ (mean)}$	0.0023	0.0025	0.0028
$E_{th \ (mean)}$, V	2.779	2.766	2.752
$\kappa_{(mean)}$, ohm^{-1}·cm^{-1}	2.05	2.10	2.22
t, min	90	90	90
$Mg_{collected}$, g	4.396	4.359	4.389
$Mg_{theoretical}$, g	4.462	4.462	4.469
I, A	6.56	6.56	6.57
A_{anode}, cm^2	5.00	5.00	5.00
j_{anode}, A·cm^{-2}	1.31	1.31	1.31
$A_{cathode}$, cm^2	15.43	15.43	15.43
$j_{cathode}$, A·cm^{-2}	0.43	0.43	0.43
$E_{average \ net}$, V	3.48	3.46	3.44
CE, %	98.5	97.7	98.2
EC, kWh·kg^{-1}	7.8	7.8	7.7
EE, %	58.2	78.2	71.4
ACD, cm	2.0	2.0	2.0

Average Net Cell Voltage dropped 42 mV while the temperature was increased from 675°C to 725°C, Figure 39. Current efficiency was not affected much from the temperature difference and was almost constant around 98% for the three experiments conducted as it can be seen from Figure 40. Energy consumption was also almost constant at 7.78kWh·kg^{-1} as given in Figure 41. Similarly the energy efficiency curve was also stable and the energy efficiencies were around 80%, Figure 42.

The decrease in the magnitude of the peaks with the increased temperature implies that the observed voltage increase is related with the molten magnesium nucleation at the stainless steel cathode. Necessary activation energy required for the nucleation decreases with the increased temperature. The decrease in the average net cell voltage is due to the increase in electrolyte conductivity and decrease in standard decomposition potential at higher temperatures.

The model used for the calculation of net cell voltage in experiments involving the study of current density was also used to determine net cell voltage from theoretical values. The bubble size and velocity used here were the same as those corresponding to the 0.43 A·cm^{-2} current density. Electrolyte conductivity increases from 1.920 to 2.005 ohm^{-1}·cm^{-1} when the temperature increases from 700 to 725ºC for a 20%$MgCl_2$-40%NaCl-40%KCl electrolyte [2]. These values are extrapolated to 675ºC to obtain corresponding conductivity value.

The results of the calculations are given in Table 11. The results are in general agreement with the experimental measurements as it can be seen in Figure 43. However the experimentally obtained voltage is slightly larger than the calculated voltage at 725°C. Slight increase in net cell voltage curve at 725°C in Figure 37, might be related with the increased loss of $MgCl_2$ due to higher evaporation rate. Similar increases were also observed for Experiments 10 and 11 in Figure 27 as a result of larger composition change when more $MgCl_2$ electrolysis was done.
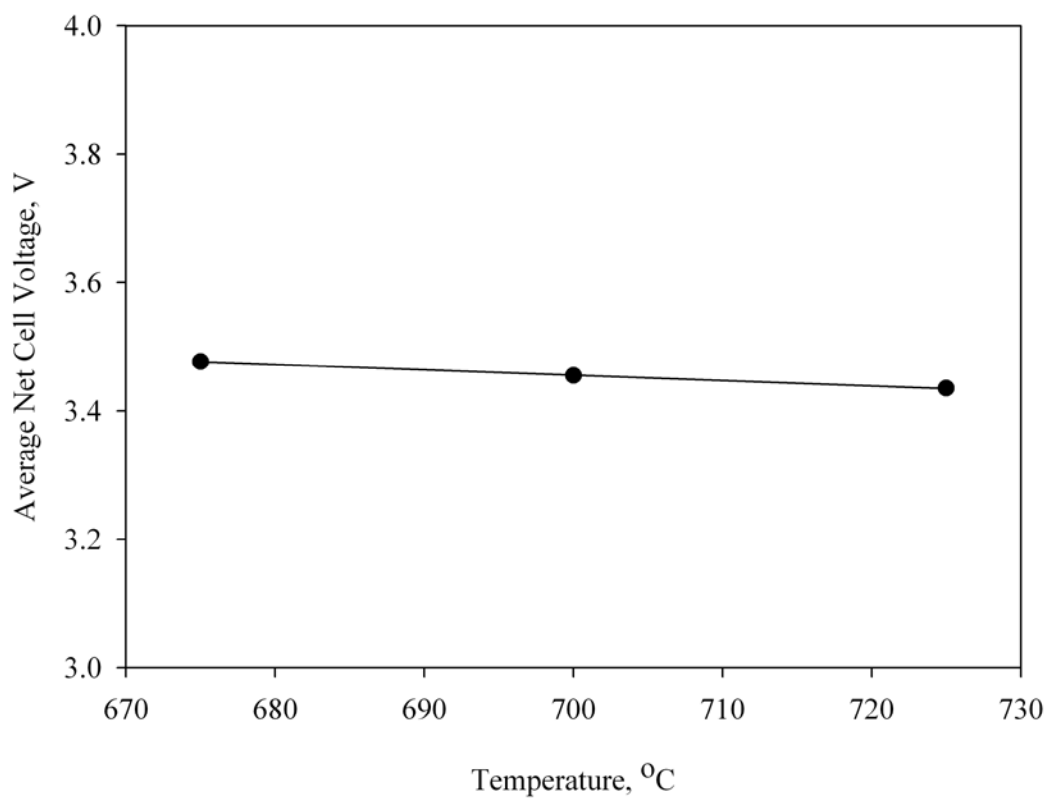
Figure 39 Average net cell voltages for the experiments involving the effect of temperature.
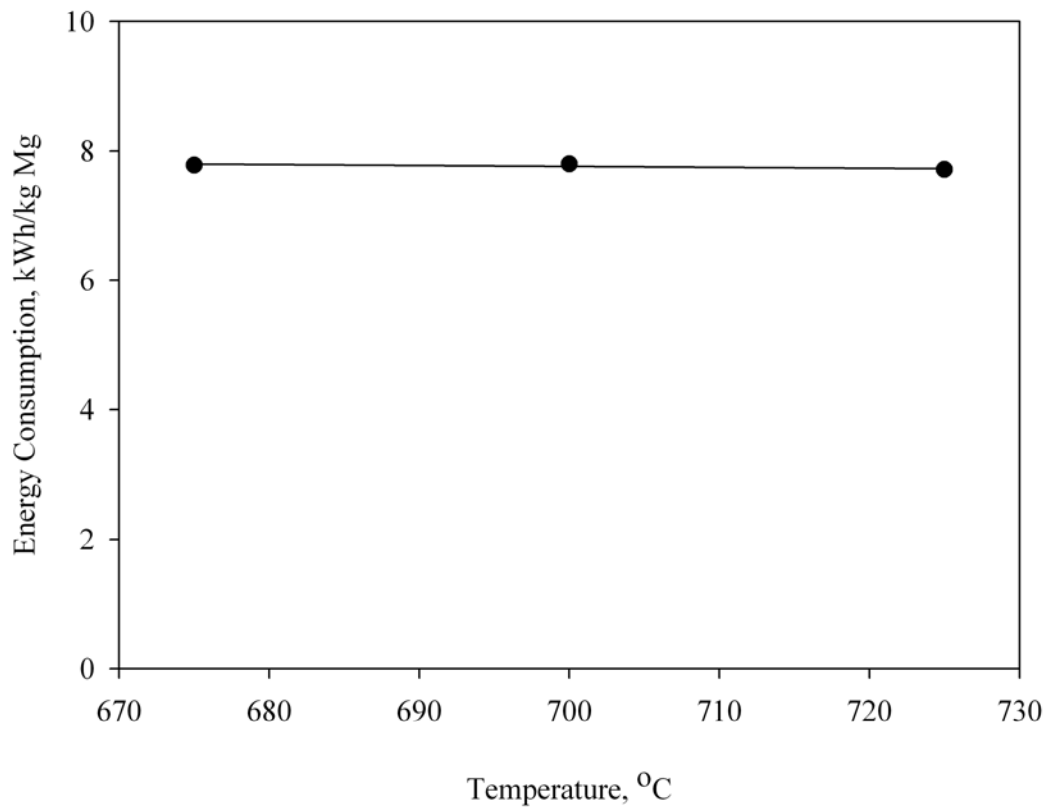
Figure 40 Current efficiencies for the experiments involving the effect of temperature.
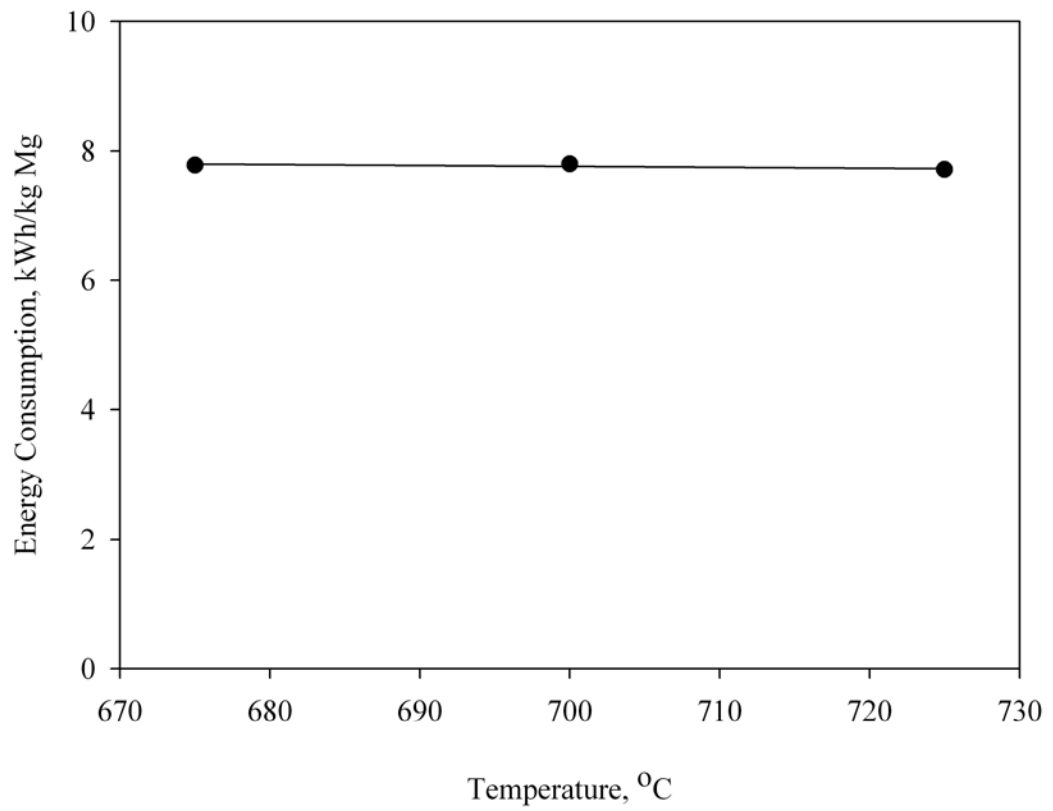
Figure 41 Energy consumptions for the experiments involving the effect of temperature.
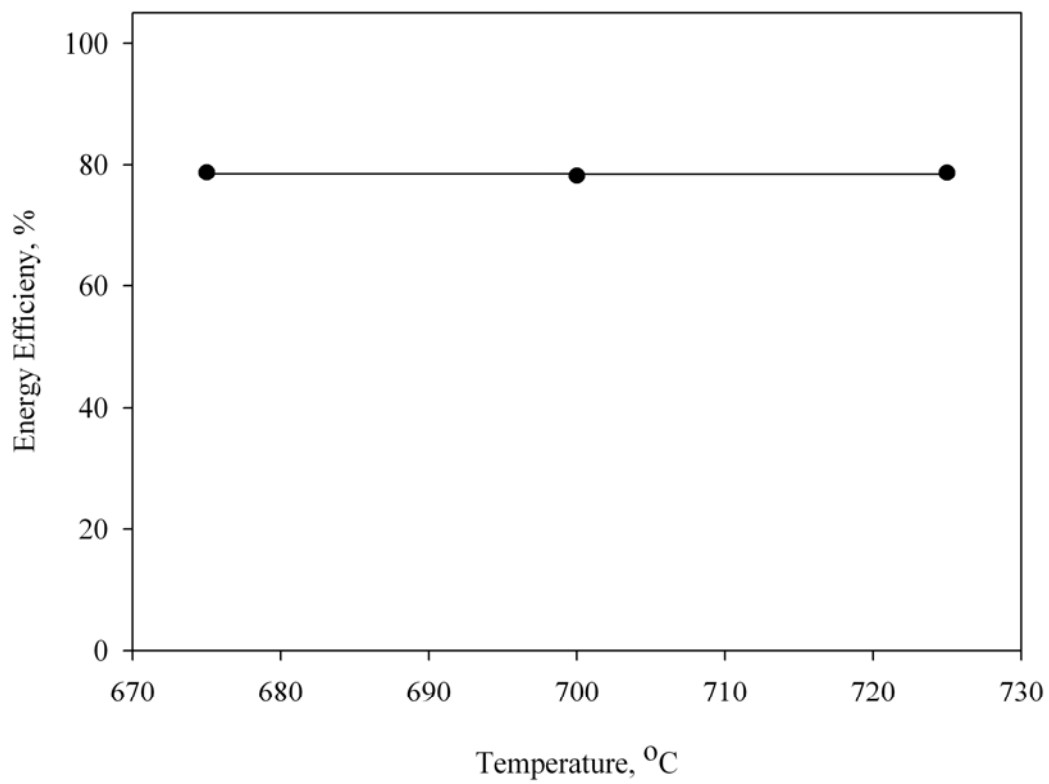
Figure 42 Energy efficiencies for the experiments involving the effect of temperature.

Table 11 Results of the net cell voltage calculations for the experiments involving the effect of temperature.

Experiment	12	9	13
ACD, cm	2.0	2.0	2.0
Mean Electrode Area, cm^2	10.22	10.22	10.22
Bubble Radius, r_b, cm	0.050	0.050	0.050
$A_{bubble\ cross\ section}$ x10^{-3}, cm^2	0.01	0.01	0.01
Residence Time, RT, second	0.050	0.050	0.050
Cl_2 production rate, $cm^3 \cdot sec^{-1}$	2.72	2.72	2.72
Bubble Volume x10^{-4}, cm^3	5.24	5.24	5.24
Bubble rate, bubbles$\cdot sec^{-1}$	5186	5186	5195
Blocked anode area, cm^2	2.04	2.04	2.04
Non blocked anode area, cm^2	2.96	2.96	2.96
Resistivity, ohm$\cdot$cm	0.49	0.48	0.45
Bubble Area Resistance, ohm	0.02	0.02	0.02
IR_{bubble}	0.11	0.11	0.10
ACD other than bubbles, cm	1.90	1.90	1.90
Electrolyte Resistance, ohm	0.091	0.088	0.084
$IR_{electrolyte}$	0.594	0.580	0.550
$E_{th}+IR_{bubble}+IR_{electrolyte}$	3.481	3.451	3.401
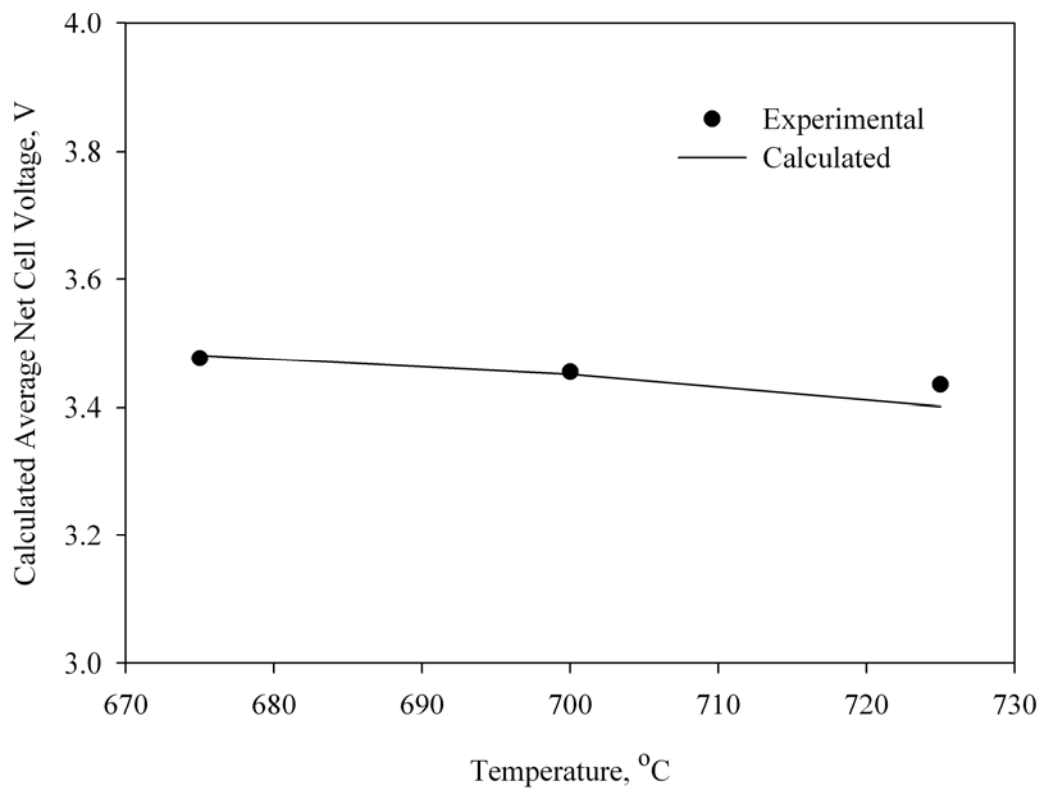
Figure 43 Calculated average net cell voltages for the experiments involving the effect of temperature.

The morphology of magnesium deposition at the cathode was not influenced much from the temperature variation, see Figure 44. Two large droplets at the 675°C experiment were detached from the cathode during withdrawal of the electrode after electrolysis. As it can be seen in pictures most of the metallic magnesium remains on cathode surface in all of these experiments. Therefore, change of temperature within the limits used in this study was not enough to change the form of magnesium on cathode. Because of the $MgCl_2$ loss inferred from the cell voltage increase, it is decided that the temperature must be kept as low as possible. Therefore 700°C was used for the remaining experiments to not to lose more $MgCl_2$ and ensure a molten electrolyte with changing chemical composition.

675°C

700°C

725°C
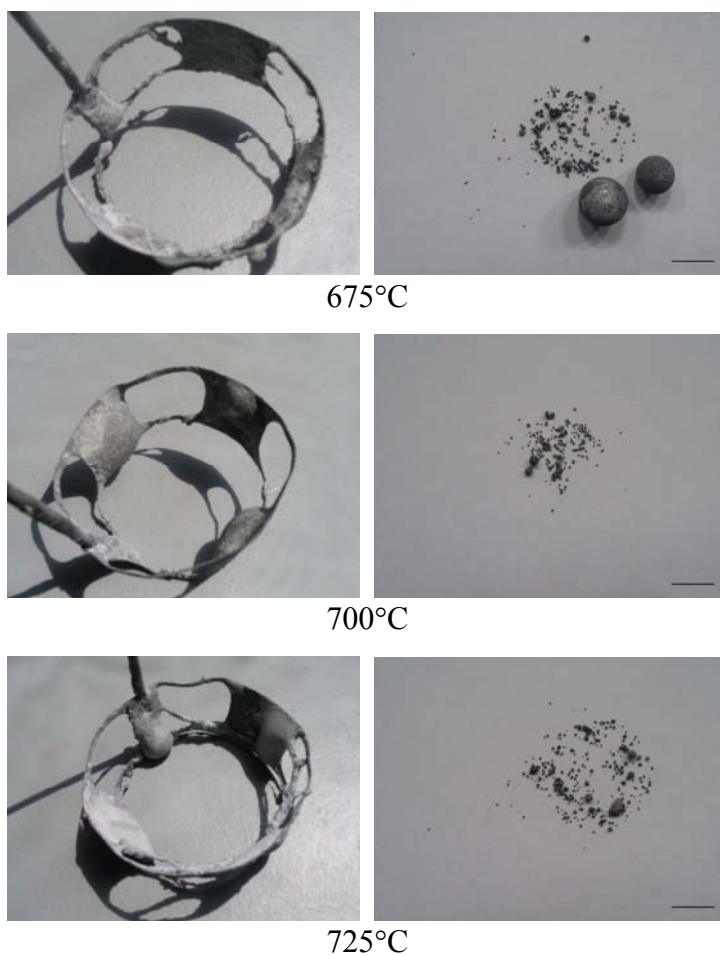
Figure 44 Cathodes and magnesium droplets for the experiments involving the effect of temperature (length of the line is 1 cm).

4.3. The Effect of Cathode Surface

Since the cathode surface condition could effect the detachment of deposited molten magnesium, experiments were conducted to see the effect of used, polished and scratched cathode surfaces. Scratched cathode was made by forming vertical scratches with no.200 abrasive paper. The electrolyte composition was again 20% $MgCl_2$, 39.5% NaCl, 39.5% KCl and 1% NaF. The ACD and the current density were 20 mm and 0.42-0.43 $A \cdot cm^{-2}$ respectively.

Peaks were observed at the beginning of the experiments and the cell voltage was stabilized afterwards as in the case of much of the previous experiments, Figure 45. The difference in cell voltage curves was remarkable between the polished and the scratched cathodes. The cell voltage showed a large peak when polished cathode was used. A steady decrease in cell voltage was observed for the scratched cathode during the initial 60 minutes electrolysis duration. A slight increase in cell voltage was observed after that period. The details of the experiments and the results obtained from the calculations based on the cell voltage and the collected metallic magnesium were summarized in Table 12.

Despite the changes in cell voltage no remarkable change obtained at different cathode surfaces conditions when current efficiency was considered. Current efficiency was around 98% for all three experiments conducted.

Energy consumption at the used cathode was similar to the energy consumption at the polished cathode, 7.78 and 7.80 $kWh \cdot kg^{-1}$ Mg respectively. 0.19 kWh decrease in energy consumption was obtained at scratched cathode with respect to polished cathode per kg of magnesium produced. Energy efficiencies were similar and they were around 80%.

90
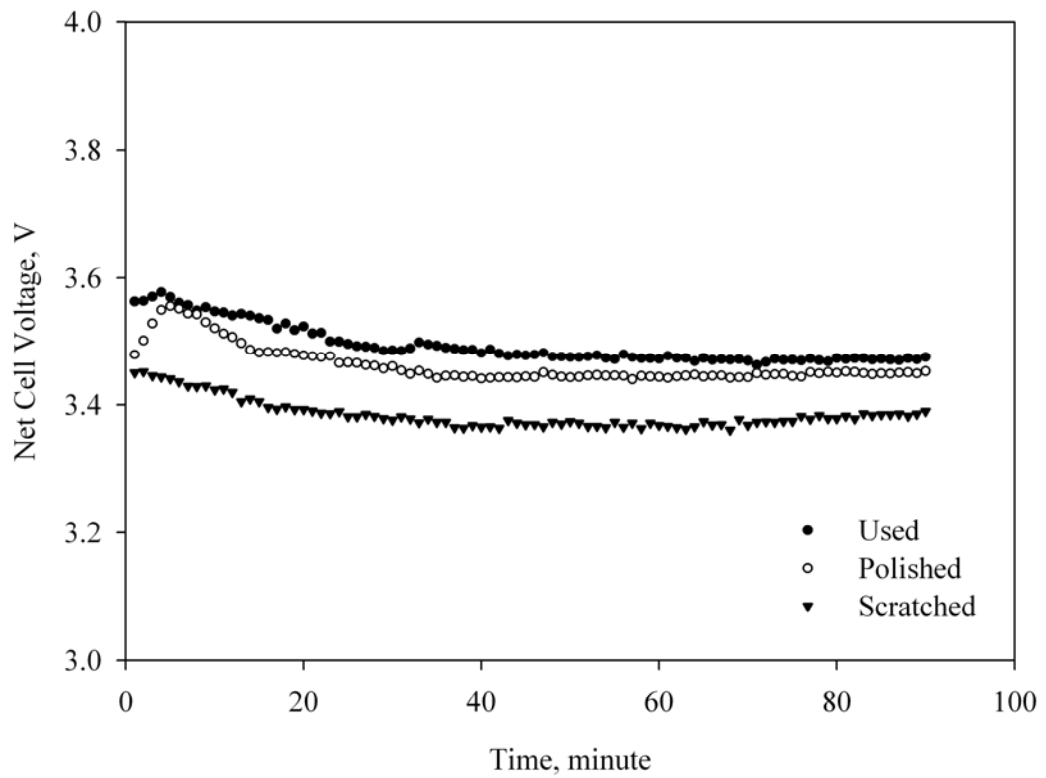
Figure 45 Net cell voltage vs. time at 20 mm ACD for the experiments involving the effect cathode surface.

Table 12 The details of the experiments involving the effect of cathode surface.

Experiment	14	9	15
Cathode Surface	Used	Polished	Scratched
$MgCl_2$, wt%	20.4	20.1	20.3
NaCl, wt%	39.3	39.5	39.3
KCl, wt%	39.3	39.5	39.3
$CaCl_2$, wt%	0.0	0.0	0.0
NaF, wt%	1.0	1.0	1.0
Total Salt, g	159.7	159.7	159.6
T, °C	700	700	700
E^0, V	2.51	2.51	2.51
a_{MgCl_2} (mean)	0.0025	0.0025	0.0025
$E_{th\ (mean)}$, V	2.77	2.77	2.77
$\kappa_{(mean)}$, ohm^{-1}·cm^{-1}	2.09	2.10	2.09
t, min	90	90	90
$Mg_{collected}$, g	4.402	4.359	4.3801
$Mg_{theoretical}$, g	4.455	4.462	4.462
I, A	6.55	6.56	6.56
A_{anode}, cm^2	5.0	5.0	5.0
j_{anode}, A·cm^{-2}	1.31	1.31	1.31
$A_{cathode}$, cm^2	15.4	15.4	15.4
$j_{cathode}$, A·cm^{-2}	0.42	0.43	0.43
$E_{average\ net}$, V	3.49	3.46	3.38
CE, %	98.8	97.7	98.2
EC, kWh·kg^{-1}	7.8	7.8	7.6
EE, %	78.4	78.2	80.4
ACD, cm	2.0	2.0	2.0

The decrease at the initial peak of the scratched cathode surface voltage variation curve demonstrated that the initial peaks were related with the nucleation phenomena. The increase in the number of available nucleation sites at the scratched cathode decreased the necessary activation energy for nucleation and the cell voltage decreased accordingly. Cell voltage at the scratched cathode remained also well below the polished cathode voltage during the entire electrolysis.

The cell voltage was higher in experiments involving the used cathode. This may be due to probably increased electrical resistance at the cathode surface. It might be due to a layer of higher electrical resistance, like magnesium bearing intermetallics or oxides unintentionally formed as a result of processes took place during or after the previous electrolysis experiments. Alternatively, chromium and nickel oxide concentrations at the surface of the stainless steel cathode might have been increased during cleaning with HCl solution.

Cathodes and the magnesium particles found in the frozen salt are shown in Figure 46. Two droplets found in scratched cathode experiment were probably formed after the electrolysis during the withdrawal of the cathode. The amount of fine magnesium particles was similar for scratched and polished cathodes. However most of the magnesium was found as droplets in used cathode experiments indicating the surface was affected by the previous experiment with the cathode. Therefore detachment of magnesium droplets from the cathode surface was obtained to a certain extent when used cathode was employed in electrolysis experiments. Detailed chemical analysis of magnesium obtained from Experiment 15 is given in Appendix.

High current efficiency obtained and many of the droplets being attached to the cathode surface right after the experiment indicates that, a large portion of the droplets were still cathodic during the experiment involving the used cathode. Therefore operation of the cell with above condition may still have the danger of short circuiting during the long electrolysis duration.

93
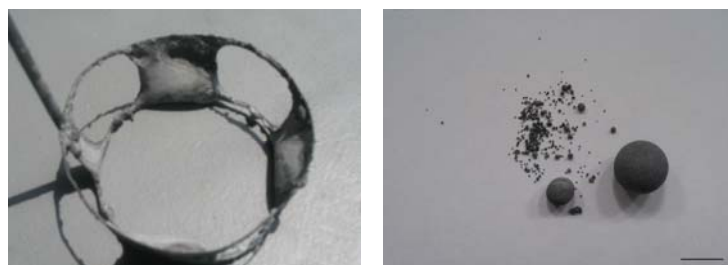
Scratched Cathode

Polished Cathode

Previously Used Cathode

Figure 46 Cathodes and magnesium droplets obtained from the experiments involving the effect cathode surface (length of the line is 1 cm).

4.4. The Effect of Sodium Chloride / Potassium Chloride Ratio

To enhance detachment of molten magnesium from cathode surface, effect of chemical composition of the electrolyte was also considered. The first set of experiments involved the use of different NaCl/KCl ratios in the electrolyte. Initial $MgCl_2$ and NaF concentrations were kept constant at 20% and 1% respectively. Two inter-electrode distances were employed and the temperature was 700°C in all these experiments.

Net cell voltage variations with time during these experiments are given in Figure 47 and Figure 48. The shapes of the curves at low NaCl concentrations are similar to the curves obtained from experiments involving the use of 0.42-0.43 $A \cdot cm^{-2}$ current density. The cell voltage formed a peak at the beginning and remained stable until the end of the experiment. However the cell voltage variation with time changes drastically at NaCl concentrations higher than 50%.

To calculate theoretical decomposition voltage, $MgCl_2$-NaCl-KCl ternary isoactivity diagram given in Figure 49 was used. The points corresponding to the initial and the final compositions of electrolytes used in this study are shown by filled and empty circles respectively. The change in specific conductivity of the electrolyte with the NaCl content at 10 and 20% $MgCl_2$ is given in Figure 50. Conductivity of the average electrolyte composition was found by interpolating the values at 10 and 20% $MgCl_2$. The summary of the results and the calculations for the NaCl/KCl ratio experiments are given in Table 13.
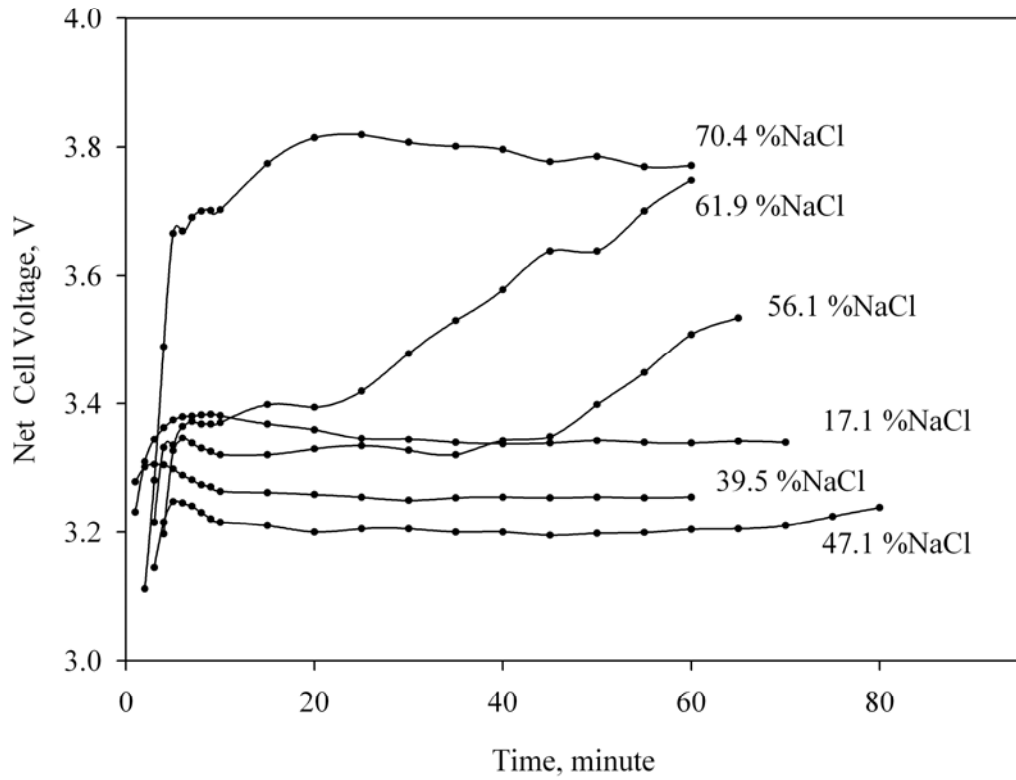
Figure 47 Net cell voltage vs. time at 13 mm ACD for the experiments involving the effect of NaCl/KCl ratio.
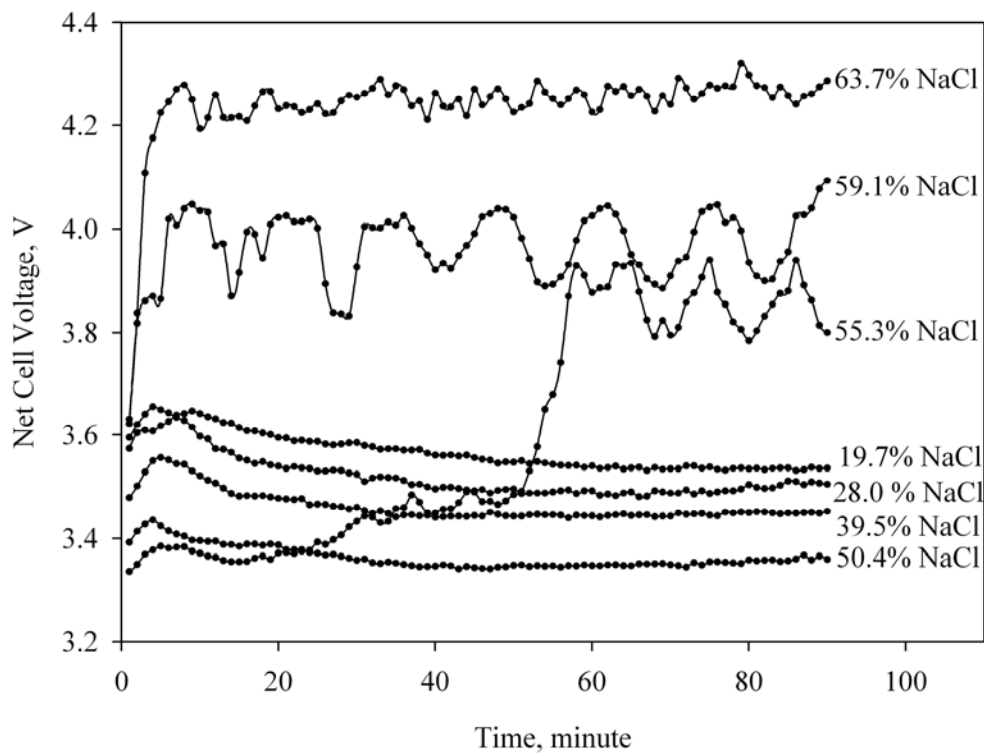
Figure 48 Net cell voltage vs. time at 20 mm ACD for the experiments involving the effect of NaCl/KCl ratio.
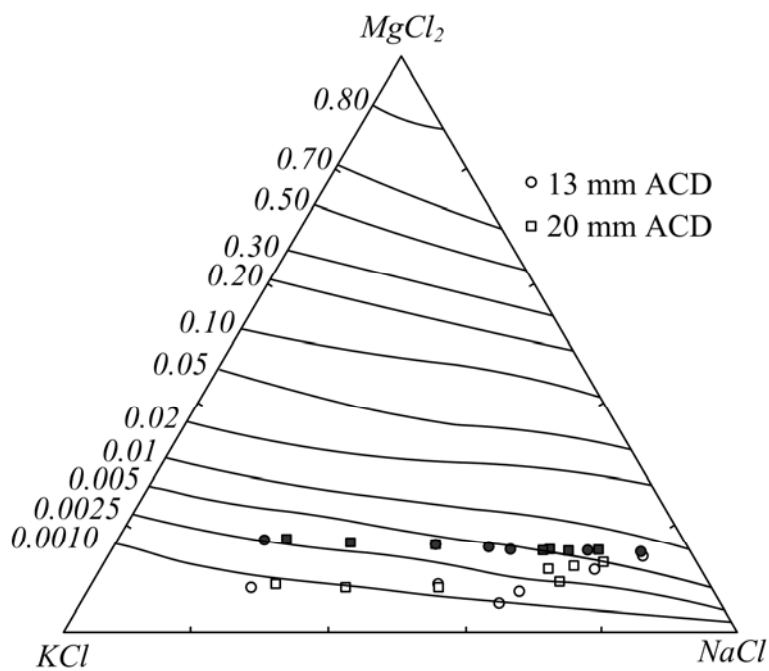
Figure 49 MgCl$_2$ isoactivity lines in MgCl$_2$-NaCl-KCl ternary [50].
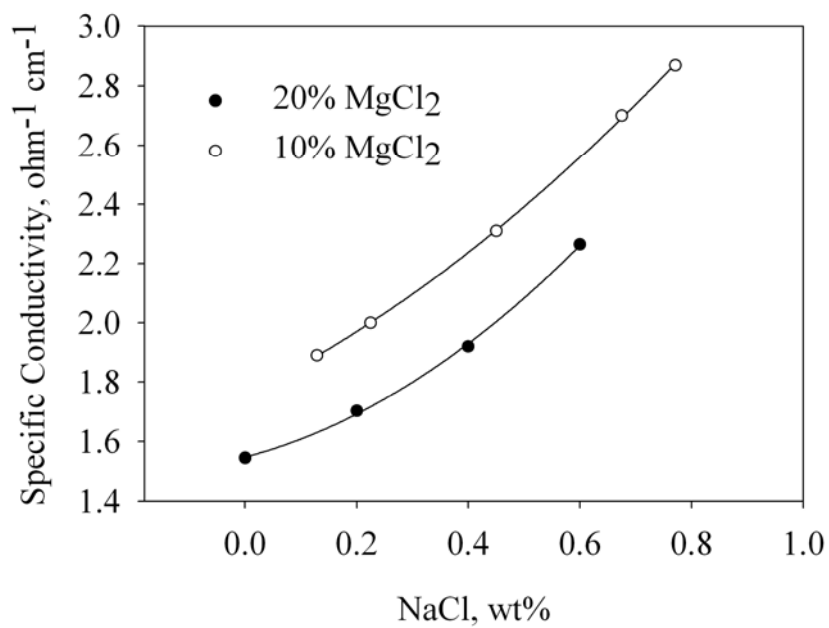
Figure 50 Specific conductivity of the MgCl$_2$-NaCl-KCl electrolyte.

Table 13 The details of the experiments involving the effect of NaCl/KCl ratio.

Experiment	15	4	16	17	18	19
$MgCl_2$, wt%	20.0	20.2	20.0	20.0	20.0	20.0
NaCl, wt%	17.1	39.4	47.1	56.1	61.9	70.4
KCl, wt%	61.9	39.4	31.9	22.9	17.1	8.6
$CaCl_2$, wt%	0.00	0.00	0.00	0.00	0.00	0.00
NaF, wt%	1.00	1.00	1.00	1.00	1.00	1.00
Total Salt, g	100.0	100.2	100.0	100.0	100.0	100.0
T, °C	700	700	700	700	700	700
E^0, V	2.514	2.514	2.514	2.514	2.514	2.514
a_{MgCl_2} (mean)	0.0015	0.0025	0.0030	0.0049	0.0059	0.0045
$E_{th\ (mean)}$, V	2.787	2.766	2.758	2.737	2.730	2.741
$\kappa_{(mean)}$, ohm^{-1}·cm^{-1}	1.813	2.085	2.300	2.354	2.398	2.494
t, min	70	60	80	65	60	60
$Mg_{collected}$, g	2.859	2.552	3.582	2.245	1.370	0.314
$Mg_{theoretical}$, g	3.153	2.702	3.603	2.928	2.702	2.702
I, A	5.96	5.96	5.96	5.96	5.96	5.96
A_{anode}, cm^2	4.5	4.5	4.5	4.5	4.5	4.5
j_{anode}, A·cm^{-2}	1.32	1.32	1.32	1.32	1.32	1.32
$A_{cathode}$, cm^2	14.1	13.0	13.0	13.1	14.1	13.1
$j_{cathode}$, A·cm^{-2}	0.42	0.46	0.46	0.45	0.42	0.45
$E_{average\ net}$, V	3.347	3.255	3.207	3.377	3.552	3.783
CE, %	90.7	94.4	99.4	76.7	50.7	11.6
EC, kWh·kg^{-1}	8.1	7.6	7.1	9.7	15.4	71.8
EE, %	49.1	60.5	71.3	53.5	34.2	7.7
ACD, cm	1.3	1.3	1.3	1.3	1.3	1.3

Table 13 (continued).

Experiment	20	9	21	22	23	24	25
$MgCl_2$, wt%	20.4	20.1	20.1	19.7	19.6	19.7	20.1
NaCl, wt%	19.7	28.0	39.5	50.4	55.3	59.1	63.7
KCl, wt%	59.0	50.9	39.5	29.0	24.1	20.1	15.3
$CaCl_2$, wt%	0.0	0.0	0.0	0.0	0.0	0.0	0.0
NaF, wt%	1.0	1.0	1.0	1.0	1.0	1.0	1.0
Total Salt, g	157.7	157.1	159.7	158.9	159.3	159.0	157.1
T, °C	700	700	700	700	700	700	700
E^0, V	2.514	2.514	2.514	2.514	2.514	2.514	2.514
a_{MgCl_2} (mean)	0.0018	0.0019	0.0025	0.0043	0.0038	0.0050	0.0071
$E_{th\ (mean)}$, V	2.779	2.777	2.766	2.743	2.748	2.737	2.722
$\kappa_{(mean)}$, ohm^{-1}·cm^{-1}	1.827	1.941	2.101	2.301	2.278	1.941	2.393
t, min	90	90	90	90	90	90	90
$Mg_{collected}$, g	4.380	4.393	4.359	4.401	2.083	1.725	1.335
$Mg_{theoretical}$, g	4.462	4.455	4.462	4.448	4.448	4.441	4.543
I, A	6.56	6.55	6.56	6.54	6.54	6.53	6.68
A_{anode}, cm^2	5.0	5.0	5.0	5.0	5.0	5.0	5.0
j_{anode}, A·cm^{-2}	1.31	1.31	1.31	1.31	1.31	1.31	1.34
$A_{cathode}$, cm^2	15.4	15.3	15.4	15.4	15.4	15.4	15.4
$j_{cathode}$, A·cm^{-2}	0.43	0.43	0.43	0.42	0.42	0.42	0.43
$E_{average\ net}$, V	3.560	3.510	3.455	3.359	3.611	3.973	4.253
CE, %	98.2	98.6	97.7	98.9	46.8	38.8	29.4
EC, kWh·kg^{-1}	8.0	7.8	7.8	7.5	17.0	22.6	31.9
EE, %	50.4	54.5	78.2	67.8	29.5	19.0	18.8
ACD, cm	2.0	2.0	2.0	2.0	2.0	2.0	2.0

As it can be seen in Figure 51, the cell voltage slightly decreased as the NaCl concentration increased. However, the average net cell voltage curve deviated considerably when NaCl concentration became higher than about 50%. Cell voltage continued to increase with increasing NaCl concentration after about 50%.

Effect of NaCl concentration on current efficiency during $MgCl_2$ electrolysis is given in Figure 52. The current efficiency increased slightly with increasing NaCl content at low concentrations, and then it decreased drastically as the NaCl content increased further beyond 50% NaCl.

From the average net cell voltage and the current efficiency values obtained, energy consumption per kg of magnesium deposited were calculated and plotted in Figure 53. From the figure it can be seen that energy consumption increased drastically when NaCl concentration became higher than 50%.

A corresponding fall in energy efficiency, as shown in Figure 54, was obtained. However energy consumptions less than 8.0 kWh for 1 kg of magnesium metal were easily obtained with the present cell design at NaCl concentrations less than 50%.
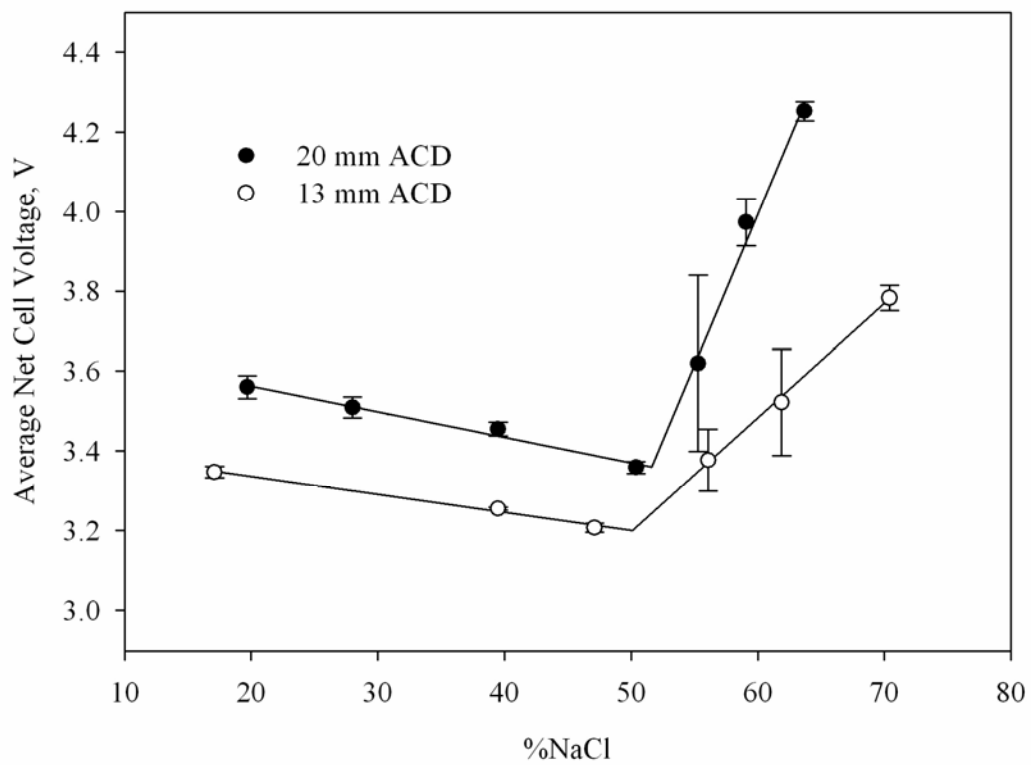
Figure 51 Average net cell voltages of the experiments involving the effect of NaCl/KCl ratio.
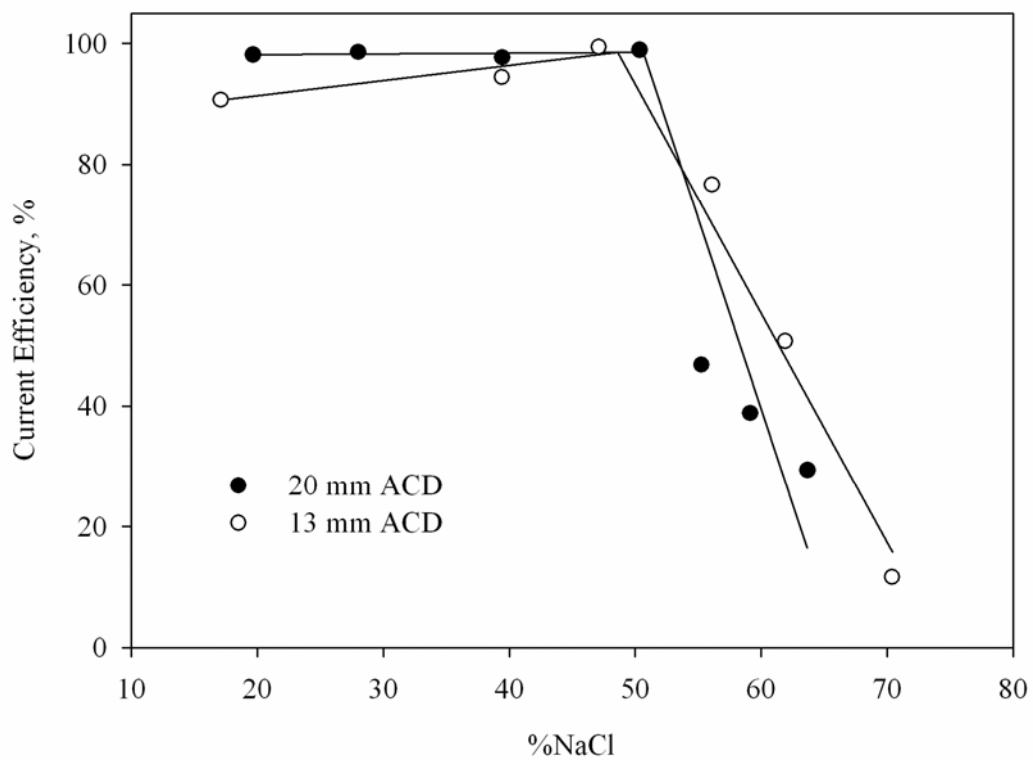
Figure 52 Current efficiencies for the experiments involving the effect of NaCl/KCl ratio.
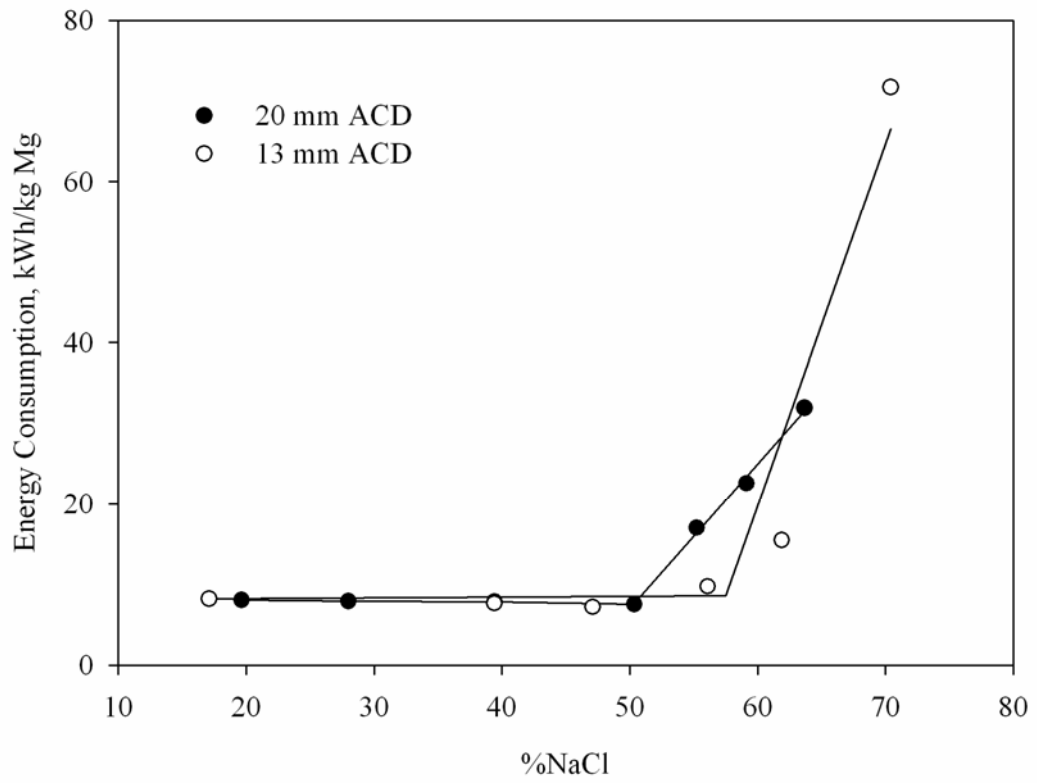
Figure 53 Energy consumptions for the experiments involving the effect of NaCl/KCl ratio.
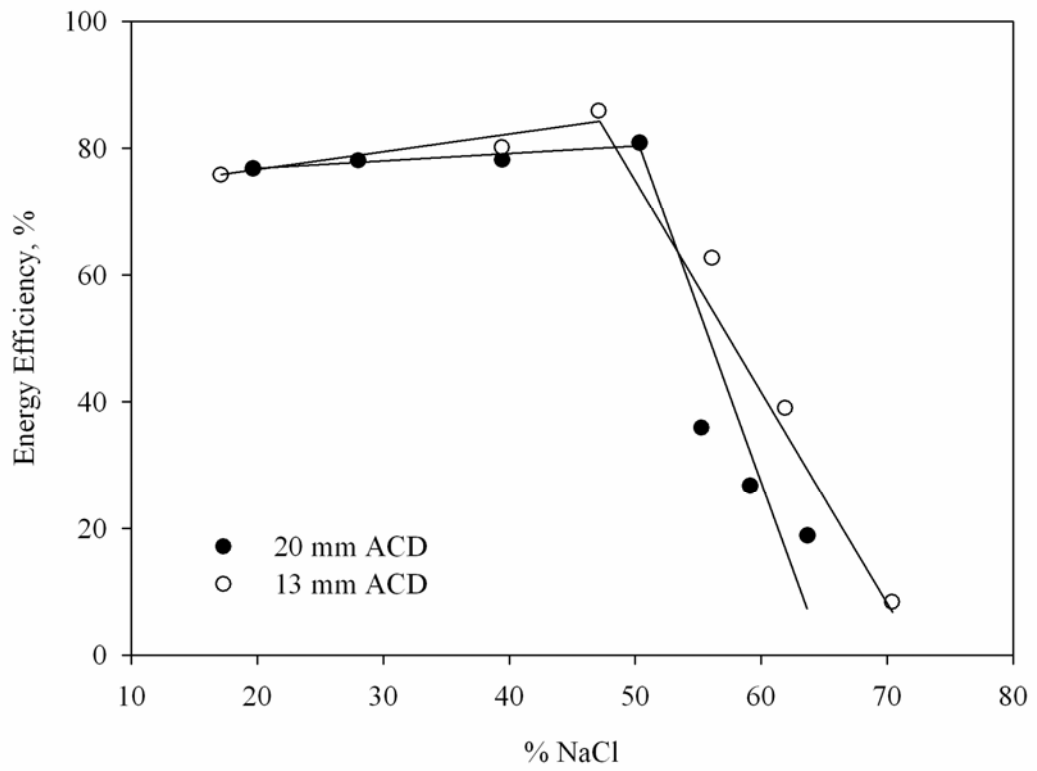
Figure 54 Energy efficiencies for the experiments involving the effect of NaCl/KCl ratio.

One of the reasons for the initial decrease in cell voltage with NaCl addition was the increase in electrical conductivity of the melt. Conductivity increased with an increase in NaCl/KCl ratio and IR drop decreased accordingly. The other reason is the increase in $MgCl_2$ activity with increasing NaCl concentration.

To calculate average net cell voltage, in addition to Eth, IR drop was necessary. The model that was used previously was applied to determine the IR drop in experiments involving the variation of NaCl:KCl ratio. The same bubble diameter and residence time, d_b=0.05 cm and RT=0.05 second respectively, were used in these computations. The resistance across the electrolyte was calculated for the two inter-electrode distances. The area current density was calculated by taking the average of the anode and cathode areas. Then IR drop was determined from Equations (61) and (62) for the specified ACD. Next the IR drops for both electrolyte and bubble region were added to the theoretical decomposition voltage to determine average net cell voltage. The results can be seen in Table 14 and the calculated cell voltages up to about 50% NaCl concentrations are given by full lines in Figure 55. Theoretical decomposition potential for $MgCl_2$ in $MgCl_2$-NaCl-KCl electrolytes were also calculated and plotted by dotted line in Figure 55. The decrease in net cell voltage due to increased $MgCl_2$ activity and electrolyte conductivity at compositions up to about 50% NaCl is in good agreement with experimentally observed values.

Table 14 Results of the net cell voltage calculations for the experiments involving the effect of NaCl/KCl ratio.

Experiment	15	4	16	20	9	21	22
ACD, cm	1.3	1.3	1.3	2.0	2.0	2.0	2.0
Mean Electrode Area, cm^2	9.31	8.75	8.75	10.22	10.15	10.22	10.22
Bubble Radius, r_b, cm	0.050	0.050	0.050	0.050	0.050	0.050	0.050
$A_{bubble\ cross\ section}$ x10^{-3}, cm^2	0.01	0.01	0.01	0.01	0.01	0.01	0.01
Residence Time, RT, second	0.050	0.050	0.050	0.050	0.050	0.050	0.050
Cl_2 production rate, $cm^3 \cdot sec^{-1}$	2.467	2.467	2.467	2.716	2.712	2.716	2.707
Bubble Volume x10^{-4}, cm^3	5.24	5.24	5.24	5.24	5.24	5.24	5.24
Bubble rate, bubbles$\cdot sec^{-1}$	4712	4712	4712	5187	5179	5187	5171
Blocked anode area, cm^2	1.85	1.85	1.85	2.04	2.03	2.04	2.03
Non blocked anode area, cm^2	2.65	2.65	2.65	2.96	2.97	2.96	2.97
Resistivity, ohm$\cdot$cm	0.55	0.48	0.43	0.55	0.52	0.48	0.43
Bubble Area Resistance, ohm	0.02	0.02	0.02	0.02	0.02	0.02	0.01
IR_{bubble}	0.12	0.11	0.10	0.12	0.11	0.11	0.10
ACD other than bubbles, cm	1.200	1.200	1.200	1.900	1.900	1.900	1.900
Electrolyte Resistance, ohm	0.071	0.066	0.060	0.102	0.096	0.089	0.081
$IR_{electrolyte}$	0.424	0.392	0.355	0.668	0.632	0.581	0.529
$E_{th}+IR_{bubble}+IR_{electrolyte}$	3.335	3.266	3.211	3.568	3.523	3.452	3.367
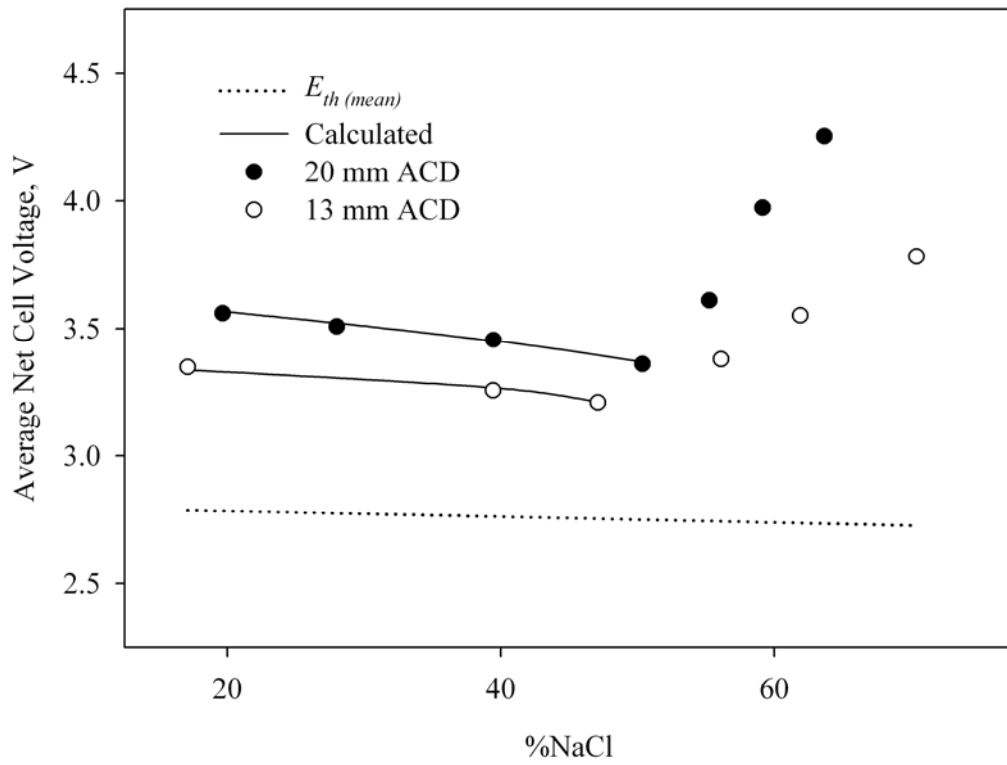
Figure 55 Calculated net cell voltages for the experiments involving the effect of NaCl/KCl ratio.

Examinations of average net cell voltages and current efficiencies at concentrations higher than 50% NaCl, indicates a different electrolysis mechanism than electrolysis at concentrations lower than 50% NaCl. In order to understand the mechanism of the processes, deposited samples obtained from experiments with NaCl concentrations higher than 39.5% were subjected to chemical analysis for Na and K. Results are given in Figure 56 and Appendix. As it can be seen from this figure, increased NaCl concentration in electrolyte increases Na codeposition. Sodium is relatively more volatile than magnesium. It has a vapor pressure of 0.197 atm at 1000K [58], that is very close to operating temperature in this study. Codeposition of Na could result in formation of Na vapor at the cathode. This could cover the electrode surface. Blocking of cathode surface could cause an increase in cell voltage at the same time a decrease in current efficiency. Therefore an average net cell voltage calculation was not done for electrolytes with NaCl concentrations higher than 50%.

Cathode and magnesium particle photographs taken after the experiments were given in Figure 57. Large droplets dropped from the cathode during the cathode withdrawal from the melt after the electrolysis while the magnesium was still molten. They should be excluded from the size comparisons. Amount of the fine particles were nearly constant up to 50%NaCl and increased after that point with the further NaCl additions. Well-wetted regions were visible even at the cathode of the highest NaCl concentration. Small particle formation could not be related with the cathode wetting by magnesium metal due to better wetting at larger NaCl concentrations. Na deposition was considered to stimulate the fine magnesium particle formation that caused an additional efficiency loss beside the Na formation.

The problem associated with the excessive magnesium accumulation at the steel cathode cannot be solved with the variation in NaCl/KCl ratio. Magnesium accumulation may cause short circuiting of the electrodes except at concentrations higher than 50% NaCl where the current efficiency is unacceptably low.
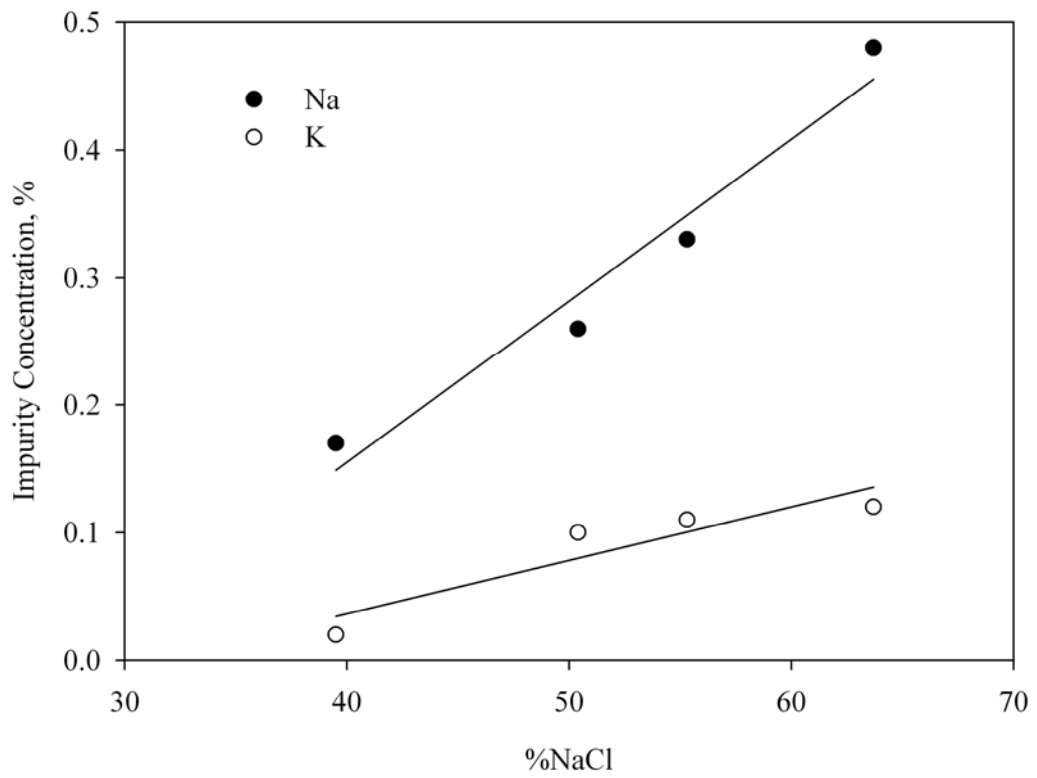
Figure 56 Sodium and Potassium concentrations in deposited magnesium.

19.7% NaCl

28% NaCl

39.5% NaCl

50.4% NaCl

Figure 57 Cathodes and Magnesium particles found among the electrolyte in NaCl
concentration experiments (length of the line is 10 mm).

55.3% NaCl

59.1% NaCl

63.7% NaCl

Figure 57 (continued).

4.5. The Effect of Calcium Chloride

Detachment of liquid magnesium from cathode surface is also affected by the density of the electrolyte. The density of the electrolyte is very close to the molten magnesium density when there is no $CaCl_2$ present. In that case the separation of the magnesium from the cathode is slow. Furthermore, MgO deposition increases the weight of the magnesium droplets and they may sink to the bottom of the electrolyte. Obviously the sinking of the magnesium particles decreases with the increased electrolyte density. Addition of $CaCl_2$ and $BaCl_2$ increase the electrolyte density and hence promote the separation of the molten magnesium from cathode.

Since calcium is commonly found in magnesium containing ores, some calcium is inevitably introduced into the electrolyte in industrial operations. Decomposition potential of $CaCl_2$ is larger than that of $MgCl_2$. Therefore calcium does not co-deposit appreciably along with the magnesium in normal operating conditions. Consequently, the calcium introduced into the cell within the feed material tends to accumulate inside the electrolyte. $CaCl_2$ was added up to about 30% to investigate its effect on cell performance. 20% $MgCl_2$ and 1% NaF was utilized along with 1:1 weight ratio of NaCl:KCl for the salt mixture. Since used cathodes yielded better detachment of magnesium droplets, these experiments employed cathodes that were previously used.

The net cell voltages recorded as a function of time are given in Figure 58 and Figure 59 for 13 mm and 20 mm ACD respectively. The cell voltage curves showed an initial peak at the beginning of the experiments and then decreased at 13 mm ACD experiments, except the experiment involving the 30% $CaCl_2$ addition. Similar behavior was observed at the 20 mm ACD experiments. However the cell voltage increased slightly after about 60 minutes in all 20 mm ACD experiments and there was an additional peak in the net cell voltage curves of experiments involving the use of more than 30% $CaCl_2$.
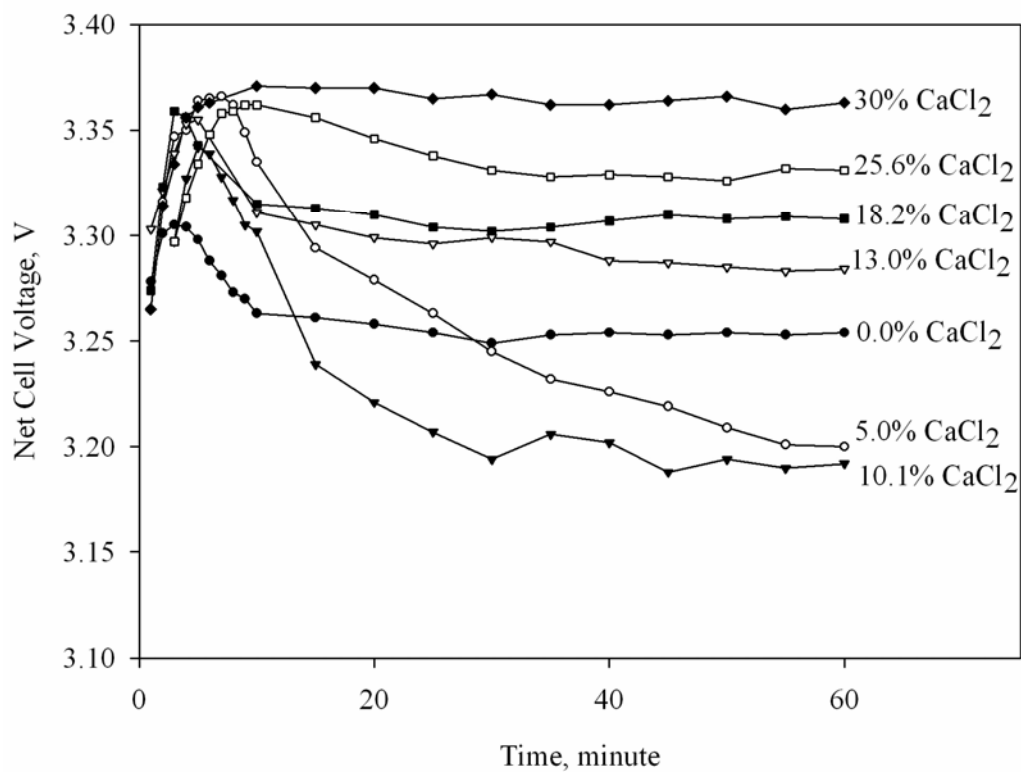
Figure 58 Net cell voltage vs. time at 13 mm ACD for experiments involving the effect of $CaCl_2$.
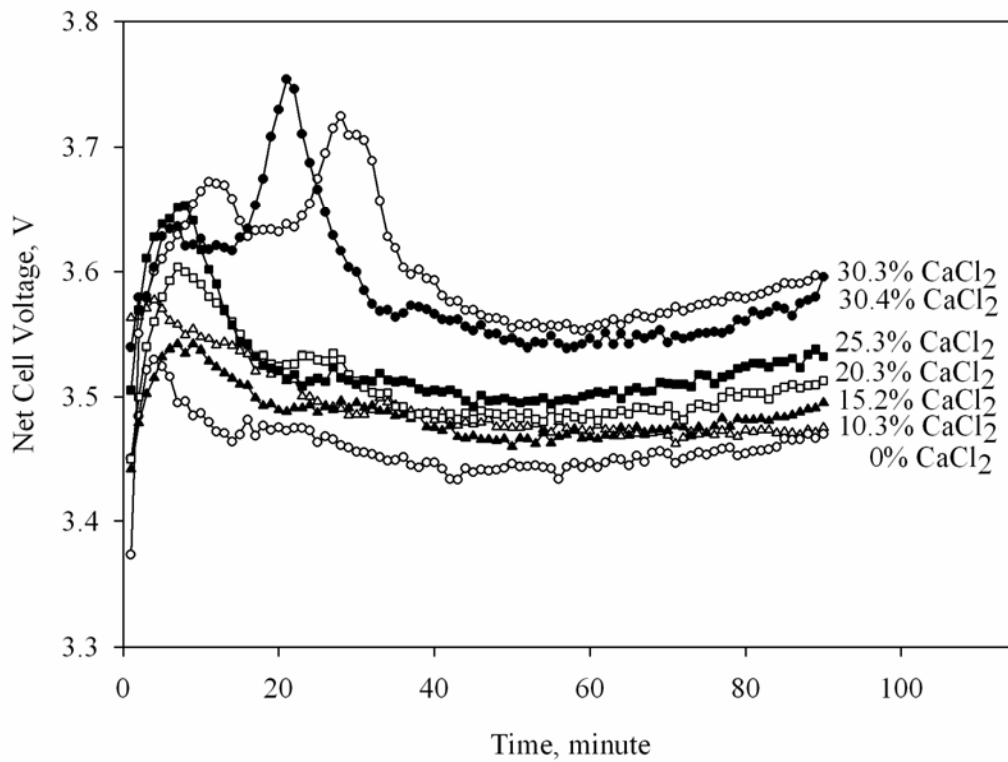
Figure 59 Net cell voltage vs. time at 20 mm ACD for the experiments involving the effect of CaCl$_2$.

Conductivity and the activity values are determined according to the average electrolyte composition during electrolysis. The conductivity of the electrolyte was determined by using experimentally determined values shown in Figure 60. The electrical conductivity value at 30% $CaCl_2$ in 20% $MgCl_2$ electrolyte was calculated from the other three data by assuming a line parallel to 10% $MgCl_2$ line. A linear variation of conductivity with $MgCl_2$ concentration was assumed to calculate conductivity of the electrolyte during electrolysis. The activities are calculated from the thermodynamic data available for $MgCl_2$-$CaCl_2$-NaCl [59] and $MgCl_2$-$CaCl_2$-KCl [60] systems at corresponding $MgCl_2$ and $CaCl_2$ concentrations. Then the average of the two activities was taken as the activity for $MgCl_2$-$CaCl_2$-1:1 NaCl:KCl electrolyte. Determined average net cell voltages along with other experimentally determined cell parameters, calculated properties of the electrolyte and experimental conditions are listed in Table 15.
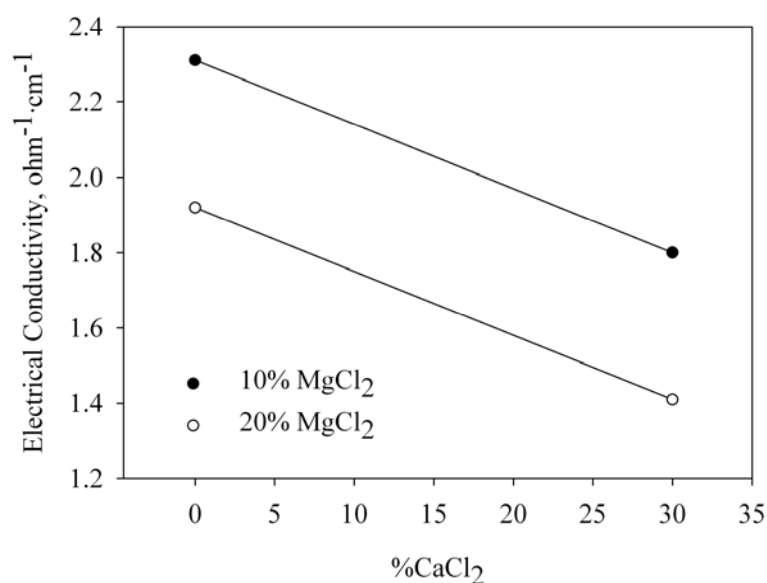
Figure 60 The conductivity of $MgCl_2$ -$CaCl_2$- balance (NaCl:KCl=1) system [2].

Table 15 The details of the experiments involving the effect of $CaCl_2$.

Experiment	4	26	27	28	29	30	31
$MgCl_2$, wt%	20.2	20.0	20.0	20.0	20.0	20.0	20.0
NaCl, wt%	39.4	37.0	34.4	33.0	30.4	26.7	24.5
KCl, wt%	39.4	37.0	34.4	33.0	30.4	26.7	24.5
$CaCl_2$, wt%	0.00	5.00	10.1	13.0	18.2	25.6	30.0
NaF, wt%	1.00	1.00	1.00	1.00	1.00	1.00	1.00
Total Salt, g	100.2	90.0	99.9	90.0	100.2	100	90.0
T, °C	700	700	700	700	700	700	700
E^0, V	2.514	2.514	2.514	2.514	2.514	2.514	2.514
$a_{MgCl_2\ (mean)}$	0.0025	0.0031	0.0045	0.0047	0.0070	0.0111	0.0141
$E_{th\ (mean)}$, V	2.766	2.756	2.741	2.739	2.722	2.703	2.693
$\kappa_{(mean)}$, ohm^{-1}·cm^{-1}	2.09	2.00	1.88	1.86	1.73	1.58	1.51
t, min	60	60	60	60	60	60	60
$Mg_{collected}$, g	2.552	2.292	2.132	2.322	2.044	1.775	1.554
$Mg_{theoretical}$, g	2.702	2.702	2.702	2.702	2.702	2.702	2.702
I, A	5.96	5.96	5.96	5.96	5.96	5.96	5.96
A_{anode}, cm^2	4.5	4.5	4.5	4.5	4.5	4.5	4.5
j_{anode}, A·cm^{-2}	1.32	1.32	1.32	1.32	1.32	1.32	1.32
$A_{cathode}$, cm^2	13.5	13.7	13.7	13.7	13.7	13.7	13.7
$j_{cathode}$, A·cm^{-2}	0.44	0.43	0.43	0.43	0.43	0.43	0.43
$E_{average\ net}$, V	3.255	3.246	3.212	3.294	3.308	3.337	3.367
CE, %	94.4	84.8	78.9	85.9	75.7	65.7	57.5
EC, kWh·kg^{-1}	7.6	8.4	9.0	8.5	9.6	11.2	12.9
EE, %	80.2	72.0	67.3	71.4	62.3	53.2	46.0
ACD, cm	1.3	1.3	1.3	1.3	1.3	1.3	1.3

Table 15 (continued).

Experiment	32	33	34	35	36	37	38
MgCl$_2$, wt%	20.4	19.2	18.8	19.0	19.0	19.2	19.2
NaCl, wt%	39.3	34.8	32.5	29.9	27.4	24.8	24.7
KCl, wt%	39.3	34.8	32.5	29.9	27.4	24.8	24.7
CaCl$_2$, wt%	0.0	10.3	15.2	20.3	25.3	30.3	30.4
NaF, wt%	1.0	1.0	1.0	1.0	1.0	1.0	1.0
Total Salt, g	159.7	158.7	157.6	157.4	158.0	158.3	158.9
T, °C	700	700	700	700	700	700	700
E^0, V	2.514	2.514	2.514	2.514	2.514	2.514	2.514
a_{MgCl_2} (mean)	0.0025	0.0036	0.0044	0.0062	0.0082	0.0117	0.0178
$E_{th \, (mean)}$, V	2.766	2.750	2.742	2.727	2.716	2.701	2.683
$\kappa_{(mean)}$, ohm^{-1}·cm^{-1}	2.09	1.95	1.88	1.77	1.68	1.57	1.57
t, min	90	90	90	90	90	90	90
$Mg_{collected}$, g	4.402	4.218	4.310	4.089	4.090	3.716	3.866
$Mg_{theoretical}$, g	4.454	4.441	4.455	4.455	4.462	4.455	4.455
I, A	6.55	6.53	6.55	6.55	6.56	6.55	6.55
A_{anode}, cm^2	5.0	5.0	5.0	5.0	5.0	5.0	5.0
j_{anode}, A·cm^{-2}	1.31	1.31	1.31	1.31	1.31	1.31	1.31
$A_{cathode}$, cm^2	15.4	15.4	15.4	15.4	15.4	15.4	15.4
$j_{cathode}$, A·cm^{-2}	0.42	0.42	0.42	0.42	0.43	0.42	0.42
$E_{average \, net}$, V	3.487	3.455	3.482	3.505	3.517	3.601	3.582
CE, %	98.8	95.0	96.8	91.8	91.7	83.4	86.8
EC, kWh·kg^{-1}	7.8	8.0	7.9	8.4	8.5	9.5	9.1
EE, %	78.4	75.6	76.2	71.4	70.8	62.6	65.0
ACD, cm	2.0	2.0	2.0	2.0	2.0	2.0	2.0

Average Net Cell Voltages obtained from 13 and 20mm ACD experiments were nearly parallel to each other, Figure 61. Curves started with a slight decrease in cell voltage until about 10% $CaCl_2$ and then increased with the further $CaCl_2$ addition. Current efficiency decreased as the $CaCl_2$ concentration increased, see Figure 62. The decrease was more pronounced at the lower ACD. As a result of the increased cell voltage and decreased current efficiency, energy consumption increased with the addition of $CaCl_2$ as can be seen in Figure 63. Energy consumption around 8kWh/kg Mg was obtained for both ACD's at small $CaCl_2$ concentrations. However, the energy consumption increased more at smaller ACD. Similarly, energy efficiency decreased more at the smaller ACD, see Figure 64.

The successive peaks observed at 20 mm ACD was considered as related with successive nucleation on top of previously deposited magnesium droplets. The cathodes of both Experiments 37 and 38 found as containing a 4-5 mm thick pile of magnesium particles below 1 mm diameter after the experiments. The successive peak formation will be discussed in more detail in the following section dealing with the effect of NaF addition.

The increases in the net cell voltage after about 60 minutes electrolysis in experiments involving the use of 20 mm ACD were due to the larger decrease in electrolyte conductivity resulting from the composition change. Similar increases were not observed in experiments involving the use of 13 mm ACD due to smaller composition change as a result of shorter duration of experiments.
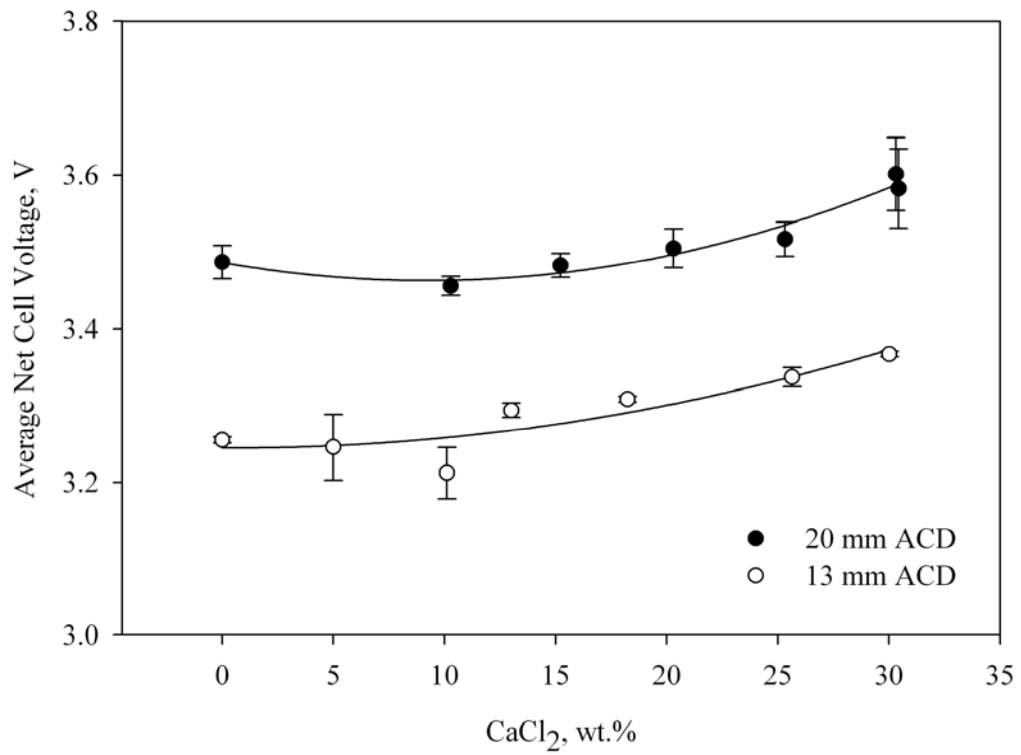
Figure 61 Average net cell voltages for the experiments involving the effect of CaCl$_2$.
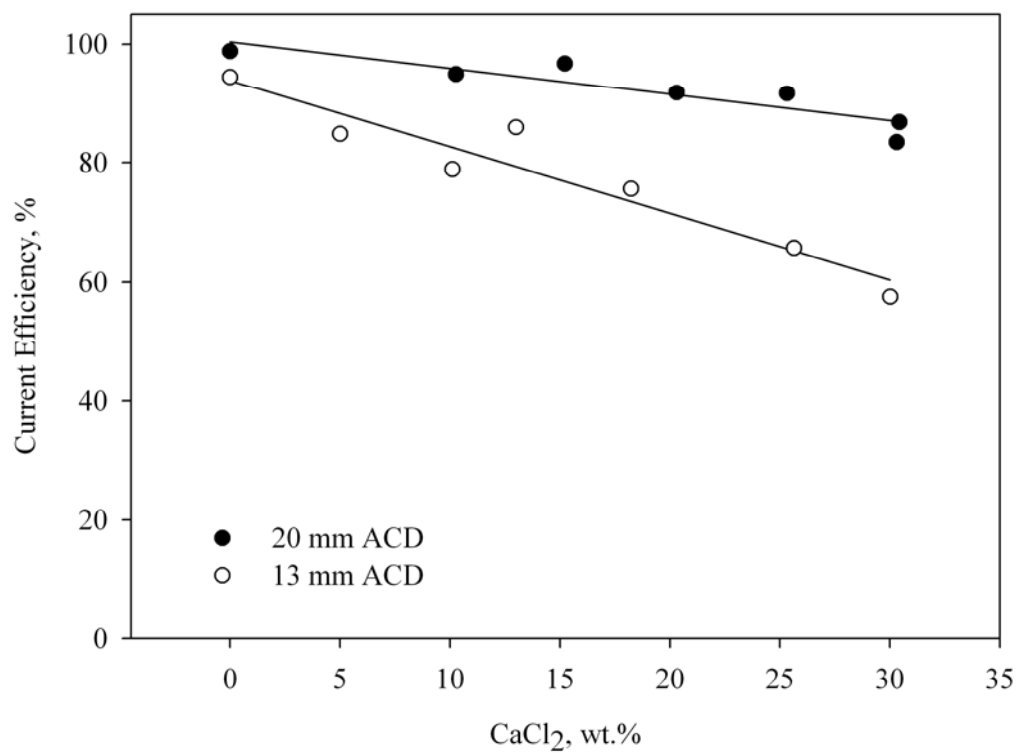
Figure 62 Current efficiencies for the experiments involving the effect of $CaCl_2$.
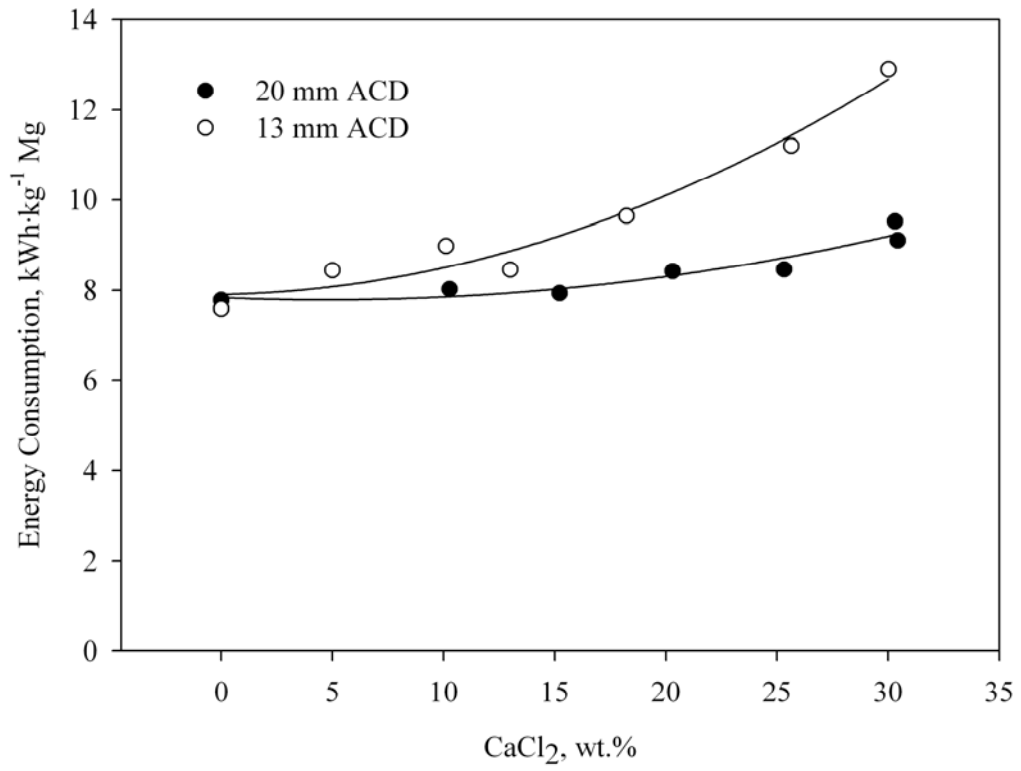
Figure 63 Energy consumptions for the experiments involving the effect of
$CaCl_2$.
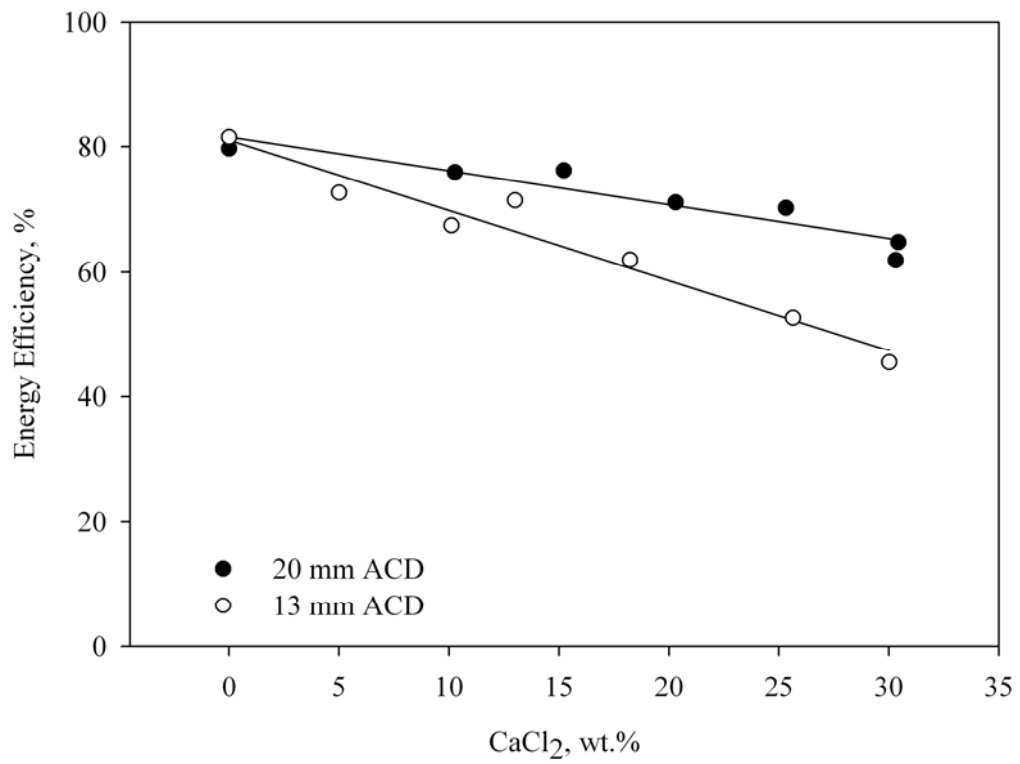
Figure 64 Energy efficiencies for the experiments involving the effect of $CaCl_2$.

CaCl$_2$ addition decreases the electrical conductivity of the electrolyte and increases the MgCl$_2$ activity. Therefore cell voltage is expected to increase due to lower electrical conductivity and decrease due to higher MgCl$_2$ activity. The calculations for cell voltage based on previously used model are given in Table 16 and Figure 65. As it can be seen from these computations, increasing CaCl$_2$ concentration made IR drop more effective and results in an increase in cell voltage in the composition range studied.

Table 16 Average net cell voltage calculations for the experiments involving the effect of CaCl$_2$.

Experiment	4	26	27	28	29	30	31
ACD, cm	1.3	1.3	1.3	1.3	1.3	1.3	1.3
Mean Electrode Area, cm^2	9.01	9.12	9.12	9.12	9.12	9.12	9.12
Bubble Radius, r_b, cm	0.050	0.050	0.050	0.050	0.050	0.050	0.050
$A_{bubble\ cross\ section}$ x10^{-3}, cm^2	0.01	0.01	0.01	0.01	0.01	0.01	0.01
Residence Time, RT, second	0.050	0.050	0.050	0.050	0.050	0.050	0.050
Cl$_2$ production rate, cm^3·sec^{-1}	2.467	2.467	2.467	2.467	2.467	2.467	2.467
Bubble Volume x10^{-4}, cm^3	5.24	5.24	5.24	5.24	5.24	5.24	5.24
Bubble rate, bubbles·sec^{-1}	4712	4712	4712	4712	4712	4712	4712
Blocked anode area, cm^2	1.85	1.85	1.85	1.85	1.85	1.85	1.85
Non blocked anode area, cm^2	2.65	2.65	2.65	2.65	2.65	2.65	2.65
Resistivity, ohm·cm	0.48	0.50	0.53	0.54	0.58	0.63	0.66
Bubble Area Resistance, ohm	0.02	0.02	0.02	0.02	0.02	0.02	0.03
IR_{bubble}	0.108	0.112	0.120	0.121	0.130	0.142	0.149
ACD other than bubbles, cm	1.200	1.200	1.200	1.200	1.200	1.200	1.200
Electrolyte Resistance, ohm	0.064	0.066	0.070	0.071	0.076	0.083	0.087
$IR_{electrolyte}$	0.381	0.392	0.417	0.421	0.452	0.495	0.521
E_{th}+IR_{bubble} +$IR_{electrolyte}$	3.254	3.260	3.277	3.281	3.305	3.340	3.363

Table 16 (continued).

| Experiment	32	33	34	35	36	37	38
Experiment	2.0	2.0	2.0	2.0	2.0	2.0	2.0
ACD, cm	10.22	10.22	10.22	10.22	10.22	10.22	10.22
Mean Electrode Area, cm^2	0.050	0.050	0.050	0.050	0.050	0.050	0.050
Bubble Radius, r_b, cm	0.01	0.01	0.01	0.01	0.01	0.01	0.01
$A_{bubble\ cross\ section}$ x10^{-3}, cm^2	0.050	0.050	0.050	0.050	0.050	0.050	0.050
Residence Time, RT, second	2.712	2.703	2.712	2.712	2.716	2.712	2.712
Bubble Volume x10^{-4}, cm^3	5.24	5.24	5.24	5.24	5.24	5.24	5.24
Bubble rate, bubbles·sec^{-1}	5179	5163	5179	5179	5187	5179	5179
Blocked anode area, cm^2	2.03	2.03	2.03	2.03	2.04	2.03	2.03
Non blocked anode area, cm^2	2.97	2.97	2.97	2.97	2.96	2.97	2.97
Resistivity, ohm·cm	0.48	0.51	0.53	0.56	0.59	0.64	0.64
Bubble Area Resistance, ohm	0.02	0.02	0.02	0.02	0.02	0.02	0.02
IR_{bubble}	0.105	0.113	0.117	0.125	0.132	0.141	0.140
ACD other than bubbles, cm	1.900	1.900	1.900	1.900	1.900	1.900	1.900
Electrolyte Resistance, ohm	0.089	0.095	0.099	0.105	0.110	0.118	0.118
$IR_{electrolyte}$	0.582	0.622	0.647	0.688	0.725	0.775	0.775
$E_{th}+IR_{bubble}+IR_{electrolyte}$	3.453	3.485	3.506	3.539	3.572	3.617	3.599
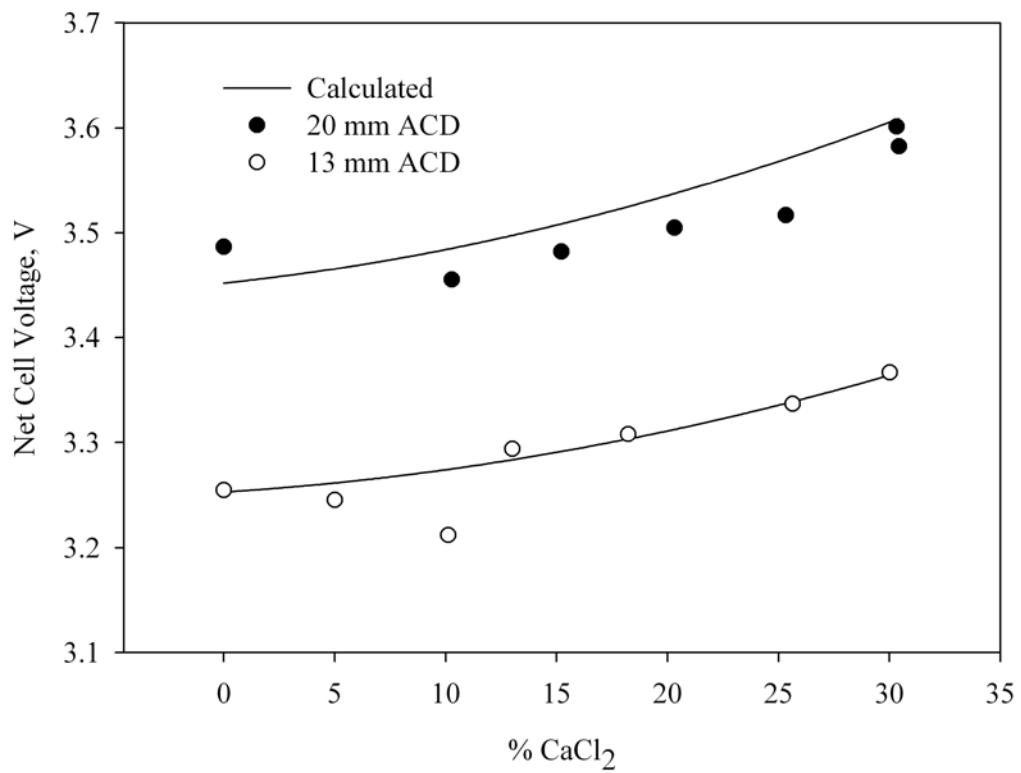
Figure 65 Calculated and experimental cell voltages for the experiments involving the effect of CaCl$_2$.

Figure 66 shows pictures of collected magnesium particles and the cathode. It is evident that detached droplets fused together during electrolysis and formed a giant particle at 10% $CaCl_2$. The fusion continued to some extent as the concentration was increased to 15% $CaCl_2$ and even beyond. Partially united magnesium droplets were easily distinguishable at 15% $CaCl_2$. However, the sizes of the united particles were smaller than those in experiments with 10% $CaCl_2$.

Unification of magnesium droplets is considered to be beneficial. Since collection of MgO at the cathode surface forms a film that hinders the coalescence of magnesium droplets addition of $CaCl_2$ up to about 10% seem to help magnesium droplets to combine together. It is not possible to completely eliminate the MgO presence inside the melt even in most controlled environments. A nucleation step is required to initiate magnesium deposition even on top of molten magnesium cathode when MgO layer formation takes place and electrolysis continues at the surface where MgO layer is thinner [61].

$CaCl_2$ was known to dissolve large amount of oxides. Hence it was possible that the $CaCl_2$ addition caused the dissolution of MgO that would deposit at the cathode surface otherwise. Therefore the magnesium particles in the melt fused easier and larger particles formed. Furthermore a small increase in net cell voltage at low $CaCl_2$ additions may in part be due to the lower oxide concentration at the cathode surface due to the MgO removal by the detached particles.

The beneficial effect of the MgO removal from the cathode surface at lower concentrations was not observed at the higher $CaCl_2$ concentrations. $CaCl_2$ is hygroscopic and more water is retained inside the melt at higher $CaCl_2$ concentrations. Therefore the amount of MgO increases with the $CaCl_2$ addition. The cell voltage increased with the increasing $CaCl_2$ concentration after 10% $CaCl_2$ mainly due to the higher electrical resistance. Increased effective ACD

because of the smaller magnesium droplets was another reason for the increased cell voltage.

Density of the melt and therefore the buoyancy forces increases with the addition of the $CaCl_2$. Magnesium particles were detached faster from the cathode surface and shorter deposition time resulted in smaller particle size. The finer magnesium droplets at the 25 and 30% $CaCl_2$ concentrations were resulted from the combination of both increased electrolyte density and the presence of MgO on magnesium particles.

The higher decrease in current efficiency at the lower ACD can be explained by the increased contact between magnesium and chlorine due to the increased turbulence in electrolyte. Smaller ACD also decreased the distance that both dissolved magnesium and chlorine had to diffuse to form back reaction.

CaCl$_2$ 0%
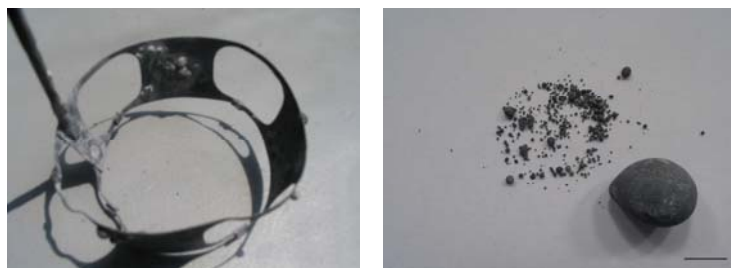
CaCl$_2$ 10%

Figure 66 Cathodes and magnesium particles at 20 mm ACD for the experiments involving the effect of CaCl$_2$ (length of the line is 10 mm,).

CaCl$_2$ 15%

CaCl$_2$ 20%

CaCl$_2$ 25%

CaCl$_2$ 30%

Figure 66 (continued).

4.6. The Effect of Sodium Flouride

NaF addition increases the coalescence of the magnesium droplets by its fluxing action at the surface of the droplets and was reported as beneficial [2,62]. A series of experiments were conducted to test the effect of NaF on the performance of the present cell. High $CaCl_2$ containing electrolyte composition was chosen to obtain large amount fine droplets to make the effect of NaF pronounced. Larger droplets were expected upon addition of NaF due to increased coalescence. The composition was 20% $MgCl_2$, 30% $CaCl_2$, 25% NaCl, 25% KCl and NaF was added by 1% increments from 1% to 5%NaF. The ACD, temperature and the current density were 20 mm, 700°C and 0.42-0.43 A cm^{-2} respectively.

The net cell voltage variations during the experiments involving the effect of NaF addition are given in Figure 67. A great fluctuation in cell voltage was observed when there was no NaF present inside the electrolyte. Two peaks were observed at the beginning and the cell voltage was stable at the second half of the experiment at 1%NaF. Cell voltage showed a single peak at 2% and higher NaF concentrations. Cell voltage was highly stable at 2%NaF but it was 100mV higher than the cell voltage at 1%NaF. The main feature of the 3%NaF was the steady increase in cell voltage after 50 minutes until the end of the experiment. A huge initial peak was observed in 4%NaF containing electrolyte and the cell voltage started to increase suddenly after 60 minutes. The experiment that involves 5% NaF could not be completed. The voltage increased further and large oscillations were observed. The summary of the NaF experiments was given in Table 17.

130
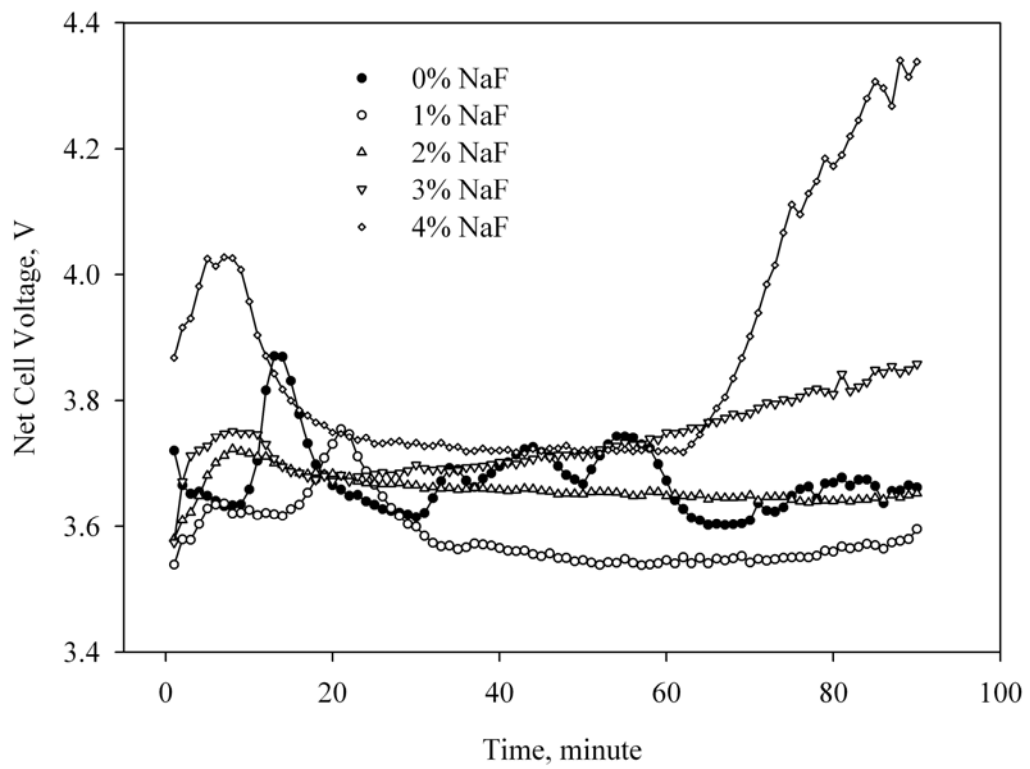
Figure 67 Net cell voltage vs. time 20 ACD for the experiments involving the effect of NaF.

Table 17 The details of the experiments involving the effect of NaF.

Experiment	39	40	41	42	43
$MgCl_2$, wt%	20.0	19.2	20.2	20.0	19.8
NaCl, wt%	25.0	24.7	23.7	23.5	23.3
KCl, wt%	25.0	24.7	23.7	23.5	23.3
$CaCl_2$, wt%	30.0	30.4	30.3	30.0	29.7
NaF, wt%	0.0	1.0	2.0	3.0	4.0
Total Salt, g	160.0	158.9	158.4	160.0	161.6
T, °C	700	700	700	700	700
E^0, V	2.51	2.51	2.51	2.51	2.51
a_{MgCl_2} (mean)	0.0025	0.0025	0.0025	0.0025	0.0025
E_{th} (mean), V	2.77	2.77	2.77	2.77	2.77
$\kappa_{(mean)}$, ohm^{-1}·cm^{-1}	1.55	1.57	1.54	1.55	1.57
t, min	90	90	90	90	90
$Mg_{collected}$, g	3.9916	3.8659	3.9281	4.0731	4.0387
$Mg_{theoretical}$, g	4.4617	4.4549	4.4413	4.4685	4.4685
I, A	6.56	6.55	6.53	6.57	6.57
A_{anode}, cm^2	5.0	5.0	5.0	5.0	5.0
j_{anode}, A·cm^{-2}	1.31	1.31	1.31	1.31	1.31
$A_{cathode}$, cm^2	15.4	15.4	15.4	15.4	15.4
$j_{cathode}$, A·cm^{-2}	0.43	0.42	0.42	0.43	0.43
$E_{average\ net}$, V	3.68	3.58	3.66	3.74	3.86
CE, %	89.5	86.8	88.4	91.2	90.4
EC, kWh·kg^{-1}	9.1	9.1	9.1	9.0	9.4
EE, %	67.3	67.0	66.9	67.4	64.8
ACD, cm	2.0	2.0	2.0	2.0	2.0

The change in cell voltage could be more easily followed in Figure 68. Addition of 1%NaF decreased the cell voltage approximately by 100mV. And the cell voltage increased after that composition. Current efficiency values obtained were around 90% and did not show any significant difference as it can be seen from Figure 69. Energy consumption slightly increased due to the increased cell voltage as it was shown in Figure 70 and the energy efficiency showed slight decrease, Figure 71.

Successive peaks observed at the 0%NaF was due to successive nucleation cycles on top of the previously deposited layer of fine droplets. Fine magnesium droplets that were smaller than 1 mm diameter accumulated on top each other and formed a pile of 3-4 mm thickness at the cathode surface at that composition.

Beneficial effect of NaF is clearly visible from the net cell voltage curves obtained from the 0% and 1% NaF experiments. Fluxing action at the magnesium surface resulted in a more stable cell voltage at the 1% NaF concentration. The decrease in the number of peaks indicated the reduced nucleation requirement at 1% NaF due to the larger particle sizes. However more nucleation required for further deposition due to MgO at the magnesium droplet surface in the absence of NaF inside the electrolyte. The nucleation took place at the cathode surface if the previous layer detached from the cathode. However, if MgO coated droplet layer remained as attached to the cathode surface, nucleation took place on top of a previously deposited magnesium droplet layer as in the case of 0%NaF.
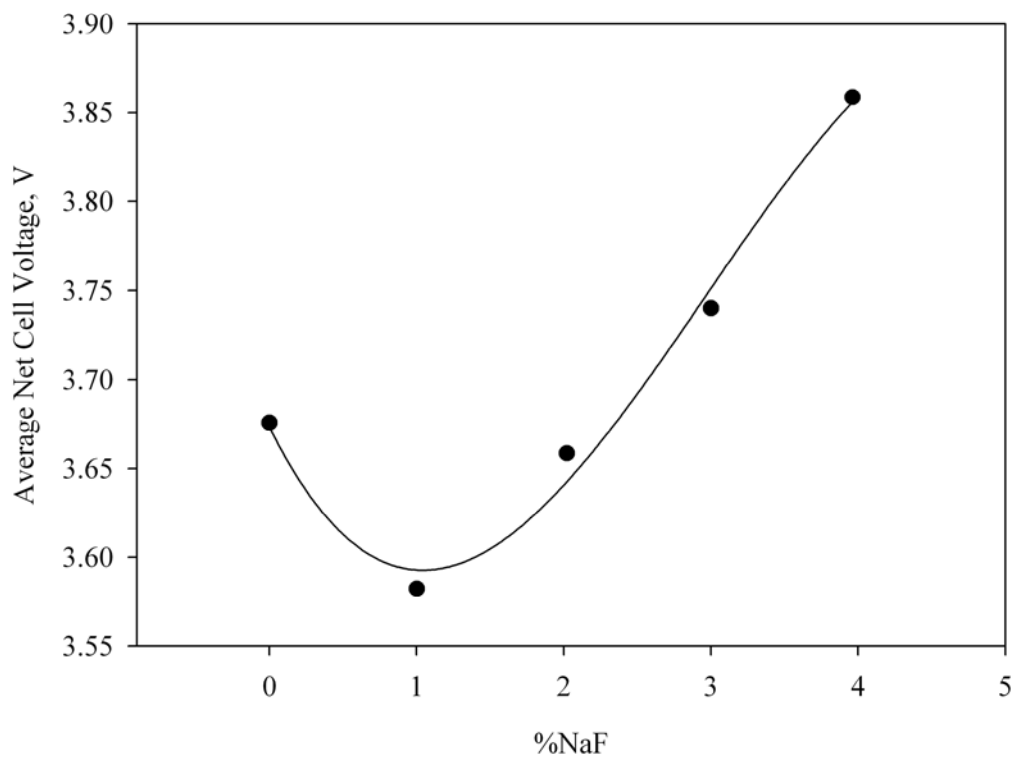
Figure 68 Average net cell voltages for the experiments involving the effect of NaF.
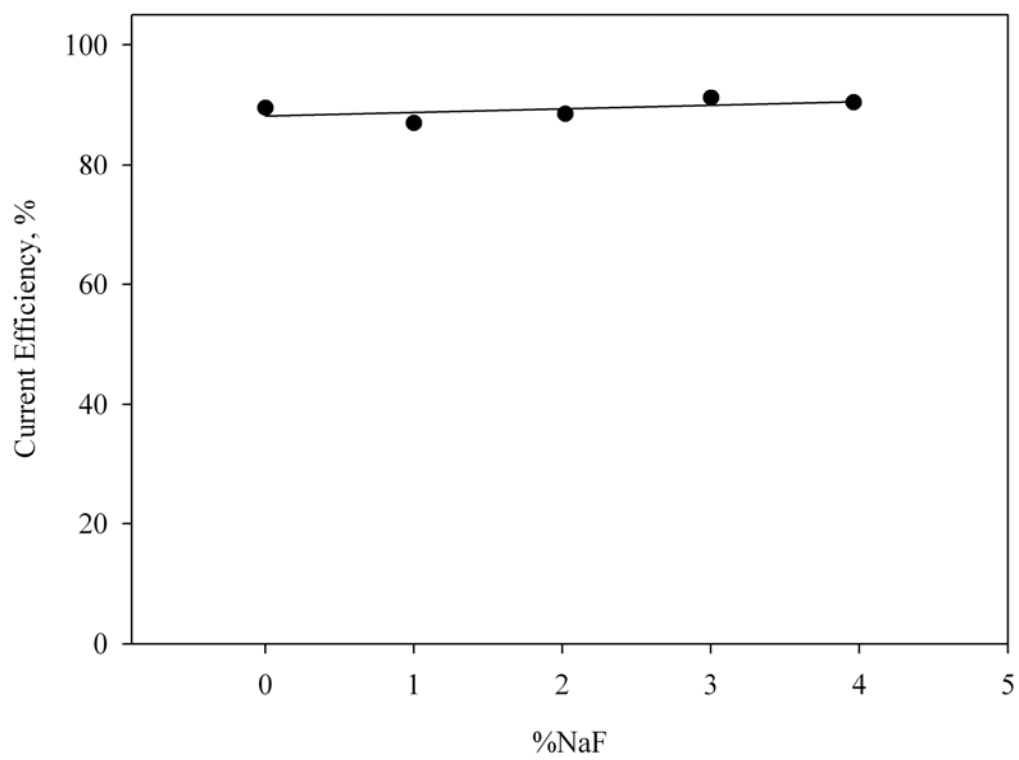
Figure 69 Current efficiencies for the experiments involving the effect of NaF.
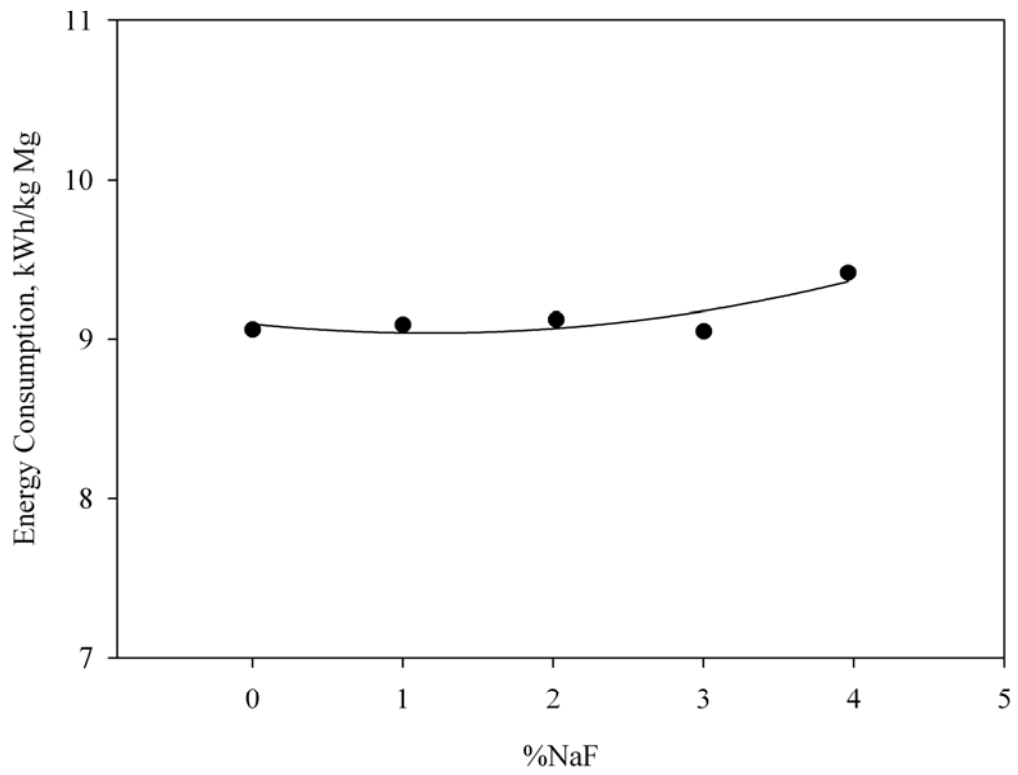
Figure 70 Energy consumption for the experiments involving the effect of NaF.
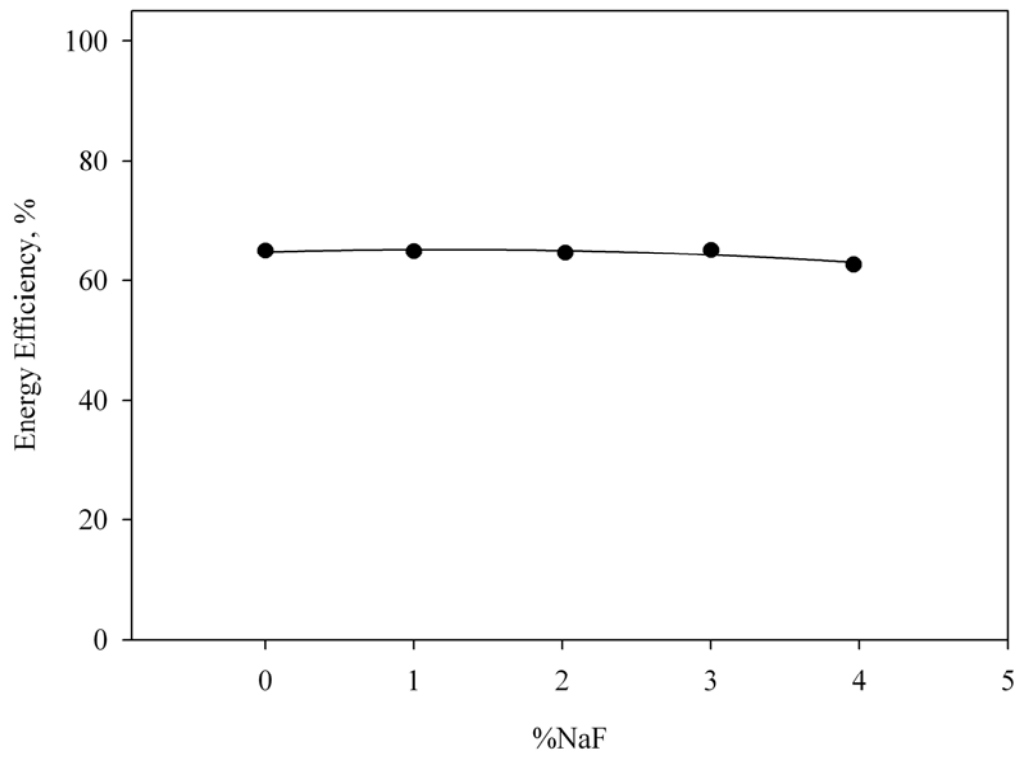
Figure 71 Energy efficiencies for the experiments involving the effect of NaF.

Droplet size increased and the number of droplets decreased by the addition of NaF as can be seen in Figure 72. The tendency of larger particle formation clearly demonstrated that NaF had a beneficial effect on the coalescence of magnesium droplets. However accompanying increase in cell voltage puts a limitation on the applicable NaF concentration.

It can be concluded that the optimum NaF concentration is around 1%NaF from the cell voltage variations. It is consistent with the results obtained in a previous study that employs a similar electrolyte [62]. Although there is no information about the cell voltages, the current efficiency is the highest around the same NaF concentration. The current efficiency increase from 70% to 84% with the corresponding increase in NaF concentration from 0% to 1% was attributed to the coalescence of magnesium droplets. Current efficiency was reported as decreasing after 1.4% NaF [62].

Corrosive action of the fluoride ions was observed from the large voltage oscillations. Cathode connection wire corroded and ruptured at an experiment involving 5% NaF. Therefore the optimum level of NaF should be high enough to affect MgO present at the magnesium metal surface and low enough to not to attack and oxidize magnesium metal.

The magnesium droplet size had a little effect on the current efficiency. This implies that the back reaction was influenced little from the size of the magnesium particles. Therefore it may be concluded that the chlorine gas evolution has a larger effect on the extent of back reaction.

0%NaF

1%NaF

2%NaF

3%NaF

4%NaF

Figure 72 Magnesium droplets for the experiments involving the effect of NaF

(length of the line is 1 cm).

CHAPTER 5

CONCLUSIONS

The effect of magnesium nucleation on the cathode is visible in most cases from the cell voltage variation with time. The magnitude of the characteristic peaks at the beginning of the voltage-time graphs increased with the increase in current density. This was related with the increased energy necessary for the larger number of nucleation sites. The decrease in the magnitude of the peaks with the increased temperature also supports that the initial peaks were related with the nucleation. In addition to this, the peak cell voltage also decreased with the scratched cathode where the available nucleation sites were increased.

Successive peaks observed in some of the experiments involving the effects of $CaCl_2$ and NaF were found as related with the successive nucleation on top of previously deposited magnesium droplet layers. Magnesium droplets were found as accumulated on the cathode surface forming a thick pile by magnesium droplets much smaller than the pile thickness at those experiments.

The latter portions of the voltage variation curves were due to $MgCl_2$ depletion during the electrolysis. Lower $MgCl_2$ content of the electrolyte results in an increase in electrical conductivity of the melt. This decreased the cell voltage. On the other hand, cell voltage increases with the decreased $MgCl_2$ activity due to lower $MgCl_2$ content. Much of the voltage curves showed continuous small decrease until the end of the electrolysis after the initial nucleation peaks. This implies that the effect of the decrease in $MgCl_2$ activity was small in those experiments. However, the cell voltage started to increase at the final portions of some of the curves as a result of decrease in $MgCl_2$ activity, and increase in cell resistance. These were the experiments where large compositional variations

were practiced due to higher electrical charges employed or higher $MgCl_2$ loss that took place due to evaporation at the higher electrolysis temperature or larger increase of cell resistance in $CaCl_2$ containing electrolytes.

Both the voltages and the current efficiencies were considered to be influenced by the amount and hydrodynamics of chlorine bubbles in inter-electrode region. Increased production rate of chlorine gas with the increased current density was assumed to affect both the diameter and residence time of the evolving bubbles. A model was used to calculate electrolyte resistance by including the resistance due to the presence of Cl_2 bubbles around the anode. Good correlations were obtained between the calculated and experimental cell voltages.

By considering the change in size and the rise velocities of the bubbles chlorine dissolution from the bubbles into the electrolyte were calculated to determine current efficiency from hydrodynamic model. Comparison of the calculated and experimental current efficiencies showed that the back reaction between dissolved magnesium and chlorine was not the only current loss mechanism. The formation and the entrance of the small magnesium particles to the anode compartment due to convection was also an important mechanism in current losses in experiments with 13 mm ACD.

Current efficiencies more than 90% were easily achieved at current densities higher than the industrial applications. The cell was capable of producing magnesium with less than the lowest energy consumption values, industrially obtained for high purity $MgCl_2$, at current densities about double the commonly practiced industrial levels.

Very high current efficiencies observed in experiments with NaCl-KCl-$MgCl_2$ electrolytes were attributed to molten magnesium being cathodic. Calculated current efficiencies support this finding.

The temperature change had no distinguishable consequence on the morphology of magnesium deposition at the cathode within the temperature range covered in this study. Cell voltages decreased with the increasing temperature as expected from ΔG of decomposition reaction and electrolyte conductivity. Slight increase of cell voltage during the electrolysis at 725°C was considered to be due to $MgCl_2$ evaporation during the electrolysis.

Detachment of magnesium droplets from the cathode surface was obtained to a certain extent when used cathode was employed. High current efficiency obtained and many of the droplets being attached to the cathode surface right after the experiment indicated that, a large portion of the droplets were still cathodic during the experiment involving the used cathode.

To enhance detachment of molten magnesium from cathode surface, different NaCl/KCl ratios were used in the electrolyte. The problem associated with the excessive magnesium accumulation at the steel cathode that could cause short circuiting of electrodes could not be solved with the variation in NaCl/KCl ratio except at concentrations higher than 50% NaCl where the current efficiency was unacceptably low. Although a continuous decrease in net cell voltage, due to increased $MgCl_2$ activity and electrolyte conductivity, was expected with increasing NaCl concentration, a considerable increase was observed at NaCl concentrations higher than 50%.

Examinations of average net cell voltages, current efficiencies and chemical analyses at concentrations higher than 50% NaCl, indicated Na codeposition. Low current efficiencies and high cell voltages for magnesium electrolysis in electrolytes with more than 50% NaCl was considered to be due to codeposited Na. Codeposition of Na could result in formation of Na vapor at the cathode because of its high vapor pressure, which could block the electrode and could cause an increase in cell voltage at the same time a decrease in current efficiency.

Na deposition was also considered to stimulate the fine magnesium particle formation that caused an additional efficiency loss.

Detachment of magnesium from the cathode was obtained when $CaCl_2$ was added to the electrolyte. This was considered to be due to increase in contact angle between liquid magnesium and steel cathode when $CaCl_2$ addition was made. Net cell voltage showed a decrease up to 10% $CaCl_2$ and then increased with further $CaCl_2$ addition at NaCl:KCl=1. The decrease in cell voltage could not be explained in terms of the electrolyte conductivity and change in decomposition voltage accompanied with the $CaCl_2$ addition. The decrease was considered as related with the beneficial effect of $CaCl_2$ at the magnesium particle surfaces that was evident from the coalescence of magnesium droplets. Cell voltage increased with the further $CaCl_2$ addition due to the increase in electrolyte resistance.

NaF had a marked effect on the coalescence of magnesium droplets and increased the droplet size of magnesium. Although it did not introduce almost any effect on the current efficiency, the cell voltage was highly sensitive to the changes in NaF concentration. Fluxing action at the magnesium surface resulted in a more stable cell voltage at the 1% NaF concentration. The cell voltage increased drastically at larger NaF concentrations. Optimum NaF concentration was determined as 1%NaF according to the cell voltage variations.

An electrolyte containing 20% $MgCl_2$, 10% $CaCl_2$, 1% NaF and 1:1 NaCl:KCl can be considered as optimum concentration for the present cell at 700˚C when ACD is 20mm. The cell consumes around 8 kWh energy per kilogram of magnesium at these conditions. That is well below the lowest industrial practice.

REFERENCES

[1] "Magnesium and Magnesium Alloys", Kirk-Othmer Encyclopedia of Chemical Technology Vol. 15, 5th ed., pp. 320-380, Wiley, New York, (2005).

[2] Kh.L. Strelets, "Electrolytic Production of Magnesium" (translated from Russian by J. Schmorak), Keter Publishing, Jerusalem, (1977).

[3] G.J. Kipouros and D.R. Sadoway, ''The Chemistry and Electrochemistry of Magnesium Production'' in Advances in Molten Salt Chemistry, Vol.6, Elsevier, Amsterdam, pp. 127-209, (1987).

[4] A.M. Martinez, B. Borresen, G.M. Haarberg, Y. Castrillejo and R. Tunold, "Electrodeposition of Magnesium from $CaCl_2$-NaCl-KCl-$MgCl_2$ Melts", Journal of Electrochemical Society, Vol.151, No.7, pp.C508-C513, (2004).

[5] R.L. Thayer and R Neelameggham, "Improving the Electrolytic Process for Magnesium Production", JOM, Vol. 53, No.8, pp.15-17, (2001).

[6] D.A. Kramer, "Magnesium Metal Statistics", Mineral Commodity Summaries, U.S. Geological Survey, (January 1996 to January 2006).

[7] M. Temkin, "Mixtures of Fused Salts as Ionic Solutions", Acta Physicochimica U. R. S. S., Vol. 4, pp. 411-420, (1945).

[8] C.H. Huang and M.H. Brooker, "Raman Spectrum of Molten $MgCl_2$", Chemical Physics Letters, Vol.43, No.1, pp.180-182, (1976).

[9] M.H. Brooker and C.H. Huang, "Raman Spectroscopic Studies of Structural Properties of Solid and Molten States of the Magnesium Chloride – Alkali Metal Chloride System", Canadian Journal of Chemistry, Vol. 58, No.2, pp.168-179, (1980).

[10] M.M. Laursen and J.H. von Barner, "Potentiometric and Raman Spectroscopic Study of the Complex Formation of Mg(II) in KCl-$AlCl_3$ Melts ", Journal of Inorganic and Nuclear Chemistry" Vol.41, No.2, pp.185-187, (1979).

[11] H. Flood and S. Urnes, "Calculation of the Activities in Magnesium Chloride-Alkali Chloride Melts from Structure Models", Zeitschrift für Elektrochemie, 59, pp.834-839, (1955).

[12] O.J. Kleppa and F. G. McCarty, "Thermochemistry of Charge-Unsymmetrical Binary Fused Halide Systems. II. Mixtures of Magnesium Chloride with the Alkali Chlorides and with Silver Chloride", Journal of Physical Chemistry, Vol.70, No.4, pp.1249-1255 (1966).

[13] D.E. Neil, H.M. Clarck and R.H. Wiswall, "Thermodynamic Properties of Molten Solutions of $MgCl_2$-KCl, $MgCl_2$-NaCl, and $MgCl_2$-KCl-NaCl", Journal of Chemical and Engineering Data" Vol.10, No.1, pp.21-24, (1965).

[14] I. Karakaya and W.T. Thompson, "Thermodynamic Properties of $MgCl_2$-NaCl Melts from EMF Measurements", Journal of the Electrochemical Society, Vol.133, No.4, pp.702-706, (1986).

[15] B.R. Davis and W.T. Thompson, "Thermodynamic Properties of Magnesium Chloride Electrolytes", International Symposium on Light Metals 1997, 36th Annual Conference on Metallurgists of CIM, Sudbury, Ontario, Canada, pp.557-566, (1997).

[16] A. Kisza, J. Kazmierczak, B. Børresen, G.M. Haarberg and R. Tunold, "Kinetics and Mechanism of the Magnesium Electrode Reaction in Molten Magnesium Chloride", Journal of Applied Electrochemistry, Vol.25, No.10, pp.940-946, (1995).

[17] R. Tunold, in Light Metals 1980, C. McMinn, ed., TMS, Warrendale, PA, pp.949, (1980).

[18] E. Aarebrot, R.E. Andresen, T. Ostvold, H.A. Oye, "A Model for the Back Reaction in the Magnesium Electrolysis", Light Metals 106th AIME Annual Meeting, 491-512 (1977).

[19] J. Wypartowicz and T. Østvold, "The Solubility of Magnesium Metal and the Recombination Reaction in the Industrial Magnesium Electrolysis", H. A. Øye, Electrochim. Acta, Vol.25, No.2, pp.151-156 (1980).

[20] J.D. Van Norman, J.J. Egan, "The magnesium--magnesium chloride system. A chronopotentiometric study", Journal of Physical Chemistry, Vol.67, 11, pp.2460-2462, (1963).

[21] P.Ficara, "The Production of Anhydrous $MgCl_2$", McGill University Thesis, Montreal, Canada, (1996).

[22] J. Thonstad, "Some Recent Trends in Molten Salt Electrolysis of Titanium, Magnesium, and Aluminum", High Temperature Materials and Processes, Vol.9, pp.135-146, (1990).

[23] G.A. Abramov, Metallurg, No.6:82, 1935. (in Kh. L. Strelets, "Electrolytic Production of Magnesium" (Translated from Russian by J. Schmorak), Keter Publishing, Jerusalem, (1977)).

[24] J.B. Belavadi, N. Rajagopalan, P.S. Desikan and U. Sen, "Fusibility study of magnesium cell electrolyte containing $MgCl_2$, $CaCl_2$, NaCl and KCl", Journal of Applied Electrochemistry, Vol.12, Iss.5, pp. 501-503, (1982).

[25] K.P. Batashev, Metallurg, No.7:100, (1935). (in Kh. L. Strelets, "Electrolytic Production of Magnesium" (Translated from Russian by J. Schmorak), Keter Publishing, Jerusalem, (1977)).

[26] R.D. Holliday and P. McIntosh, "Laboratory Cell and Hydrodynamic Model Studies of Magnesium Chloride Reduction in Low-Density Electrolytes", Journal of the Electrochemical Society, Vol.120, No.7, pp.858-866, (1973).

[27] V.P. Mashovets and Z.F. Lundina, Trudy Nisalyuminiya, No.10:5, (1935) (in Kh.L. Strelets, "Electrolytic Production of Magnesium" (Translated from Russian by J. Schmorak), Keter Publishing, Jerusalem, (1977)).

[28] Kh.L. Strelets and O.G. Desyatnikov, Zhurnal Prikladnoi Khimii, No:2:201, p.41, (1955) (in Kh.L. Strelets, "Electrolytic Production of Magnesium" (Translated from Russian by J. Schmorak), Keter Publishing, Jerusalem, (1977)).

[29] R.L. Quintero, "On the Thermodynamic Properties of Hydrates and Ammines of Magnesium Chloride", MSc. Thesis, Department of Mining and Metallurgical Engineering, McGill University, Montreal, Canada, (1981).

[30] K.K. Kelly, "Energy Requirements and Equilibria in the Dehydration, Hydrolysis, and Decomposition of Magnesium Chloride", Technical Paper 676, U.S. Bureau of Mines, Washington DC, (1945).

[31] J.E. Vindstad, H. Mediaas and T. Ostvold, "Hydrolysis of $MgCl_2$ containing Melts", Acta Chemica Scandinavica, Vol.51, pp.1192-1200, (1997).

[32] S. Kashani-Nejad, K.W. Ng and R. Harris, "MgOHCl Thermal Decomposition Kinetics", Metallurgical and Materials Transactions, 36B, pp.153-157, (2005).

[33] K.W. Ng, S. Kashani-Nejad and R. Harris, "Kinetics of MgO Chlorination with HCl Gas", Metallurgical and Materials Transactions, 36B, pp.405,409, (2005).

[34] Kh.L. Strelets and K.D. Muzhzhavlev, "Application of Radioactive Isotopes to Investigation of Mechanism of Passivation of Cathodes in Magnesium Electrolyzers", Tsvetnye Metally, Vol.30, No.6, pp.52-56, (1957).

[35] H. Mediaas, J.E. Vindstad and T. Ostvold, "Solubility of MgO in MgCl$_2$-NaCl-NaF Melts", Light Metals 1996, pp.1129-1137, (1996).

[36] U.S. Pat. 3,742,100 (June 26, 1973) O. Boyum et.al. (to Norsk-Hydro AS), U.S. Pat. 3,760,050 (Sept. 18, 1973) I. Blaker et.al. (to Norsk-Hydro AS), U.S. Pat. 5,112,584 (May 12, 1992) G. T. Mejdell et.al. (to Norsk-Hydro AS), U.S. Pat. 5,120,514 (June 9, 1992) K. W. Tveten et.al. (to Norsk-Hydro AS).

[37] U.S. Pat. 3,907,651 (Sept. 23, 1975) K.A. Anderassen and K.B. Stiansen (to Norsk-Hydro AS), U.S. Pat. 4,308,116 (Dec. 29, 1981) K.A. Andreassen et.al. (to Norsk-Hydro AS).

[38] U.S. Pat. 4,058,448 (Nov. 15, 1977) K.D. Muzhzhavlev et.al..

[39] U.S. Pat. 4,514,269 (Apr. 30, 1985) Sivilotti O.G. (to Alcan), U.S. Pat. 4,518,475 (May 21, 1985) Sivilotti O.G. (to Alcan), U.S. Pat. 4,560,449 (Dec. 21, 1985) Sivilotti O.G. (to Alcan), U.S. Pat. 4,604,177 (Aug. 5, 1986) Sivilotti O.G. (to Alcan), U.S. Pat. 4,960,501 (Oct. 2, 1990) O. G. Sivilotti (to Alcan).

[40] U.S. Pat. 4,647,355 (Mar. 3, 1987) H. Ishizuka, U.S. Pat. 4,495,037 (Jan. 22, 1985) H. Ishizuka, U.S. Pat. 4,481,085 (Nov. 6, 1984) H. Ishizuka, U.S. Pat. 4,334,975 (June 15, 1982) H. Ishizuka.

[41] Ullmann's Encyclopedia of Industrial Chemistry, Vol.A15, Barbara Elvers, Stephen Hawkins, Gail Schulz, eds., VCH, New York, p. 559, (1990).

[42] U.S. Pat. 4,800,003 (Jan. 24, 1989) J. G. Peacey and G. B. Harris (to Noranda, Inc.), U.S. Pat. 5,091,161 (Feb. 25, 1992) G. B. Harris and J. G. Peacey (to Noranda, Inc.).

[43] D.R. Hodgson, A. Fones, D.J. Fray, I. Mellor, S. Brewer, D. Jackson, L. Slevin and S.E. Male, "Development and Scale-up of the FFC Cambridge Process for Production of Metals", ECS Transactions, Vol. 2, No.3, pp. 365-368, (2006).

[44] D.R. Sadoway, "New Opportunities for Metals Extraction and Waste Treatment by Electrochemical Processing in Molten Salts", Journal of Materials Research, Vol.10, No.3, pp.487-492, (1995).

[45] M.Güden and I. Karakaya, "Electrolysis of MgCl$_2$ with a Top Inserted Anode and Mg-Pb Cathode", Journal of Applied Electrochemistry, Vol.24, pp.791-797, (1994).

[46] R. Sharma, "An Electrolytic Process for Magnesium and Its Alloys Production", Light Metals 1996, W. Hale, ed., TMS, Warrendale, PA, p. 1113, (1996).

[47] E.F. Emley, Principles of Magnesium Technology, Pergamon Press, New York, p. 120, (1966).

[48] U.S. Pat. 2,267,862 (Dec. 30, 1941) J.D. Hanawalt et.al.(to Dow Chemical Co.), U.S. Pat. 5,147,450 (Sept. 15, 1992) B.A. Mikucki et.al. (to Dow Chemical Co.).

[49] G.Song, A.Atrens, D. St John, X. Wu and J. Nairn, "The Anodic Dissolution of Magnesium in Chloride and Sulphate Solutions", Corrosion Science, Vol.39, No.10-11, pp.1981-2004, (1997).

[50] E.I. Savinkova, R.P. Lelekova, "Equilibrium of Magnesium Chloride Hydrolysis in Chloride Melts", Zhurnal Prikladnoi Khimii, Vol.51, No.7, pp.1453-1456, (1978).

[51] O.A.Lebedev, "Basic Spefications of Electrolyte for the Production of Magnesium", The Soviet Journal of Non-Ferrous Metals, Vol.25, p.52 (November,1984).

[52] I. Leibson, E.G. Holcomb, A.G. Cacoso and J.J. Jasmic, "Rate of Flow and Mechanics of Bubble Formation from Single Submerged Orifices", American Institute of Chemical Engineers Journal, Vol.2, No.3, pp.296-206, (1956).

[53] G. Demirci, "Molten salt electrolysis of magnesium and its hydrodynamics", MSc. Thesis, Middle East Technical University, Ankara, (1998).

[54] P.H. Calderbank, Transactions of the Institution of Chemical Engineers, "Physical Rate Processes in Industrial Fermentation; Part2- Mass Transfer Coefficients in Gas-Liquid Contacting with and without Mechanical Agitation" Vol.37, pp.173-185, (1959).

[55] Aarebrot E., Andresen R.E., Ofstvold T. and Oye H.A., "A Model for the Back Reaction in the Magnesium Electrolysis", Light Metals 106th AIME Annual Meeting, pp.491-512, (1977).

[56] Q.Zhuxian, F. Liman, K.Grjotheim and H. Kvande, "Formation of Metal Fog During Molten Salt Electrolysis Observed in a See Through Cell", Journal of Applied Electrochemistry, Vol.17, pp.707-714, (1987).

[57] B.R. Davis, "A Thermodynamic Study of Magnesium Chloride-Alkali Chloride Electrolytes for Use in Magnesium Production", PhD. Thesis, Queen's University, Kingston, Canada (1994).

[58] J.K. Fink and L. Leibowitz, "Thermodynamic and Transport Properties of Sodium Liquid and Vapor", Argonne National Labaratory, Report no. ANL/RE-95/2, (January 1995).

148

[59] İ.Karakaya, W.T. Thompson, "A Thermodynamic Study of the System $MgCl_2$-NaCl-$CaCl_2$ Melts", Canadian Metallurgical Quarterly, Vol.25, No.4, pp.307-317, (1986).

[60] J. Zhu, İ.Karakaya, W.T. Thompson, "Partial Molar Properties of $MgCl_2$ in $MgCl_2$-KCl-$CaCl_2$ melts", Journal of the Electrochemical Society, Vol. 135, No.1, pp.122-126, (1998).

[61] B. Boressen, G.M. Haarberg and R. Tunold, "Electrodeposition of Magnesium from Halide Melts – Charge and Diffusion Kinetics", Electrochimica Acta, Vol.42, 10, pp.1613-1622, (1997).

[62] G.M. Rao, "Effect of Fluorspar on Electrowinning of Magnesium", Journal of Applied Electrochemistry, Vol.16, pp.626-628, (1986).

[63] N. Howell Furman editor, "Standart Methods of Chemical Analysis, Sixth Edition, Vol One – The Elements", D. Van Nostrand Company, Inc. Princeton, New Jersey, (1962).

APPENDIX

QUALITY OF THE PRODUCT

Chemical analyses of magnesium collected were done after certain experiments that were involving the study of the effect of NaCl:KCl ratio. Sodium (Na) and potassium (K) analyses were performed by PFP7 Jenway Flame Photometer while Ca, Cr, Cu, Fe, Mn, Ni and Pb analyses were made by ATI Unicam 929 Atomic Absorption Spectrometry. The flame photometry is suitable for the determination of 0.01 to 1.0% sodium, 0.01 to 1.0% potassium in magnesium alloys [63].

One gram of magnesium metal was dissolved in 20 ml concentrated HCl and then diluted. Na and K analyses were given in graphical form in Figure 56. They are given in tabular form in Table 18. Concentrations of other elements in metallic magnesium obtained from Experiment 15 that had an electrolyte with 39.5% NaCl are also included in Table 18. This electrolyte composition was used in most of the experiments.

Examination of this table indicates that sodium and nickel concentrations were higher than those in electrolytic magnesium. As it was discussed before high sodium concentrations were mainly due to Na co-deposition in selected samples obtained from high NaCl containing electrolytes. The high nickel concentration is attributable to the corrosion of the steel cathode. The cathode was left unprotected before and after the electrolysis. It is obvious that some dissolution occurred and nickel was deposited in magnesium. It is expected to have smaller Na, K, Fe, Ni and Cr concentrations for a continuous electrolysis process. Therefore the system is considered to provide electrolytic grade magnesium.

Table 18 Results of the chemical analyses.

	Description	%Na	%K	%Ca	%Cu	%Pb	%Cr	%Ni	%Fe	%Mn
Experiment 15	39.5%NaCl	0.17	0.02	0.06	0.01	0.01	0.01	0.35	0.07	0.04
Experiment 22	50.4% NaCl	0.26	0.1							
Experiment 23	55.3% NaCl	0.33	0.11							
Experiment 25	63.7% NaCl	0.48	0.12							
Experiment 37	30%CaCl2	0.19	0.04	0.08						
Experiment 38	30%CaCl2	0.18	0.03							

CURRICULUM VITAE

PERSONAL INFORMATION

Surname, Name: Demirci, Gökhan

Nationality: Turkish (TC)

Date and Place of Birth: 21 September 1972, Trabzon

Marital Status: Married

Phone : +90 312 210 45 17

Fax   : +90 312 210 12 61

E-mail : demirci@metu.edu.tr

EDUCATION

Degree	Institution	Year of Graduation
MS	METU Metallurgical and Materials Engineering	1998
BS	METU Metallurgical Engineering	1995
High School	Çanakkale Lisesi	1989

WORK EXPERIENCE

Year	Place	Enrollment
January 2005-Present	METU Department of Electrical and Electronics Engineering	Research Scientist
September1995-September 2003	METU Department of Metallurgical and Materials Engineering	Teaching Assistant

MILITARY SERVICE November 2003 - November 2004 / TRNC TUPFICYP

FOREIGN LANGUAGE English